Development of a Longitudinal Cracking Fatigue Damage Model for Jointed Plain Concrete Pavements Using the Principles of Similarity

A Dissertation

SUBMITTED TO THE FACULTY OF THE UNIVERSITY OF MINNESOTA

BY

Rita Elizabeth Lederle

IN PARTIAL FULFILLMENT OF THE REQUIREMENTS

FOR THE DEGREE OF

DOCTOR OF PHILOSOPHY

Adviser: Lev Khazanovich

July 2014

Acknowledgements

First and foremost, I would like to thank my adviser Lev Khazanovich for his guidance throughout my career at the University of Minnesota. I appreciate the time, and advice he gave me. I would also like to thank Dr. Mihai Marasteanu, for chairing my committee and Dr. Henryk Stolarski and Dr. Adam Rothman for serving on my committee. Research is never conducted alone, and I received help and encouragement from my research group, in particular from Mary Vancura, Kyle Hoegh, and Sam Paitich. Without Brad Aylsworth's programming genius, this project would not have been completed and his efforts are immensely appreciated.

I am indebted to my tri-state dissertation writing support group of Rose Kantor, Khatereh Vagehfi, and Chris DeDene, who were always just a phone call away to share experiences and encourage me to keep going. I'm so glad we all went through this together.

Finally, I would like to thank my family, who provided endless love, encouragement, and support to help me through this process.

For Andrew,

and in memory of my grandfather Charles Asgian
Պիտի կարօտնամ ձեզի, Պապա

Abstract

Mechanistic-empirical (M-E) pavement design computes stresses induced in a concrete slab due to applied traffic and environmental loads, and correlates these stresses to distress levels using empirical correlations. Currently, the Mechanistic-Empirical Pavement Design Guide (MEPDG) is one of the most advanced and prevalent methods of M-E pavement design. While the MEPDG predicts transverse cracking, longitudinal cracking is not predicted, even though longitudinal cracking is commonly observed in jointed plain concrete pavements (JPCPs). In this research, an MEPDG compatible model was developed to predict longitudinal cracking fatigue damage in JPCPs. This modeled adapts the framework of the MEPDG specifically for longitudinal cracking.

In order to develop an M-E longitudinal cracking fatigue damage model, it is necessary to compute stresses at the critical location for longitudinal cracking due to the various traffic and environmental loads to which a pavement could be exposed. The principles of similarity were used to map the original problem into similar space, which drastically reduces the complexity of the problem without introducing any error. To avoid the computational inefficiency associated with embedding a finite element program within the program, neural networks are used for rapid stress solutions. Stresses determined in similar space are converted back into real space for damage computation. Modifications were made to the MEPDG fatigue damage computation process to eliminate simplifying assumptions and to make the procedure applicable to longitudinal cracking.

A study was also conducted to determine characteristics of pavement susceptible to longitudinal cracking based on various parameters. This study made use of the principles of similarity to examine almost all pavements which could be considered in M-E design. By identifying the characteristics of pavements susceptible to longitudinal cracking, engineers can identify pavements for which longitudinal cracking analysis should be conducted. The model and design procedure developed in this research provides the tools needed to conduct such an analysis.

Table of Contents

List of Tables

List of Figures

Chapter 1. Introduction

Mechanistic-empirical (M-E) design of pavements uses mechanics to predict stresses induced in a pavement by traffic and environmental loads and empirical correlations to convert stress levels to predicted distresses. Of the many M-E design procedures in existence (ex. Darter 1977; Darter et al. 1995; Packard & Tayabji 1985; PCA 1984; Thompson & Barenberg 1992; Zollinger & Barenberg 1989), the most advanced is the recently introduced Mechanistic-Empirical Pavement Design Guide (MEPDG) (NCHRP 2006). The MEPDG computes damage from each applied load using Miner's cumulative fatigue law (Miner 1945). Cumulative fatigue damage is then correlated to distress levels using empirical data from hundreds of pavements throughout the United States and Canada collected as part of the Long Term Pavement Performance (LTPP) project (FHWA 2009).

While the MEPDG predicts the amount of transverse cracking (i.e. cracks perpendicular to the direction of traffic) expected in a jointed plain concrete pavement (JPCP), longitudinal cracking (cracks parallel to the direction of traffic) is not considered as a failure method. With the increased use of widened lanes, longitudinal cracking is routinely observed in the field, including in Minnesota (Khazanovich et al. 2008; Owusu-Ababio & Schmitt 2013) and the need for a longitudinal cracking model in the MEPDG has been expressed (Hiller et al. 2012; Khazanovich & Darter 2012).

The lack of an MEPDG longitudinal cracking model has implications on pavement design decisions. When widened slabs are used, the MEPDG treats thin slabs as a viable design option. If these pavements are built and used however, they fail in unpredicted longitudinal cracking. This shows the need to develop an MEPDG compatible procedure to account for longitudinal cracking which can be used in conjunction with the current transverse cracking model.

1.1 Problem Statement

In order to predict JPCP longitudinal cracking within the MEPDG framework, it is necessary to compute the stresses in the pavement which would cause longitudinal

cracking caused by various loads to which the pavement will be subjected in its lifetime. Stresses must be computed for many different cases, including different vehicle loads at different locations on a pavement subjected to different temperature and moisture gradients. There is also a need to account for changes in the pavement structure over time. For example, seasonally adjusted values for subgrade moduli are considered on a monthly basis throughout pavement life; similarly, load transfer efficiency and the friction level between the concrete and underlying layers degrade as the pavement ages. Accounting for these factors means that hundreds of thousands of scenarios must be considered in the analysis of a single pavement (NCHRP 2004). Embedding a finite element analysis program within the MEPDG is so computationally intensive as to be prohibitive. Therefore, a computationally efficient tool for such stress analysis should be developed and incorporated into the MEPDG framework.

1.2 Research Goal

The goal of this research was to develop a longitudinal cracking fatigue damage model for JPCP, which is compatible with and implementable in the existing MEPDG framework. This model must analyze the same range of pavement parameters as the MEPDG, and require minimal user information beyond that which is already provided when using the MEPDG. This will allow pavement engineers to account for longitudinal cracking in the design process.

1.3 Research Approach

A model developed to be compatible with the MEPDG must follow its existing framework. In the MEPDG, incremental damage is computed based on stresses for each load application seen by the pavement throughout its life. Stresses are computed within the MEPDG using neural networks trained with many finite element runs conducted using the finite element analysis program ISLAB2000 (Khazanovich et al. 2000a). By running a large finite element factorial in advance and using its results to train neural networks, computation of such a large number of stresses for each pavement analyzed in the MEPDG becomes possible on a time scale with which a user would be comfortable.

The use of neural networks eliminates the need to embed a finite element analysis within the program and allows for greater computational efficiency.

The neural networks used for rapid stress analysis in the MEPDG cannot be used when considering longitudinal cracking because the critical stress locations for longitudinal and transverse cracking are different. Therefore, to develop a longitudinal cracking fatigue damage model, new neural networks are needed, which means new stress analyses must be conducted.

Constructing a finite element factorial which will cover all of the cases needed to train a neural network to predict stresses for any pavement which could be inputted into the MEPDG results in a staggeringly large number of cases. The MEPDG used the equivalent structure concept (also known as similarity) to reduce the size of the factorial without introducing any error (Khazanovich et al. 2001). Similarity states that the stresses and deflections in an unknown system can be computed for those in a known system as long as the deflection basins of the two systems are proportional. Running the factorial and training neural networks in similar space reduces the size of the problem to a manageable level. The results of this stress analysis are converted back into real space and the stresses produced are used to calculate damage and, ultimately, distress levels.

To train the neural networks for the longitudinal cracking fatigue damage model, the range of pavements over which the factorial must be conducted must be defined. The principles of similarity can be used to transform the problem into similar space and reduce the size of this factorial. By using similarity, the stresses induced in a slab can be determined based on the stressed induced in a similar slab, rather than through computationally intensive analysis. By implementing similarity differently than was done in the MEPDG, certain difficulties encountered in the creation of the MEPDG can be avoided.

By employing the principles of similarity, a new longitudinal cracking model was developed. This model has the capability of being incorporated into the MEPDG without drastically impacting the computational efficiency of the program or changing the user experience. With the addition of a longitudinal cracking damage model, design engineers will be given a more accurate picture of the potential failure modes of pavements they design. This will be particularly useful when designing pavements with widened slabs, which are more prone to longitudinal cracking.

One of the main differences between transverse and longitudinal cracking is the independence of cracks. While the presence of a transverse crack in one slab does not affect the stress distribution in an adjacent slab, this is not the case for a longitudinal crack. The lack of independence prevents the relationship between damage levels and cracking levels from being used to predict longitudinal cracking. Therefore, it is necessary to modify the design procedure typically used in pavement design to consider fatigue damage directly instead of cracking levels.

Using similarity to define a reduced factorial also provides useful information about the stress states of many different pavement types under different axle and thermal load conditions. By comparing the stresses which cause longitudinal cracking to those which cause transverse cracking for many different pavement types and loads, it is possible to determine the characteristics common to pavement susceptible to longitudinal or transverse fatigue damage. Without using similarity, it would not have been possible to conduct such an analysis on this large of a scale because of the computational intensity of stress calculation.

1.4 Dissertation Organization

This dissertation is organized sequentially based on how the longitudinal cracking model was developed and used. From the perspective of a reader wishing to know all of the procedural details in order to recreate this type of model, this is the best format to use. For the casual reader however, certain chapters will be more helpful than others. of Chapter 3 provides more detailed information on why cracking cannot be predicted even

though fatigue damage is computed. Chapter 4 provides a detailed account of exactly how this research was conducted, and may not be as useful to the casual reader as Chapters 3, 5, and 6, which explain the significance and use of this research. A summary of each chapter is provided below to assist the reader in determining which chapters may be of interest to him or her.

Background information is provided in **Chapter 2**. This includes a literature review and a further exploration of both the problem which served as an impetus for this research and methods which will be used in its solution.

The difficulties of modeling longitudinal cracks are outlined in **Chapter 3**. While transverse cracks are independent of each other, longitudinal cracks are not. The influence of a longitudinal crack on adjacent slabs is investigated to explore how the lack of independence in longitudinal cracking affects the modeling process. Implications of this lack of independence on design philosophy are also detailed.

Chapter 4 discusses the development of the finite element factorial used for stress analysis. The inputs for the finite element model are discussed and the ranges of these variables needed to encompass all typical pavement designs are identified. The principals of similarity are employed to transform the problem into equivalent space and reduce the overall size of the factorial. Locations of stress analysis points and details of the analysis process are provided. The results of the reduced finite element analysis are used to develop neural networks in similar space. These neural networks can be used to determine stresses in a pavement without conducting a finite element analysis. This chapter discusses how the neural networks were created and validated. The methods to transform a pavement system from real space to similar space, compute stresses using the neural network, and then transform the problem back into real space are discussed.

Based on the stresses in the many reduced factorial determined in Chapters 4, an analysis was conducted to compare transverse and longitudinal cracking in all of the pavements in the reduced factorial. The results of this analysis are presented in **Chapter 5**. By using

similarity to consider almost all possible pavement types, it was possible to identify characteristics common to pavements which are susceptible to longitudinal cracking.

Chapter 6 shows how the incorporation of the longitudinal cracking fatigue damage model into the current MEPDG will affect pavement design. Case studies are provided to further illustrate now to interpret model results in the context of a pavement design problem.

Conclusions and design recommendations based on this research are given in **Chapter 7**. Future research needs identified based on this project are also described.

Chapter 2. Background and Literature Review

Longitudinal cracks form parallel to the direction of traffic in a Portland cement concrete (PCC) jointed plain concrete pavements (JPCPs), as shown in Figure 2.1. Historically, longitudinal cracking has not been considered in pavement design because transverse cracking is predicted by standard analysis of a typical pavement designs. However, recent changes in design practice have made longitudinal cracking a more likely distress and ignoring it in design may cause premature pavement failure.

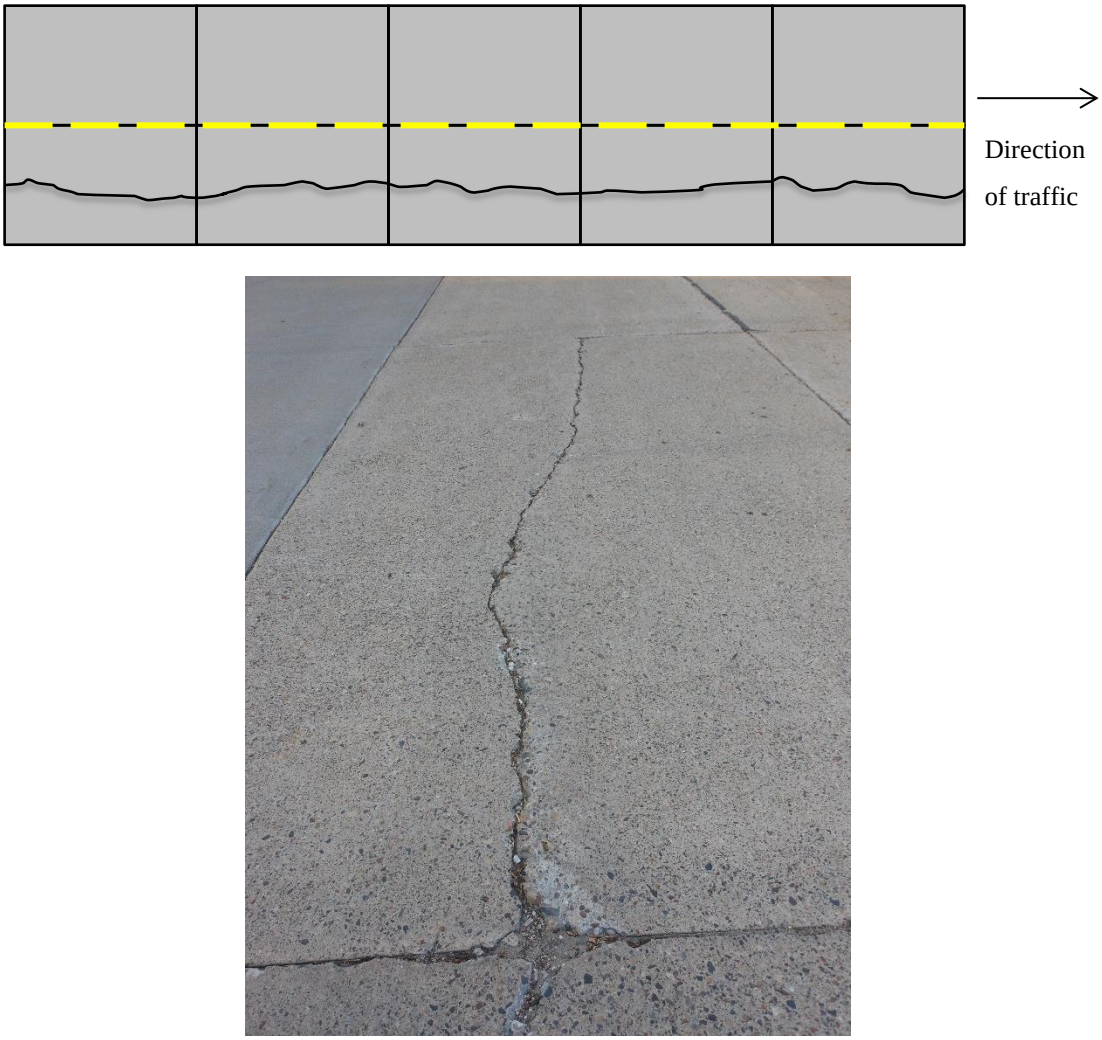

Figure 2.1: Schematic of a longitudinal crack (top) and photo of longitudinal cracking on a low volume road in Minnesota (bottom)(photo courtesy of Andrew Lederle)

Widened slabs are commonly used to mitigate transverse cracks, and as they have become more prominent, so have longitudinal cracks. Longitudinal cracking has been

observed in various Midwestern states, including Minnesota (Khazanovich et al. 2008) and Wisconsin (Owusu-Ababio & Schmitt 2013). Given the prominence of longitudinal cracking, the need for a way to account for it in design has been identified (Khazanovich & Darter 2012).

Longitudinal cracks can also be caused by site conditions and construction errors. Studies have found that pavements constructed over soils which are prone to heaving (Janda 1935) or swelling (Ardani et al. 2003) can experience longitudinal cracking as soil movement causes changes in support conditions, which, in turn, change how stresses are distributed in the slab. The same effects can also be observed when underlying layers are improperly compacted (Ardani et al. 2003) or undergo settlement (Voight 2002). Restraint from the base layer can cause longitudinal cracks, particularly when stabilized bases are used. One study (Corley-Lay & Morrison 2002) of 33 year-old pavements on cement stabilized bases in North Carolina found 80 and 82% of slabs had longitudinal cracks for the pavements with and without dowels, respectively. Other sections of the same pavement with a crushed aggregate base experienced 0-7% cracking. Construction errors resulting in longitudinal cracking can include miss-aligned dowels (Owusu-Ababio & Schmitt 2013), sawing joints too late (Voight 2002) and inadequate vibration from the paver during placement (Ardani et al. 2003; Owusu-Ababio & Schmitt 2013).

2.1 Long Term Pavement Performance Project SPS-2 Case Study

The Long Term Pavement Performance (LTPP) project consists of over 2500 monitored test pavements throughout the United States and Canada. Detailed information regarding the design and construction of these pavements is available, as are results of periodic testing and distress surveys. These test pavements are subdivided into categories for specific studies. The SPS-2 pavement sections were used in the Strategic Study of Structural Factors for Jointed Plain Concrete Pavements to investigate the role of various JPCP design features on long term performance, including the use of widened lanes. This study featured standard JPCPs sections constructed specifically for this test in 13 different states covering a wide range of climatic conditions (FHWA 2009).

A study of the initial performance of these sections was conducted while all sections were less than 10 years old (Jiang & Darter 2005). 78% of the 155 test sections examined were found to have no longitudinal cracking present. Twenty sections were found to have some longitudinal cracking, but the total crack length was less than fifty meters. Of the six test sections which had severe longitudinal cracking, five were at sites which had been constructed using poor practices; these sections were excluded from further analyses.

It was found that pavements located in so-called dry no-freeze zones (ex. California, Arizona) had the most longitudinal cracking, while those in wet no-freeze zones (Ex. North Carolina, Arkansas) had the least. Sections with a permeable asphalt treated base had less longitudinal cracking that those with a dense graded aggregate base, while pavements constructed on a lean concrete base had the most longitudinal cracking. Thinner slabs had more longitudinal cracks than thicker ones, and wider slabs had more longitudinal cracks than standard slabs. Thin, widened slabs were found to be the most susceptible to longitudinal cracking.

2.2 Widened Slabs

Widened lanes have become more prominent in the last 20 years as a means of mitigating transverse cracking. When a widened lane is used, the pavement slab itself is constructed wider, but the traffic lane is not widened and the lane line is located some distance from the slab edge, see Figure 2.2. This moves the wheel load away from the slab edge causing the average wheel path to be 42 inches from the longitudinal edge of the slab, rather than 18 inches.

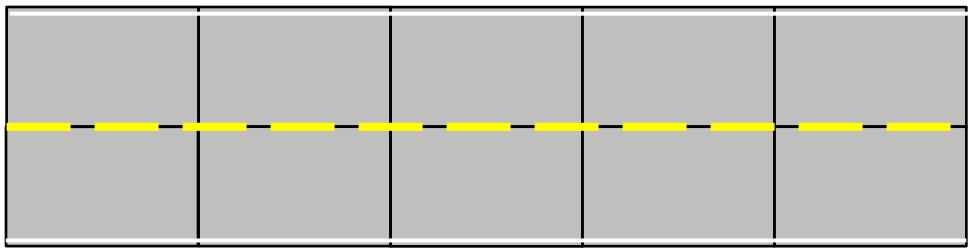

Standard width slab: Lane width is approximately equal to slab width

Widened slab: Lane width is less than to slab width

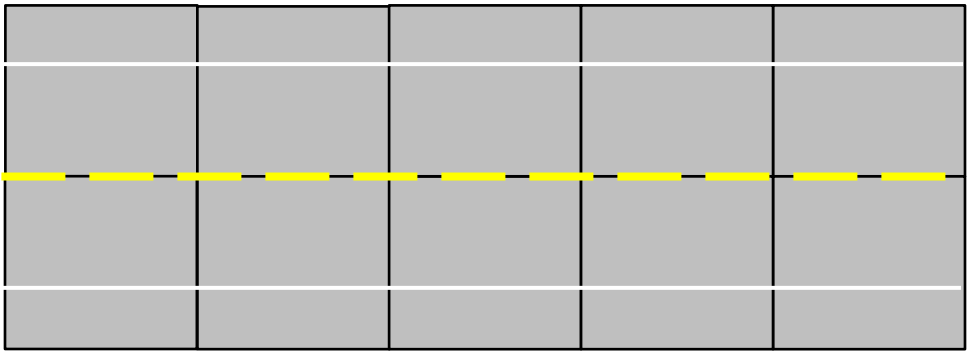

Figure 2.2: Widened slabs move the load away from the slab edge because the lane line does not correspond with the slab edge.

The benefit of using a widened slab can be seen by examining classical Westergaard (1926) theory, which provides closed form solutions for determining the stresses induced by a load placed at the interior, corner, and edge of the pavement. Of these loading cases, an edge load will produce the highest stresses while interior loading is associated with the lowest stresses. When widened lanes are used, the load is moved further from the slab edge, creating a condition more like interior loading, which produces lower stresses. Lower stresses, in turn, are associated with lower amounts of damage and distresses, such as cracking.

Placing wheel loads further from the slab edge reduces the stresses induced in the longitudinal edge of the slab and therefore the cracking potential. This is illustrated in Figure 2.3 which shows how the presence of a widened slab can drastically reduce the

percent of slabs predicted to have cracked over the life of a pavement as compared to other traditional support methods

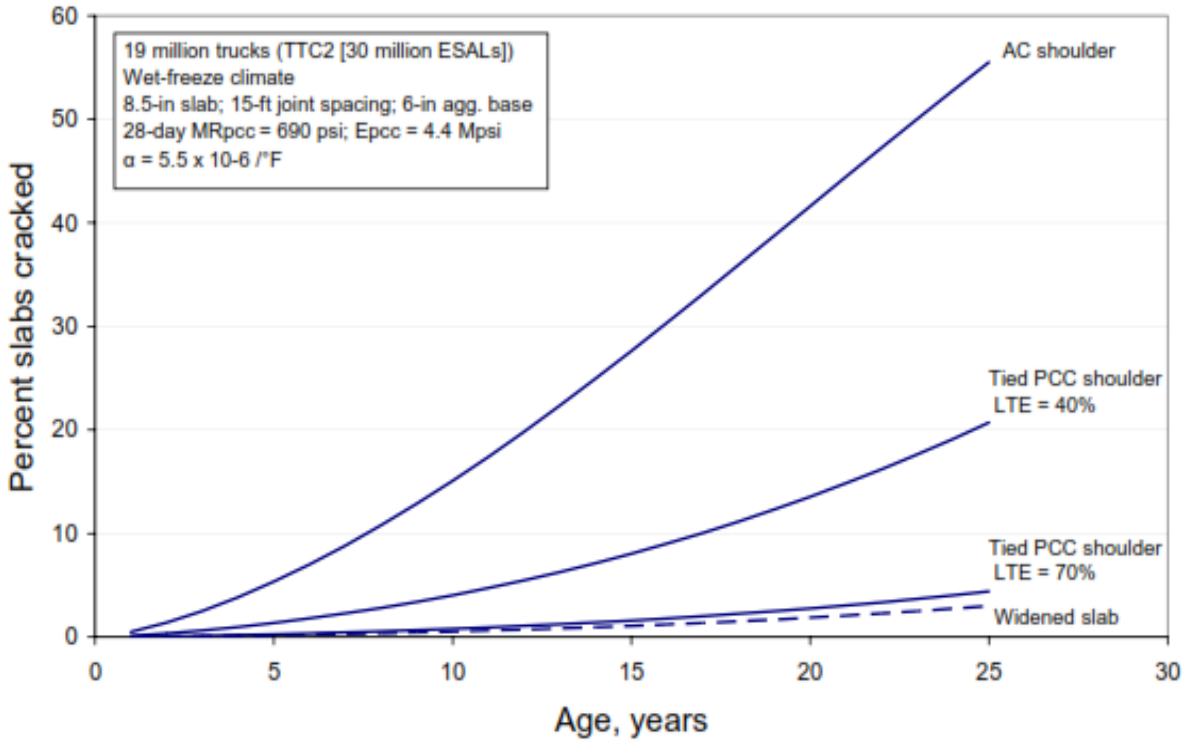

Figure 2.3: Effects of lateral support methods on transverse cracking (NCHRP 2003a)

2.3 Differential Volume Change

One element which can contribute to the formation of longitudinal cracks in properly constructed concrete pavements is changes in support condition due to differential volume changes. Differential volume change occurs when the top of the slab expands or contracts more or less than the bottom of the slab, and is caused by shrinkage and environmental factors. For example, if the top of the slab is warmer than the bottom (as commonly occurs during the day when the sun warms the surface of the slab), then the top of the slab will expand while the bottom does not. This results in a slab which is curled downwards, see Figure 2.4a. At night, when the temperature gradient is reversed, the slab curls upwards into a bowl shape, see Figure 2.4b. The same phenomenon also can be observed due to changes in moisture (relative humidity), shrinkage gradients, etc.

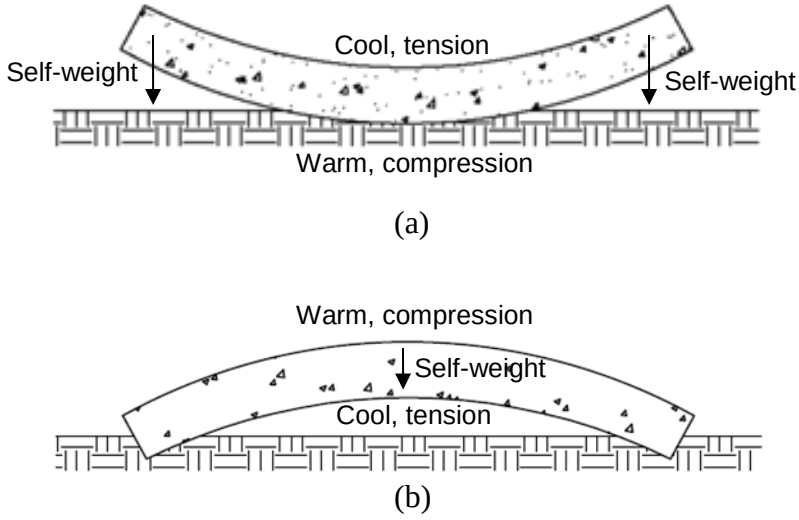

Figure 2.4: A slab curled due to a temperature gradient a) upwards and b) downwards, and associated stress state.

For the purposes of research and modeling, differential volume change is typically divided into five components: temperature curling, moisture warping, differential drying shrinkage, construction curl, and creep. Construction curl, differential drying shrinkage and creep together are collectively referred to as built-in curl. While in reality all of the components of differential volume change influence the others, they are treated as independent for the sake of modeling. Differential volume change is quantified by the equivalent temperature gradient required to deform an identical, but theoretically flat, slab to the same shape as the actual slab. By summing the equivalent temperature gradient from each of the components of differential volume change, the total equivalent temperature difference needed to characterize the shape of the slab can be determined.

2.3.1 Temperature Curling

Temperature curling is caused by an actual temperature difference between top and bottom surfaces of the slab. During the day, a positive temperature gradient (the slab is warmer on the top than on the bottom) causes the slab to curl downwards, while at night, a negative temperature gradient curls the slab upwards. It has been shown that temperature gradients in the field are nonlinear (Armaghani et al. 1987; Beckemeyer et al. 2002; Choubane & Tia 1995; Poblete et al. 1988; Teller & Sutherland 1935) and due

to this non-linearity, stresses will develop in the slab to maintain equilibrium even when that slab is unrestrained (Timoshenko & Goodier 1951). The nonlinear temperature gradient can be divided into three components (Bradbury 1938; Thomlinson 1940), as shown in Figure 2.5. These components are the axial or uniform component, the linear component and the non-linear or self-equilibrating component.

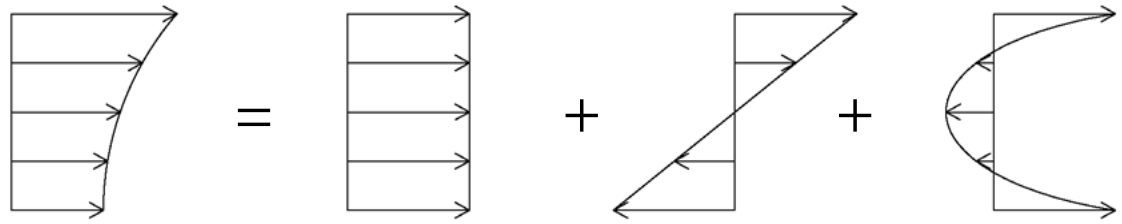

Figure 2.5: Total temperature gradient and constituent components.

The axial component of temperature gradient is due to the uniform portion of the temperature distribution and causes axial expansion and contraction. The assumption in plate theory that plane sections remain plane and perpendicular to the neutral axis during bending means that the axial volume change does not induce bending (Timoshenko & Goodier 1951); this has been found to be the case for most pavements (Pane et al. 1998). The axial component of the temperature gradient as a function of depth can be given as (Khazanovich 1994):

$$T_c(z) = T_0 + \frac{\int_h \alpha(z)E(z)[T(z) - T_0]dz}{\alpha(z)\int_h E(z)\,dz} \qquad (2.1)$$

Where:

$T_c(z)$ = constant strain component of the temperature distribution

T_0 = temperature at which the slab is flat

α = coefficient of thermal expansion

E = modulus of elasticity

z = depth of the slab, defined positive downwards starting at the neutral axis of the slab

h = thickness of the slab

Assuming that neither the modulus of elasticity or the coefficient of thermal expansion vary through the depth of the slab, this equation simplifies to, for the concrete layer in the unbonded case (NCHRP 2003b):

$$T_{c,PCC}(z) = \frac{1}{h_{PCC}} \int_{-\frac{h_{PCC}}{2}}^{\frac{h_{PCC}}{2}} T(z)dz \tag{2.2}$$

and for the bonded case:

$$T_c(z) = T_0 + \frac{\int_{-x}^{h_{PCC}-x} \alpha_{PCC}E_{PCC}(T(z)-T_0)dz + \int_{h_{PCC}-x}^{h_{PCC}+h_{base}-x} \alpha_{base}E_{base}(T(z)}{\alpha(z)(E_{PCC}h_{PCC} + E_{base}h_{base})} \tag{2.3}$$

Where:

h_{PCC} = thickness of the concrete layer

h_{base} = thickness of the base layer

E_{PCC} = modulus of elasticity of the concrete layer

E_{base} = modulus of elasticity of the base layer

α_{PCC} = coefficient of thermal expansion of the concrete

α_{base} = coefficient of thermal expansion of the base

$$x = \frac{E_{PCC}h_{PCC}\frac{h_{PCC}}{2} + E_{base}h_{base}\left(h_{PCC} + \frac{h_{base}}{2}\right)}{E_{PCC}h_{PCC} + E_{base}h_{base}} \tag{2.4}$$

Bending in the slab is due to the linear portion of the temperature gradient, which causes the warm surface of the slab to expand and/or the cool surface of the slab to contract. The linear component of the temperature gradient is given as (Khazanovich 1994):

$$T_L(z) = T_0 + \frac{z}{\alpha(z)} \frac{\int_h \alpha(z)E(z)[T(z) - T_0]zdz}{\alpha(z)\int_h E(z)z^2\,dz} \tag{2.5}$$

Where:

$T_L(z)$ = linear component of the temperature distribution

Assuming that neither the modulus of elasticity or the coefficient of thermal expansion vary through the depth of the slab, this equation simplifies, for the concrete layer in the unbonded case, to (NCHRP 2003b):

$$T_L(z) = T_0 + 12 * \frac{\xi}{\alpha_{base}} \left[\frac{\int_{-\frac{h_{PCC}}{2}}^{\frac{h_{PCC}}{2}} \alpha_{PCC}E_{PCC}(T(z) - T_0)zdz}{E_{PCC}h_{PCC}^3 + E_{base}h_{base}^3} + \frac{\int_{-\frac{h_{base}}{2}}^{\frac{h_{base}}{2}} \alpha_{base}E_{base}\left(T\left(\frac{h_{PCC} + h_{base}}{2} + \xi\right) - T_0\right)\xi d\xi}{E_{PCC}h_{PCC}^3 + E_{base}h_{base}^3} \right] \tag{2.6}$$

Where:

$$\xi = z - \frac{h_{PCC}+h_{base}}{2}$$

Because this component is responsible for all bending deformations, if an equivalent linear temperature gradient is defined for the system, it must induce the same bending deformation and the linear component of the total temperature gradient.

The non-linear, or self-equilibrating, component of temperature gradient is the difference between the effects of the actual gradient and the sum of the effects of the uniform and linear gradients components. The total temperature gradient is given as (Khazanovich 1994):

$$T(z) - T_0 = [T_c(z) - T_0] + [T_L(z) - T_0] + [T_{NL}(z) - T_0] \quad (2.7)$$

Where:

T_{NL} = the nonlinear portion of the temperature gradient

Solving for the nonlinear component of the temperature gradient (Khazanovich 1994):

$$T_{NL}(z) = T(z) - T_c(z) - T_L(z) + 2T_0 \quad (2.8)$$

The nonlinear component of the temperature gradient serves to balance out the thermal stress profile in the slab and ensure that there is no total force acting on the slab (i.e. to ensure equilibrium). Thus, additional stresses, but no deformations are induced (Choubane & Tia 1995; Ioannides & Khazanovich 1998a; b). Typically, temperature gradients in slabs are modeled as quadratic (Choubane & Tia 1992; 1995; Richardson & Armaghani 1987); using a linear temperature distribution is unconservative (Choubane & Tia 1995; Mohamed & Hansen 1997; Rao et al. 2001; Reddy et al. 1963; Siddique et al. 2006). In the MPEDG, temperature gradients are computed by the enhanced integrated climatic model, EICM, (Larson & Dempsey 1997).

2.3.2 Moisture Warping

Moisture warping is caused by variation in the moisture gradient through the slab coupled with the fact that a portion of drying shrinkage is reversible. Moisture gradients are nonlinear within the top few inches of the surface and fairly uniform through the rest of the slab (Janssen 1987). As the ambient relative humidity changes, the top surface of the slab either shrinks or experiences a reversal of previous shrinkage. The amount of shrinkage which is reversible is dependent on the properties of the concrete mix, the curing regime and the degree and duration of wetting (Helmuth & Turk 1967; L'Hermite 1947; L'Hermite et al. 1949; Lederle & Hiller 2013; Shacklock & Keene 1957). For a typical paving mix, it has been found that approximately 30% of the total shrinkage is reversible (Lederle & Hiller 2013). The amount of moisture warping a pavement will

experience depends on the location of the pavement and the climate to which it is exposed (Hiller et al. 2011; Lederle & Hiller 2013). It has been found that moisture effects are of a similar magnitude as temperature effects (Hveem & Bailey 1957), and that neglecting moisture warping in pavement design is unconservative (Rao et al. 2001). In the MEPDG, moisture warping is considered on a monthly basis (NCHRP 2004); in the field, moisture warping has been found to vary seasonally (Granger et al. 1994).

2.3.3 Differential Drying Shrinkage

Similar to moisture warping, differential drying shrinkage is also caused by changes in moisture through the depth of the slab. While moisture warping is caused by reversible shrinkage, differential drying shrinkage is caused by irreversible, or permanent, drying shrinkage. A portion of drying shrinkage is permanent due to the nature of the calcium silicate hydrate (C-S-H) bonds which form as the cement hydrates. Neville (1997) hypothesized that C-S-H gels form in fairly close proximity as the concrete shrinks during drying. When the concrete swells during re-wetting, it cannot grow back to its original size because it is restrained by the C-S-H bonds. Given that moisture movement only occurs in the top few inches of the slab (Janssen 1987), drying shrinkage is larger in the top few inches of the slab compared to the bottom of the slab (Wells et al. 2006), which causes an upwardly warped shape. Differential drying shrinkage does not vary with time after the concrete is fully cured, and is considered as part of the built-in curl input in the MEPDG. A model does exist to predict differential drying shrinkage (Lederle & Hiller 2012), but it is not currently used by the MEPDG.

2.3.4 Construction Curl

Construction curl occurs when the slab is cast in the presence of a temperature gradient (Eisenmann & Leykauf 1990). While a temperature gradient would normally cause the slab to deform, the plastic concrete cannot change its shape. Therefore, the slab sets as a flat slab and deforms anytime the temperature gradient does not match the gradient which was present at the time of casting (Yu & Khazanovich 2001). Typically, slabs are cast in the morning in the spring or summer, resulting in a slab which sets with a temp gradient that is warm on the top and cooler on the bottom, a positive gradient. Once the actual

temperature gradient is smaller than the gradient at the time of set, the slab responds as though the positive gradient has been removed (i.e. as though a negative gradient was applied). This so called negative construction curl is experienced by most slabs (Armaghani et al. 1987; Guo 2001; Poblete et al. 1988; Rao & Roesler 2005), and therefore a large positive gradient is necessary to overcome this construction curl and induce a downward curl (Poblete et al. 1988). Due to this, slabs are typically curled upwards at all times, though the amount of curl present varies with ambient temperature and moisture conditions. Construction curl is considered in the built-in curl input of the MEPDG.

2.3.5 Creep

Creep is deformation due to sustained loading, in this case the self-weight of the slab. All deformations induced by the other components of differential volume change are countered by creep. Creep has been found to counteract shrinkage (Altoubat & Lange 2001), curl (Rao et al. 2001; Sondag & Snyder 2003; Teller & Sutherland 1935), and warp (Bissonnette et al. 2007; Teller & Sutherland 1935). Though many creep models exist (ex. Bazant & Baweja 1995; Gardner & Lockman 2001), they often require more inputs for material characterization than are considered by the MEPDG. Thus, creep is not independently computed by the MEPDG, instead creep is considered in the built-in curl input.

2.3.6 Effects of Differential Volume Change

Slabs with built-in curl experience longitudinal cracking because they have different support conditions than flat slabs. Most pavements are found to have some type of negative built-in curl (i.e. an upwardly curled bowl shape) (Armaghani et al. 1987; Guo 2001; Poblete et al. 1988; Rao & Roesler 2005), with typical values on the order of -10°F, but reaching as high as -44°F (Hiller 2007). With these high levels of built-in curl, it is possible for slabs to have the corners lift off of the underlying layers for several feet (Hveem 1951; Rao & Roesler 2005), though built-in curling of this extreme magnitude is not common. However, it is common for most slabs to be at least partially unsupported (Harr & Leonards 1959; Poblete et al. 1991). Figure 2.6 shows an example of the area of

a pavement which is unsupported for various negative temperature gradients, as determined through finite element analysis (Hiller 2007). Note that the actual area is for this specific pavement only and various parameters, such as self-weight, will influence how the slab deforms and how much of it is unsupported.

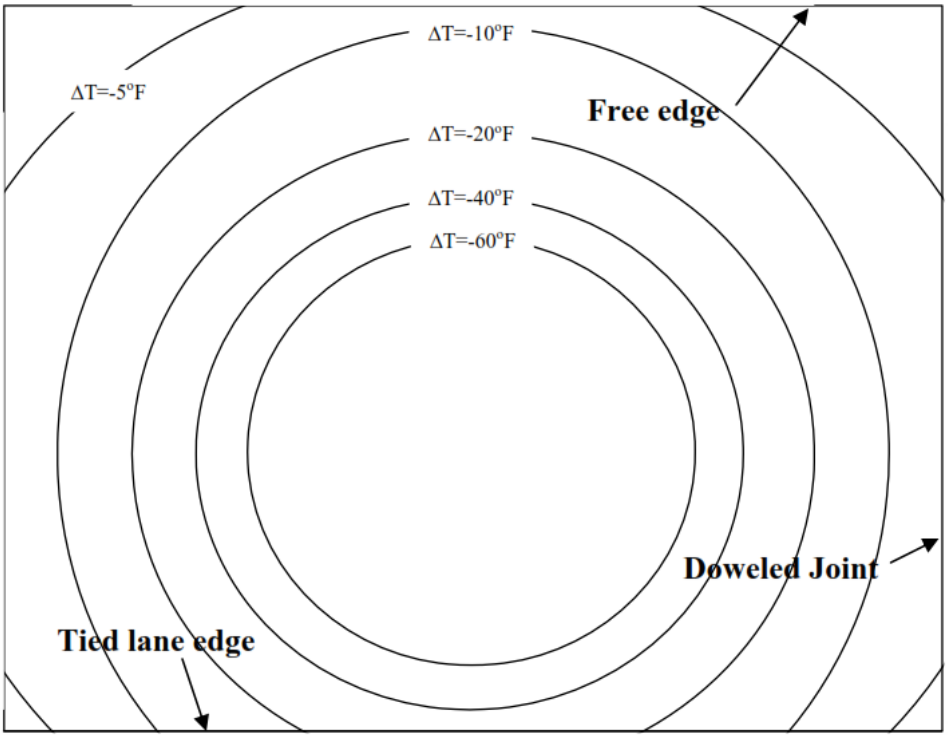

Figure 2.6: Area of support under a slab subjected to a negative temperature gradient (from Hiller 2007)

From this figure, it can be seen that as the magnitude of the temperature gradient becomes larger, less and less of the slab is supported. While the extreme case shown of a -60°F temperature gradient is uncommon, this figure shows that a significant portion of the slab is unsupported when the total equivalent temperature gradient is only -5 or -10°F, which is a commonly seen value (NCHRP 2003a). When any portion of the pavement becomes unsupported, the stiffness of the entire pavement system is degraded (Armaghani et al. 1987). The changes in support conditions associated with differential volume changes can lead to longitudinal cracking.

2.4 The Mechanistic-Empirical Pavement Design Guide

Until recently, concrete pavements were typically designed using the AASHTO-93 design method (AASHTO 1993). This method is completely empirical and is based solely on data from the AASHTO road test, which was conducted in only one location. Because pavement performance is highly dependent on location specific parameters, such as climate and soil type, the very limited scope of the AASHTO road test is seen as one of its major limitations. The AASHTO-93 method does not predict individual distresses, but instead gives a composite decrease in ride quality index. This does not give the designer information on how the pavement fails.

The Mechanistic-Empirical Pavement Design Guide (MEPDG) is a paradigm shift from the completely empirical methods used previously to an approach based in mechanics. The MEPDG calculates stresses in the pavement based on predicted traffic and environmental loads. These stresses are then empirically correlated to damage based on a national database of observed pavement distresses. The designer can compare the predicted distresses to acceptable levels and determine if the design is acceptable or if some aspect of the design must be changed. Thus the MEPDG is an analysis tool, and the design process becomes much more analogous to design in structural engineering.

There are two main schools of thought on how pavements are damaged by loading. The first is that any application of load causes some fatigue damage and it is the accumulation of all the damage which leads to failure. Therefore the damage caused by each and every load application must be accounted for in design. The second school of thought is that pavements fail from an application of a single load under critical conditions (Ioannides et al. 1998). However, determining which combinations of vehicle and environmental loads constitute critical loads is not a trivial task.

The MEPDG uses an incremental damage approach to determine the fatigue damage caused by different load combinations. This approach involves determining the pavement structure properties as they vary with time, as well as the vehicle and thermal loads to which the pavement will be exposed. For each load combination and pavement

structure, stresses are computed. From these stresses, fatigue damage can be computed and this cumulative damage is correlated with distress levels. Details of this procedure are given below.

2.4.1 Traffic Loading

Traffic loads are characterized by volume, axle type, axle load level and traffic path/wander, and may vary with age based on the assumed traffic growth as specified by the user. Lateral traffic wanted is assumed to be normally distributed using the mean wheel path and a standard deviation, which are user inputs in the MEPDG. Stresses in the slab do not drop off immediately when the wheel goes partially off the pavement. Instead, a load x inches outside from the edge of the pavement is assumed to have the same effect as a load x inches inside from the edge of the pavement. This is accounted for by changing the probability of a load being located x inches from the pavement edge, as shown in Figure 2.7.

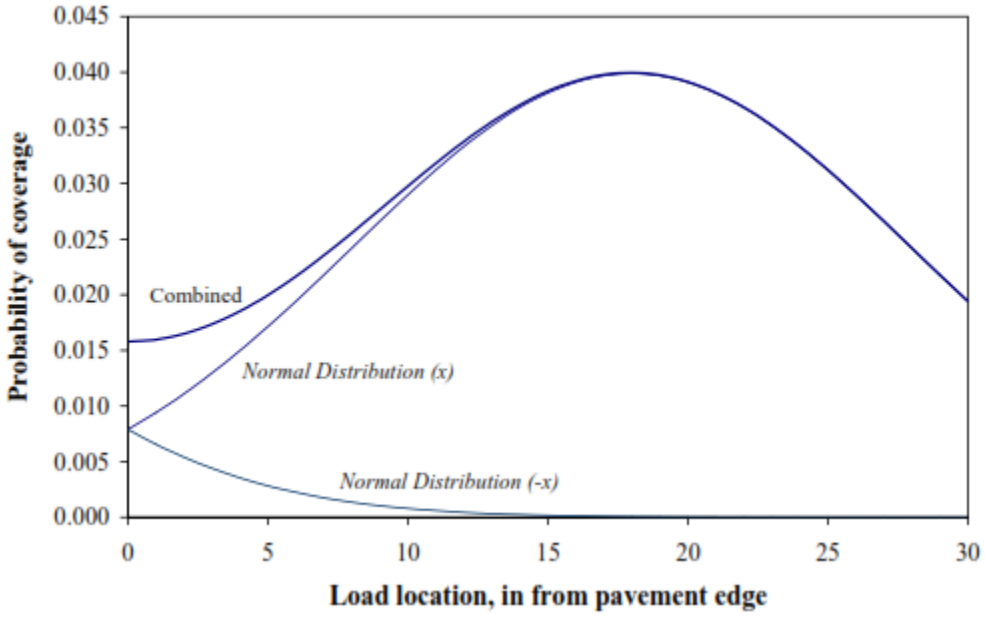

Figure 2.7: Probability of a load being x inches from the pavement edge inside the slab and –x inches from the pavement edge outside of the slab when an axle is partially off the pavement (from NCHRP 2003a)

Traffic inputs are used differently to predict bottom-up and top-down cracking. For bottom-up cracking, traffic inputs processed to determine a number of equivalent single, tandem, or tridem axles for each load level. One actual single axle is equal to one effective single axle of the same load placed at mid-span, see Figure 2.8a (note that this is different than the AASHTO-93 equivalent single axle load concept). One actual tandem axle load is equal to two effective tandem axle loads of the same load level placed alternately so that the front and then the rear axle is at mid-span., see Figure 2.8b.

To compute n for top-down cracking, the total number of trucks is multiplied by the percent of trucks with short, medium, and long wheel bases. This information is used instead of effective axle loads. For both top-down and bottom-up cracking, the number of monthly loads (either by effective axle or load base) is multiplied by the hourly truck distribution factor to compute hourly traffic loading. This information is then combined with hourly temperature data to determine the number of loads of a certain load level and axle type which occur in conjunction with specific temperature gradients. This number of loads is what is compared to allowable loads, which are computed from stress determined for specific load and temperature combinations.

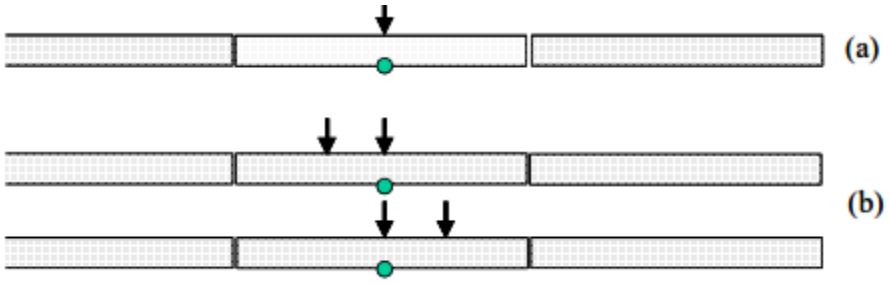

Figure 2.8: Procedure to account for different axle types when computing the number of applied loads for bottom-up cracking fatigue damage computations for a) single axle loads, and b) tandem axle loads. (from NCHRP 2003a)

2.4.2 Thermal Loads

Temperature loads are affected by month of pavement life and total equivalent temperature difference. Temperature gradients in the pavement are computed for every hour of an average twenty four hour period in each month. Thus, there will be one

temperature for the hour from 2 to 3 AM in February and one for the same time period in March. The day is irrelevant.

The month of pavement life affects environmental loads due to relative humidity. In the MEPDG, moisture effects are accounted for monthly by computing an equivalent temperature gradient due to moisture warping.

Hourly nonlinear temperature gradients are computed in the EICM as a temperature profile at 11 equally spaced points through the thickness of the concrete layer and constant through the base layer. As was discussed in Section 2.3.1, temperature gradients can be divided into three components, of which the linear and nonlinear components must be considered in stress computations. Both of these components must also be considered in determining the number of applied loads because different combinations of linear and nonlinear temperature gradients can be considered as different thermal load cases and the number of applied loads is computed for each load case. The simplifying process by which the MEPDG accounts for linear and nonlinear temperature gradients when computing n is called linearization.

2.4.3 Linearization

As previously discussed, the number of applied loads is a function of pavement age, month, axle type and load level, traffic wander and equivalent linear temperature distribution. Essentially, it is necessary to compute the total number of loads of each axle type and weight occurring at a specific location (wander) at a specific equivalent temperature in each month. To accomplish this, frequency distributions are used. For example, a frequency distribution is created during the traffic analysis of the MEPDG to compute the frequency distribution of each type of axle load and axle type. This is used in conjunction with the hourly frequency distribution to determine how many loads of each type are seen in each hour of the day. To determine the number of loads of each type which occur in conjunction with a specific temperature gradient, temperature frequency distributions must be created.

This entire process can be computationally intensive in terms of the amount of data which must be generated and stored. At the time the MEPDG was created, available computer time was a major limitation which had to be considered when creating programs which made many computations. The linearization process was created to reduce the RAM demands of the MEPDG when computing the number of applied loads in cumulative damage computations.

Linearization eliminates the need to compute the number of loads as a function of both linear and nonlinear temperature gradients by equating stresses due to nonlinear gradients with those due to linear gradients, which removes one dimension of the problem and reduces computational time. The first step in this process is to compute and tabulate the stresses in the pavement at critical locations for linear temperature gradients, ΔT_{LZ} in 2°F increments. For bottom-up damage accumulation, a 18 kip single axle load is placed at the mid-slab edge where it will produce the maximum stress according to conventional pavement theory, shown in Figure 2.9.

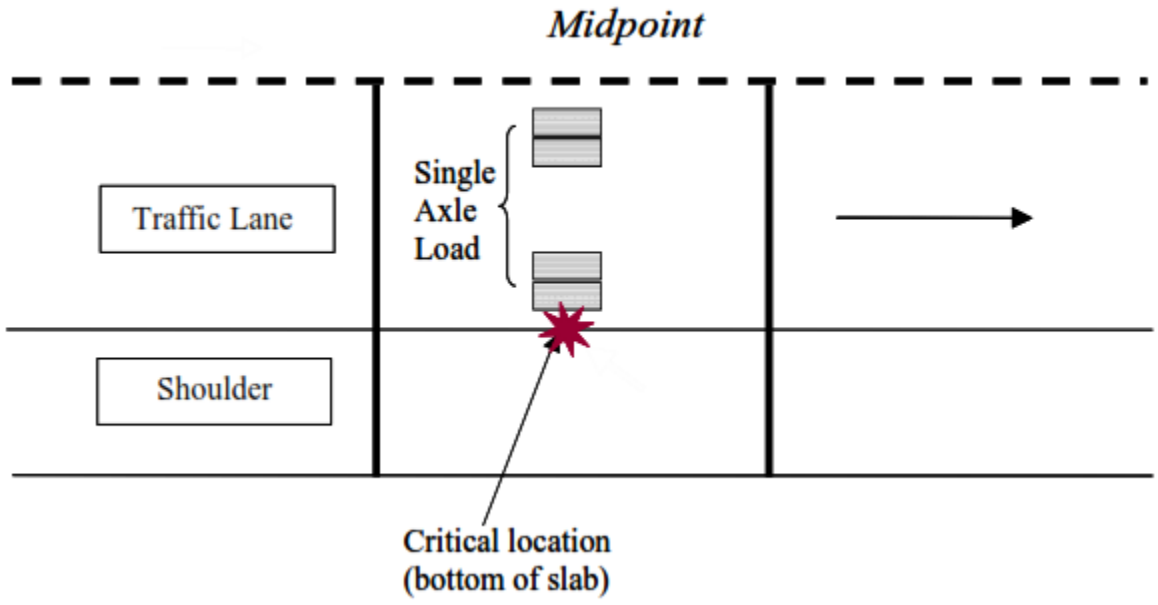

Figure 2.9: Critical load and stress locations for bottom-up cracking (from NCHRP 2003a)

For top-down damage accumulation, a 12 kip single axle load and a 34 kip tandem axle load with a medium wheel base is placed at the critical loading location, as shown in Figure 2.10.

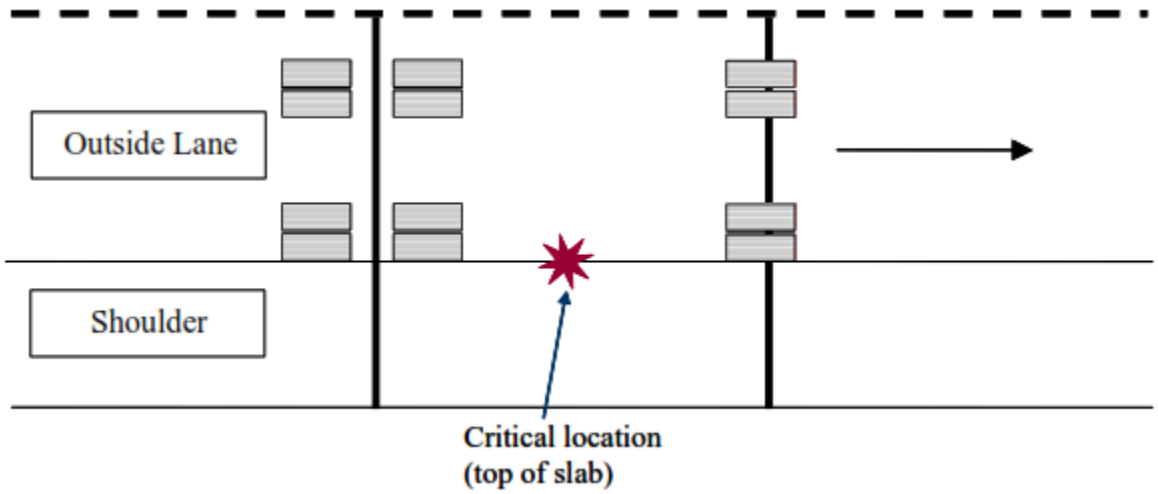

Figure 2.10: Critical load and stress locations for top-down cracking (from NCHRP 2003a)

A second table is made for stresses computed using the same axle loads, but using different thermal loads. In this case, the total thermal load applied to the system is a sum of the actual temperature load (consisting of both the linear and nonlinear portions of the temperature gradient) and the permanent curl/warp user input (-10°F default value). Call this temperature gradient ΔT^*.

For each stress computed using ΔT^* (the second table), the same stress due only to traffic and ΔT_{LZ} is located in the first table. The linear temperature gradient corresponding to this stress is then determined. This linear temperature gradient ΔT_{LZ}, when applied with traffic loads, will produce the same stress as the traffic loads applied with a temperature gradient equal to ΔT^*, which incorporates nonlinear effects. It should be noted that the deflection profiles for these slabs will be different even though the maximum stresses in the system are the same.

The temperature frequency distribution for each month and hour based on ΔT_{LZ}, rather than ΔT^*. A different temperature frequency distribution is created for each load and offset condition. However, this process drastically reduces the number of stress computation which must be made because only one calculation is conducted for each bin in the temperature frequency distribution. This temperature frequency distribution is used in conjunction with the traffic frequency distributions to compute n for each load case.

Though linearization reduces computational time needed by the MEPDG, it does have some drawbacks. The main disadvantage to this process is that it assumes that the component of stress due to the interaction between nonlinear temperature and traffic is constant for all traffic loads. While the validity of this claim has not been fully investigated, it is obviously a simplifying assumption.

2.4.4 Stress Analysis in The MEPDG

Neural networks are used in the MEPDG to avoid running an embedded finite element model as part of the stress analysis procedure. The MEPDG design process for rigid pavements requires stress analysis to be conducted for different load cases, including different vehicle loads at different locations a pavement subjected to different temperature and moisture gradients. There is also a need to account for changes in the pavement structure over time. For example, seasonally adjusted values for subgrade moduli are considered on a monthly basis throughout pavement life; similarly, load transfer efficiency degrades as the pavement ages while concrete strength and modulus of elasticity increase. Accounting for these factors means that hundreds of thousands of finite element models must be considered in the analysis of even a single pavement (NCHRP 2004). Conducting a finite element analysis for each of these cases within an MEPDG analysis is so computationally intensive as to be prohibitive.

To make stress calculations more efficient in the MEPDG, neural networks are used to calculate stresses in the pavement at the desired locations. Neural networks are a commonly used tool for solving large and repetitive problems in a computationally

efficient manner. They have been used in the design and analysis of standard concrete pavements (Banan & Hjelmstad 1996; Khazanovich et al. 2001; Meier & Rix 1994) and airfield pavements (Ceylan et al. 1999; 2000; Ceylan et al. 1998; Haussmann et al. 1997).The neural network is trained using many cases with known solutions. For example, pavements with different geometries, loading, thermal gradients, support conditions, etc. can be analyzed using finite element analysis and the stresses at various points obtained. Both the problem and the solution are used to train the neural network. Then, the neural network is presented with a new problem for which the solution is not already known, in this example, a pavement with a different combination of factors than was used in training. Based on the answers of all the known problems with which it was trained, the neural network can predict the solution, in this case the stresses at certain points on the slab.

By running a large finite element factorial in advance and using its results to train neural networks, computation of such a large number of stresses for each pavement analyzed in the MEPDG becomes possible. Constructing a finite element factorial which will cover all of the cases needed to train a neural network results in a staggeringly large number of cases. The MEPDG used the principles of similarity (see Section 2.6) to reduce the size of the factorial without introducing any error. Similarity states that the stresses and deflections in an unknown system can be computed for those in a known system as long as the deflection basins of the two systems are proportional. Running a factorial and training neural networks in similar space reduces the size of the problem to a manageable level. The results of this stress analysis are converted back into real space and the stresses produced are used to calculate damage and, ultimately, distress levels. While conducting the stress analysis in advance and creating neural networks has many obvious advantages, the main disadvantage to this approach is that the range of applicability of the neural networks cannot be expanded without completely retraining them.

The MEPDG uses neural networks was built using a modified Monte Carlo Hierarchical Adaptive Random Partitioning (MC-HARP) neural network architecture (Banan & Hjelmstad 1994; 1995; Khazanovich & Roesler 1997).

2.4.5 Incremental Damage Accumulation

The MEPDG uses the incremental damage approach combined with Miner's cumulative damage hypothesis (Miner 1945). It defines the total fatigue damage in the pavement by equation (2.9).

$$Fatigue\ Damage = \sum_i \sum_j \sum_m \sum_p \sum_q \sum_r \frac{n_{ijklmn}}{N_{ijklmn}} \quad (2.9)$$

Where:

n_{ijklmn} = number of applied loads at condition i, j, m,…

N_{ijklmn} = number of allowable load applications at condition i,j,m,…

i = pavement age

j = month

k = axle type

l = load level

m = equivalent temperature difference (to account for curling, warping, and built-in curl)

n = traffic path/wander

The number of allowable load applications, N, is given as (NCHRP 2003b):

$$Log(N_{ijklmn}) = 2\left(\frac{MOR}{\sigma_{ijklmn}}\right)^{1.22} \quad (2.10)$$

Where:

MOR = the modulus of rupture of the concrete

σ_{ijklmn} = stress due to load condition i, j,m,…

The percent of slabs cracked is computed based on the fatigue damage calculated using equation (2.9) as (NCHRP 2003a):

$$CRK = \frac{1}{1 + FD^{-1.68}} \quad (2.11)$$

Where:

CRK = fraction of slabs predicted to be cracked

FD = fatigue damage as computed by equation (2.9)

This equation was derived empirically by plotting the computed fatigue damage 516 real pavements against the actual percentage of crack slabs observed in the field. A sigmoidal curve was best fit to the data to determine the constants in the equation.

In the current MEPDG JPCP cracking model, two types of cracking are considered: bottom-up and top-down. It is assumed that each slab has only one failure mechanism (i.e. that slabs cannot fail in different types of cracking at the same time). For each of these types of cracking, fatigue damage and percent of slabs cracked are computed separately using equations (2.9) and (2.11), respectively. The total amount of cracking is then computed, assuming that an individual slab can only crack either from the top-up or the bottom-down, but not both (NCHRP 2003a):

$$TCRACK = (CRK_B + CRK_T - CRK_B * CRK_T) * 100\% \quad (2.12)$$

Where:

TCRACK = total cracking as a percent

CRK_B = predicted amount of bottom-up cracking, as a fraction

CRK_T = predicted amount of top-down cracking, as a fraction

Currently the MEPDG computes only transverse cracking, and does not consider longitudinal cracking.

2.5 Previous Investigations of Longitudinal Cracking

There has been relatively little research in the area of longitudinal cracking from a mechanistic-empirical design perspective. The potential for longitudinal cracking to occur in pavements with certain characteristics was investigated by Hiller (Hiller 2007; Hiller & Roesler 2002). Hiller also developed a mechanistic-empirical longitudinal cracking model based on influence line analysis (Hiller 2007; Hiller & Roesler 2005), though it has many limitations.

2.5.1 Relative Reference Stress

The concept of relative reference stress has been used to determine when longitudinal cracking is more likely to be the mode of failure than transverse cracking (Hiller & Roesler 2002). The relative reference stress is the ratio of the tensile stress at a specified location (the location of interest) induced by a load placed at a specified location (the load of interest) and the maximum tensile stress at the mid-slab edge induced by a load placed at the mid-slab edge. If the relative reference stress is greater than one, then the typically considered stress at the mid-span edge induced by a load at the mid-span edge is not the critical stress case. In other words, transverse cracking is not the most likely failure mechanism. It should be noted that the relative reference stress does not indicate if the pavement will crack or not because the strength of the concrete is not considered. Instead, it can be used to identify situations in which longitudinal cracking must be considered in design.

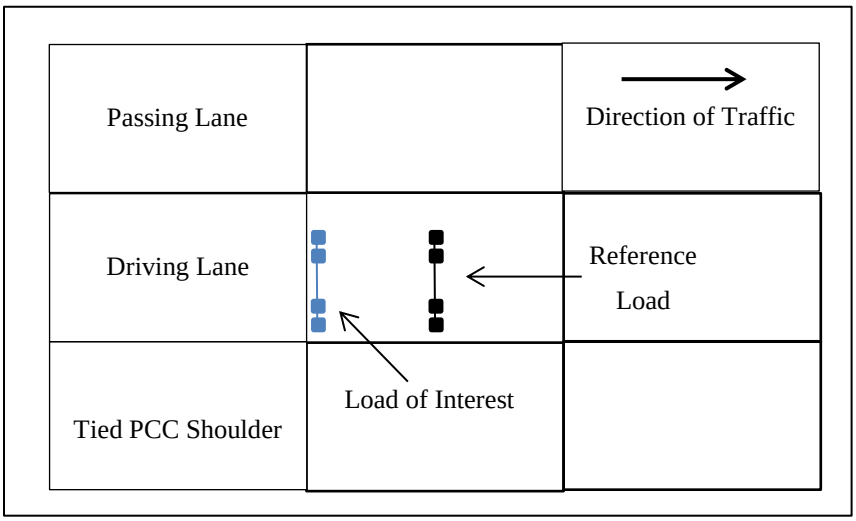

Figure 2.11: Location of loads in relative reference stress parametric study, (adapted from Hiller & Roesler 2002)

The parametric study (Hiller & Roesler 2002) considered 2160 cases and investigated the impact of load position, slab geometry, modulus of subgrade reaction, thermal gradients, and the presence of a shoulder, among other things. The load positions used for the investigation are shown in Figure 2.11. It was found that widened slabs resulted in a relative reference stress greater than one, for both the top and the bottom of the slab.

This indicates that both top-down and bottom-up longitudinal cracking must be considered in design. Regular width slabs were also found to have a relative reference stress greater than one in some instances, which shows that longitudinal cracking can occur in pavements without widened slabs, though other factors must be present for this to occur, such as a tied PCC shoulder. Longer joint spacing was found to increase the potential for top-down longitudinal cracking. Thickness was not found to have much of an effect on the relative reference stress because it would decrease the value of stress at both the location of interest and the mid-slab edge. However, thinner pavements have nonetheless been found to be more susceptible to longitudinal cracking (Owusu-Ababio & Schmitt 2013).

While this study was able to identify some characteristics which could make a pavement more susceptible to longitudinal cracking, it was also very limited in scope. These limitations are due to the fact that each pavement case had to be analyzed individually. For each case considered, a separate finite element model had to be constructed and run, which was much more computationally expensive at the time the study was conducted than it is now. Additionally, in order to investigate the effect of many parameters, relatively few cases of each parameter could be examined. While this allows general trends to be determined, it does not allow specific criteria to be identified.

2.5.2 RadiCAL Longitudinal Cracking Program

After conducting the relative reference stress study discussed in Section 2.5, Hiller (2007) developed a longitudinal cracking model which mechanistically computes stresses and failure modes in JPCPs. The results of 1.3 million ISALB2000 runs encompassing many different slab configurations, and load types and patterns were used to train a neural network to create a database of different stress cases for different load configurations. This database is used by RadiCAL to find maximum and residual stresses, which are converted into damage through transfer functions.

One of the main limitations of Hiller's model is that it has fixed inputs, and therefore can only predict longitudinal cracking for slabs with given geometry, materials properties,

etc. Table 2.1 shows the fixed values and ranges of inputs which can be used in RadiCAL. From this table, it can be seen that some parameters cannot be changed, and others only have a small range of variables. For example, only slabs with a thickness of 8, 10, or 12 inches can be analyzed, while the modulus of elasticity of the concrete is fixed at a single value. Additionally, Hiller's model was developed using California specific traffic and climates. These limitations are due to the computing capabilities which existed at the time the model was developed, making it necessary to limit the number of cases considered. One way to avoid such limitations is to use the principles of similarity (which will be discussed in Section 2.6), as was done in the MEPDG to transform the problem into similar space and reduced the size of the factorial which must be considered.

Table 2.1: Inputs for the RadiCAL program, fixed or ranges (modified from Hiller 2007)

Geometry		**Traffic**	
Joint spacing	12 or 15 ft	Two way AADTT	variable
Slab width	12 or 14 ft	Trucks in design direction	variable
Slab thickness	8, 10, or 12 in	Trucks in design lane	variable
PCC Mateirals/ Support		Design life	variable
flexural strength	variable		
Elastic Modulus	$4*10^6$ psi	**CA Average Vehicle Class Distribution**	
Coefficient of thermal expansion	$5.5*10^{-6}$ / °F	Class 4	1.14%
Poisson's ratio	0.15	Class 5	20.03%
Modulus of Subgrade Reaction	250 psi/in	Class 6	5.18%
Built-in curl	0 to -40 °F	Class 7	0.28%
Load Transfer Efficiency		Class 8	6.66%
Transverse joints	20-90%	Class 9	50.63%
Longitudinal joints	50%	Class 10	0.63%
Lateral Wheel Wander Distribution		Class 11	8.78%
Mean	variable	Class 12	1.06%
Standard Deviation	variable	Class 13	0.10%
		Class 14	2.52%

2.6 Similarity Principle

To increase the number of cases which can be analyzed without increasing computing time, concept of similarity, also called equivalency, can be used. Similarity is already used in the MEPDG transverse cracking model for both CRCP (Khazanovich et al. 2001) and JPCP pavements (NCHRP 2003b). These models used three different equivalencies combined to create an equivalent structure, and in doing so, decreased the number of required variables. For example, by implementing the principles of similarity, the number of variables required to analyzed all pavements considered in the continuously reinforced concrete pavement transverse cracking model was decreased from 17 to 7 (Khazanovich et al. 2001).

2.6.1 Similarity Principle

The concept of similarity can be summarized as using the solution of a known system to obtain the solution of an unknown, but similar system. For concrete pavements, systems are similar if their deflection basins are proportional. This can be demonstrated by examining the equilibrium equation for a Kirchhoff plate on a Winkler foundation (Timoshenko & Woinowsky-Krieger 1959):

$$D\nabla^4 w(x,y) + k(x,y) * w(x,y) = q(x,y) \tag{2.13}$$

where:

$$\nabla^4 = \frac{\partial^4 w(x,y)}{\partial x^4} + 2\frac{\partial^4 w(x,y)}{\partial x^2 \partial y^2} + \frac{\partial^4 w(x,y)}{\partial y^4}$$

$$k(x,y) = \begin{cases} constant\ k, when\ in\ full\ contact\ with\ base\ at\ point\ (x,y) \\ 0\ when\ no\ contact\ with\ base\ at\ point\ (x,y) \end{cases}$$

D = flexural stiffness of the plate

k = modulus of subgrade reaction

w = deflections

q = pressure on the slab (due to self-weight, applied load, etc)

x and y define the horizontal coordinate system

Non-dimensional variables scaled by the radius of relative stiffness ℓ are introduced.

$$x^* = \frac{x}{\ell}, \qquad y^* = \frac{y}{\ell} \tag{2.14}$$

Where:

ℓ = radius of relative stiffness is (Westergaard 1927):

$$\ell = \sqrt[4]{\frac{E_{PCC} h_{eq}^3}{12 * (1 - \mu^3) * k}} \tag{2.15}$$

Where:

ℓ = radius of relative stiffness

E_{PCC} = modulus of elasticity of concrete

h_{eq} = effective concrete thickness

μ = Poisson´s ratio

k is the modulus of subgrade reaction

Rearranging the non-dimensional variables in (2.14):

$$x = x^* \ell, \qquad y = y^* \ell \tag{2.16}$$

Differentiating (2.16):

$$\partial x = \ell \partial x^*, \qquad y = \ell \partial y^* \tag{2.17}$$

Introducing the non-dimensional variables in (2.17) into the equilibrium equation (2.13)

$$\frac{D}{\ell} \nabla^4 w(x^*, y^*) + k(x^*, y^*) * w(x^*, y^*) = q(x^*, y^*) \tag{2.18}$$

Dividing both sides of (2.18) by k(x^*, y^*):

$$\nabla^4 w(x^*, y^*) + w(x^*, y^*) = \frac{q(x^*, y^*)}{k(x^*, y^*)} \tag{2.19}$$

From equation (2.19), it can be seen that the deflection basins of the two slabs are proportional if the loads are proportional in non-dimensional space, and the boundary conditions scale. This can also be represented as:

$$w_1(a_1x_1, b_1y_1) = \lambda_{def} w_2(a_2x_2, b_2y_2) \tag{2.20}$$

Where:

a and b are scaling factors independent of coordinates

λ_{def} = scaling factor for deflections dependent only on the properties of the pavement structure

subscripts 1and 2 indicate the two systems

Using similarity decreases the dimensions of the problem, but without introducing any new sources of error.

2.6.2 Equivalencies

Relationships between similar slabs are called equivalencies. Three equivalencies are used to reduce the dimensions of a problem: equivalent thickness, equivalent temperature gradient, and equivalent slab/structure. The concept of equivalent thickness is used to transform the problem from a two layer system to a one layer system, and can be used to solve for stresses in pavement loaded only by traffic. The concept of equivalent temperature gradient can be used to solve for stresses in pavements exposed only to environmental loads. The equivalent slab/system concept combines these two equivalencies to solve problems with both traffic and environmental loads.

The general form for computing stresses in one system from those in another is:

$$\sigma_{1,total}(a_1x_1, b_1y_1) = \lambda_{stress}\sigma_{2,linear}(a_2x_2, b_2y_2) + \sigma_{2,nonlinear}(x_2, y_2) \tag{2.21}$$

Where:

σ_{total} = total stress at the surface (top or bottom) of the slab

λ_{stress} = scaling factor for stress

σ_{linear} = linear component of stress at the surface of the slab due to traffic and thermal loading

$\sigma_{nonlinear}$ = nonlinear linear component of stress at the surface of the slab only due to thermal loading

All of the components of stress are independent of coordinates. The scaling factor for stress is dependent only on the properties of the pavement structure.

2.6.2.1 *Equivalent Thickness*

The concept of equivalent thickness (Ioannides et al. 1992) is used to transform a two layer system into an equivalent single layer system which will have a deflection basin proportional to the original system. This transformation is illustrated in Figure 2.12.

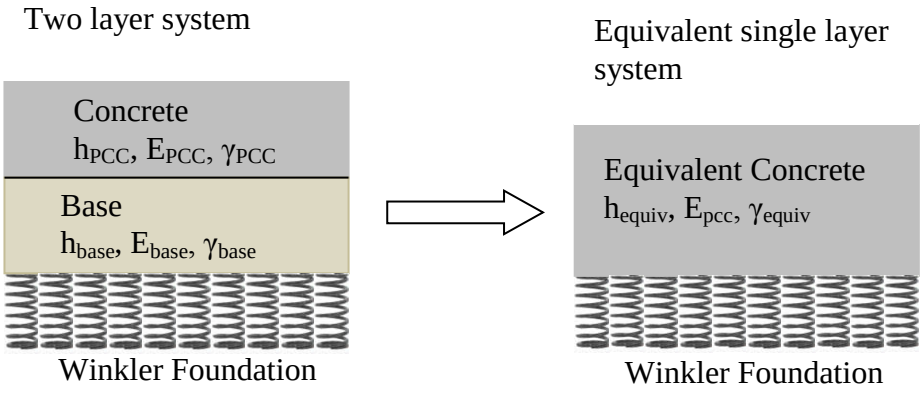

Figure 2.12: Transformation from a two layer original system to an equivalent single layer system.

Using the equivalent thickness concept, stress in a slab can be found based on known stresses in a similar slab which has the same deflections, provided both slabs have the same elastic modulus and Poisson's ratio, and either no bond or full friction between layers. Both slabs must also have the same flexural stiffness D, given as:

$$\mathcal{D} = \frac{Eh^3}{12(1-\mu^2)k} \tag{2.22}$$

Where:

D = flexural stiffness

E = concrete modulus of elasticity

h = concrete layer thickness

μ = Poisson's ratio of the concrete

k = modulus of subgrade reaction

To define the equivalent single layer system, an equivalent thickness and equivalent unit weight must be calculated. The equations used for these calculations are dependent on the nature of the bond between the concrete and base layers in the original system. For unbonded systems, the equivalent thickness is given as (Ioannides et al. 1992):

$$h_{equiv} = \sqrt[3]{{h_{PCC}}^3 + \frac{E_{base}}{E_{PCC}} {h_{base}}^3} \tag{2.23}$$

while for the bonded case, the equivalent thickness is given as (Ioannides et al. 1992):

$$h_{eq} = \sqrt[3]{{h_{PCC}}^3 + \frac{E_{base}}{E_{PCC}} {h_{base}}^3 + 12\left[\left(x - \frac{h_{PCC}}{2}\right)^2 h_{PCC} + \frac{E_{base}}{E_{PCC}}\left(h_{PCC} - x + \frac{h_{base}}{2}\right)^2 h_{base}\right]} \tag{2.24}$$

Where:

$$x = \frac{E_{PCC}h_{PCC}\frac{h_{PCC}}{2} + E_{base}h_{base}\left(h_{PCC} + \frac{h_{base}}{2}\right)}{E_{PCC}h_{PCC} + E_{base}h_{base}}$$

h_{eq} = equivalent slab thickness

E_{PCC} = modulus of elasticity of the concrete

E_{base} = modulus of elasticity of the base layer

h_{pcc} = thickness of the concrete layer

h_{base} = thickness of the base layer

The equivalent unit weight is (Khazanovich 1994):

$$\gamma_{equiv} = \frac{\gamma_{PCC}h_{PCC} + \gamma_{base}h_{base}}{h_{equiv}} \tag{2.25}$$

Where:

γ_{eq} = equivalent concrete unit weight

γ_{pcc} = unit weight of the concrete layer

γ_{base} = unit weight of the base layer

For the unbonded case, γ_{base} is equal to zero, while for the bonded case, it is equal to the actual unit weight of the base material.

The equivalent thickness and unit weight defined using these equations are used in the other equivalencies. The stresses at the bottom of the original concrete slab can be determined from the stresses of the equivalent slab using the following equations (NCHRP 2003b). For the unbonded case:

$$\sigma_{PCC} = \frac{h_{pcc}}{h_{equiv}} \sigma_{equiv} \tag{2.26}$$

For the bonded case:

$$\sigma_{PCC} = \frac{2\left(h_{pcc} - x\right)}{h_{equiv}} \sigma_{equiv} \tag{2.27}$$

This equivalency cannot be used to account for changes in shape and support condition curling induced by temperature gradients.

2.6.2.2 *Equivalent Temperature Gradient*

The equivalent linear temperature gradient concept (Ioannides & Khazanovich 1998b; Khazanovich 1994) is needed to account for environmental loading. This allows the computation of thermally induced stresses in one slab based on those of another if both slabs have the same length, width, flexural stiffness, self-weight, boundary conditions, applied pressure, rest on the same foundation, and the thermal gradients through the thickness of each slab satisfy the following equation:

$$\begin{aligned} &\int_{h_a} E_a(z) * \alpha_a(z) * \left(T_a(z) - T_{0,a}\right) * z \, dz \\ &= \int_{h_b} E_b(z) * \alpha_b(z) * \left(T_b(z) - T_{0,b}\right) * z \, dz \end{aligned} \tag{2.28}$$

Where:

a and b = the two slabs

E = concrete modulus of elasticity

α = concrete coefficient of thermal expansion

z = distance from the neutral axis

T_0 = temperature gradient required to induce flat slab conditions

If these conditions are satisfied, then an equivalent linear temperature gradient which produces the same bending moment in the equivalent system as the original non-linear gradient produced in the original system can be defined. This equivalent temperature gradient, for the unbonded case, is given as (NCHRP 2003b):

$$\Delta T_{lin,eq} = \frac{12}{h_{eq}^2} * \left(\int_{-\frac{h_{PCC}}{2}}^{\frac{h_{PCC}}{2}} (T(z) - T_0) z dz + \frac{\alpha_{base} E_{base}}{\alpha_{PCC} E_{PCC}} * \int_{-\frac{h_{base}}{2}}^{\frac{h_{base}}{2}} \left(T\left(\frac{h_{PCC} + h_{base}}{2} + \xi \right) - T_0 \right) \xi d\xi \right) \quad (2.29)$$

And for the bonded case:

$$\Delta T_{lin,eq} = \frac{12}{h_{eq}^2} \left(\int_{-x}^{h_{PCC}-x} (T(z) - T_0) z dz + \frac{\alpha_{base} E_{base}}{\alpha_{PCC} E_{PCC}} \int_{h_{PCC}-x}^{h_{PCC}+h_{base}-x} (T(z) - T_0) z dz \right) \quad (2.30)$$

Where:

$\Delta T_{lin,eq}$ = equivalent temperature gradient in the equivalent single layer system

T(z) = temperature distribution in the original two layer system

T_0 = temperature at which the slab is flat

α_{PCC} = coefficient of thermal expansion of the concrete

α_{base} = coefficient of thermal expansion of the base

z = depth through the thickness of the system as measured positive downwards from the neutral axis of the slab for the unbonded case and the slab-base system for the bonded case

$$\xi = z - \frac{h_{PCC} + h_{base}}{2}$$

If it was assumed that the coefficient of thermal expansion of the concrete and the base are equal, that the temperature at the bottom surface of the concrete is equal to the temperature at the top surface of the base, and that T_0 is equal to the temperature at the bottom surface of the concrete layer, then (2.29) and (2.30) reduce to (NCHRP 2003b):

For the unbonded case:

$$\Delta T_{lin,eq} = \frac{12}{h_{eq}^2} \int_{-\frac{h_{PCC}}{2}}^{\frac{h_{PCC}}{2}} \left(T(z) - T\left(\frac{h_{PCC}}{2}\right) \right) z dz \tag{2.31}$$

And for the bonded case:

$$\Delta T_{lin,eq} = \frac{12}{h_{eq}^2} \int_{-x}^{h_{PCC}-x} \left(T(z) - T(h_{PCC} - x) \right) z dz \tag{2.32}$$

The original temperature gradient can be divided into 10 increments, thus 11 points will be known. Numerically integrating (2.31) and (2.32) over those 11 points gives:

For the unbonded case:

$$\Delta T_{lin,eq} = \frac{h_{PCC}}{5h_{eq}^2} \sum_{i=1}^{10} \left(T_i * (3i - 17) * \frac{h_{PCC}}{10} + T_{i+1}(3i - 16) * \frac{h_{PCC}}{10} \right) \tag{2.33}$$

And for the bonded case:

$$\Delta T_{lin,eq} = \frac{h_{PCC}}{5h_{eq}^2}\sum_{i=1}^{10}\left(T_i\left((3i-2)\frac{h_{PCC}}{10}-3x\right)\right.$$
$$\left.+\,T_{i+1}\left((3i-1)\frac{h_{PCC}}{10}-3x\right)\right) \qquad (2.34)$$
$$-\frac{T_{11}}{2}h_{PCC}(h_{PCC}-2x)$$

Where:

T_1, T_2, …, T_{11} = temperature at evenly spaced points from top of slab (T_1) to bottom of slab (T_{11})

Stresses at the bottom of the original concrete slab can be determined using the following equations:

For the unbonded case:

$$\sigma_{PCC} = \frac{h_{pcc}}{h_{equiv}}\sigma_{equiv} - \frac{E_{PCC}\alpha_{PCC}}{(1-\mu_{PCC})}$$
$$*\left(\frac{\Delta T_{lin,eq}}{2h_{eq}}h_{PCC} - \frac{\sum_{i=1}^{10}T_i}{10} + \frac{T_1}{20} + \frac{21T_{11}}{20}\right) \qquad (2.35)$$

For the bonded case:

$$\sigma_{PCC} = \frac{2\left(h_{pcc}-x\right)}{h_{eq}}\sigma_{eq} - \frac{E_{PCC}\alpha_{PCC}}{(1-\mu_{PCC})}$$
$$*\left(\frac{\Delta T_{lin,eq}}{h_{eq}}(h_{PCC}-x)\right. \qquad (2.36)$$
$$\left.-\frac{h_{PCC}}{h_{PCC+\left({E_{base}}/{E_{pcc}}\right)h_{base}}}\left(\frac{\sum_{i=1}^{10}T_i}{10}+\frac{T_1}{20}+\frac{21T_{11}}{20}\right)\right)$$

While the equivalent thickness can be used to solve for stresses due to wheel loads, and the equivalent temperature concept can be used to determine stresses due to thermal gradients, the results of the two cannot be superimposed. This is because temperature changes cause slab deformations, which lead to different stress distributions when an axle load is applied to a curled slab. Simply summing the stresses due to thermal and axle loads does not produce the same results as analysis of a load on a curled slab (Ioannides & Salsilli-Murua 1989; Teller & Sutherland 1935).

2.6.2.3 *Korenev's Equivalent Slab*

To analyze the effects of temperature and axle loads applied simultaneously, Korenev's equivalent slab can be used (Korenev & Chernigovskaya 1962). This principle allows the calculation of stresses in a single circular slab on a Winkler foundation due to axle loading and the effects of thermal gradients based on the stresses in a similar slab. To use Korenev's equivalent slab, Korenev's non-dimensional temperature gradient ϕ must first be defined:

$$\phi = \frac{2\alpha(1+\mu)\ell^2 k}{h^2\gamma}\Delta T \tag{2.37}$$

Where:

α = coefficient of thermal expansion

μ = Poisson's ratio

ℓ = radius of relative stiffness

k = modulus of subgrade reaction

γ = unit weight

h = slab thickness

ΔT = temperature gradient

The stresses in one slab can then be determined based on those in another slab using equation (2.38). Korenev's equivalent slab concept does not build off of the equivalent thickness or equivalent temperature gradient concepts, and therefore refers to the similar slabs as Slab 1 and Slab 2, where neither slab is the "equivalent" slab.

$$\sigma_{comb,2}(\xi) = \frac{h_1\gamma_2\ell_2^2}{h_2\gamma_1\ell_1^2}\sigma_{comb,1}(\xi) \quad (2.38)$$

Where:

$$\sigma_{comb}(\xi) = \frac{6\gamma\ell^2}{h}M^*\left(\frac{P}{Q}, \frac{L}{\ell}, \phi^*, \xi\right)$$

ξ = normalized radial distance r/L

r = radial distance as measured from the center fo the slab

L = slab radius

γ = concrete unit weight

h = slab thickness

ℓ = radius of relative stiffness

M^* = non-dimensionalized moment distribution

P = total applied load

Q = total slab self-weight

ϕ = Korenev's non-dimensional temperature gradient

To use this equation, both slabs must be circular and have the same L/ℓ ratio, same Korenev's equivalent temperature gradient ϕ, and same P/hγ ratio.

While Korenev's equivalent slab concept represents a leap forward in modeling the interaction between axle and thermal loads, it is not without limitations, namely that it can only be used with single, circular slabs. Khazanovich et al. (2001) used Korenev's equivalent slab in conjunction with the equivalent thickness and equivalent temperature gradient concepts to define an equivalent structure, which can be used to solve for stresses induced by axle and environmental loads on a rectangular multi-slab system. The equivalent structure model also accounts for the non-liner, self-equilibrating stresses induced in the pavement by temperature gradients, in addition to the stresses from the linear portion of the temperature gradient. To use the equivalent structure concept, the following conditions must be satisfied with regard to the two slabs:

$L_1 = L_2$

$\ell_1 = \ell_2$

$\phi_1 = \phi_2$

$$\frac{AGG_1}{k_1\ell_1} = \frac{AGG_2}{k_2\ell_2}$$

$$\frac{P_1}{h_1\gamma_1} = \frac{P_2}{h_2\gamma_2}$$

$s_1 = s_2$

$f_1 = f_2$

Where:

AGG = aggregate interlock factor determined from the load transfer efficiency (Crovetti 1994)

$$AGG = \frac{0.00546k\ell}{\left(\frac{1}{LTE} - 0.01\right)^{1.178}}$$

s = distance from slab edge to outer wheel edge

f = tire footprint

Subscripts 1 and 2 denote the two slabs considered

Because Khazanovich's equivalent structure concept is based on Korenev's equivalent slab concept, neither of the slabs considered is an "equivalent" slab. However, by selecting one slab to be the equivalent slab and using the appropriate properties as determined through the equivalent thickness and equivalent temperature gradient concepts, Khazanovich made the equivalent structure compatible with the other principles of similarity. In this case, the original two layered system is considered as Slab 1, while Slab 2 is the similar, single layer system. Slab 2 does not necessarily have to be the equivalent system for Slab 1, it need only be similar. The stresses in the unbonded bottom surface of the unbonded original system can be determined from those in the equivalent system using equation (2.39) (Khazanovich et al. 2001).

$$\sigma_{PCC,1} = \frac{h_{PCC,1}^2 h_{PCC,2} \gamma_{PCC,1}}{h_{equiv}^3 \gamma_{PCC,2}} \sigma_{equiv} - \frac{E_{PCC,1} \alpha_{PCC,1}}{(1 - \mu_{PCC,1})} * \left[\frac{T_{top} + T_{bott} - 2T_{mid}}{3} + \frac{h_{equiv}^3 - h_{pcc,1}^3}{2h_{equiv}^3} (T_{top} - T_{bott}) \right] \quad (2.39)$$

Where:

$h_{PCC,1}$ = thickness of slab 1

$h_{PCC,2}$ = thickness of slab 2

h_{eq} = equivalent thickness for slab 1

$E_{PCC,1}$ = concrete elastic modulus for slab 1

$\alpha_{PCC,1}$ = concrete coefficient of thermal expansion for slab 1

$\mu_{PCC,1}$ = concrete Poisson's ratio for slab1

T_{top} = temperature at the top surface of the concrete slab

T_{bott} = temperature at the bottom surface of the concrete slab

T_{mid} = temperature at the mid-depth of the concrete slab

2.7 Finite Element Analysis Software

Though many different finite element modeling programs exist, ISLAB2000 (Khazanovich et al. 2000b) is often used to model JPCPs because it is computationally efficient, accurate to the degree necessary for pavement applications, and much more user friendly than other generic finite element modeling packages (NCHRP 2003b). ISLAB2000 is also the software that was used in the development of MEPDG (NCHRP 2003b), and was used by Hiller (2007) to develop the factorial used for neural network training for the program RadiCAL.

ISLAB2000 is an improved version of the rigid pavement analysis program ILLISLAB (Tabatabaie & Barenberg 1978), and its subsequent incarnation ILSL2 (Khazanovich & Yu 1988). Some of the main advantages of ISLAB2000 are its graphical user interface, its ability to perform analyses in batch mode, and its inherent efficiency (Saxena 2011). In one study which examined the robustness and user friendliness of ISLAB2000, it was

determined that ISLAB2000 is easy to use and produces solutions of acceptable accuracy for pavement analysis (Buch et al. 2004). This study compared the results of analyses of rigid pavements with the classic solutions of Westergaard (1926). Good agreement was found between the ISLAB2000 finite element solution and the theoretical Westergaard solution, provided that correction factors (Ioannides et al. 1985) were used to account for Westergaard's assumptions.

The creators of the MEPDG considered several finite element programs before deciding to use ISLAB2000. As part of their work, a study was conducted to determine which commercially available program would be best suited for their purposes. This study found that ISLAB2000 is superior to other pavement specific finite element programs available because it can analyze one and two layered pavement systems, both linear and non-linear temperature gradients can be used, and a variety of subgrade models are available (NCHRP 2003b). Though not all of these capabilities will be required to run the reduced factorial, they may be needed for verification. For example, though the factorial will consist only of equivalent single layer systems, analyses of multi layered systems will be needed to verify results. Additionally, ISLAB2000 was found to be more computationally efficient than the other pavement analysis programs investigated. The MEPDG study also compared ISLAB2000 with generic finite element programs, but found that their generalness contributed to inefficiency and maladroitness when used to solve pavement systems. For these reasons, it was determined that ISLAB2000 was the best option for use in the MEPDG (NCHRP 2003b). These same reasons contributed to the selection of ISLAB2000 for this research as well.

2.8 Summary

Longitudinal cracking is a commonly observed distress in concrete pavements, especially those with widened slabs. While longitudinal cracking is not typically considered in design, there has been a renewed interest in developing a longitudinal cracking model which is compatible with current design procedures.

The Mechanistic-Empirical Pavement Design Guide (MEPDG) (NCHRP 2006) is a fairly new pavement design procedure. Based on estimated traffic levels and climatic data specific to the pavement location, stresses in the pavement are computed mechanistically. These stresses are then used to calculate damage, which is empirically correlated with distress levels based data from on thousands of test sections. For all of its advantages, one of the most notable disadvantages of the MEPDG is its inability to predict longitudinal cracking.

The MEPDG provides a good framework for mechanistic-empirical design and contains many advanced models to predict various pavement parameters. To develop a longitudinal cracking fatigue damage model, the methods used in the MEPDG can be followed and many of its models can be used to produce needed inputs. One crucial component which cannot be reused in new models is the neural networks, which the MEPDG uses for rapid stress solutions. Because longitudinal and transverse cracks are induced by stresses at different locations, stress analysis must be completely repeated to consider different loading conditions and to compute stresses at different locations.

One tool used in the development of the MEPDG to facilitate stress analysis is similarity. This concept states that the solution of a system can be determined from the solution of another system, provided that the two systems are similar, meaning that their deflection basins are proportional. This eliminates the need to analyze every pavement system which could be considered in a design program. Similarity was used in the transverse cracking models of the MEPDG (Khazanovich et al. 2001; NCHRP 2003b), which employs three equivalencies: equivalent thickness (Ioannides et al. 1992), equivalent temperature gradient (Khazanovich 1994), and equivalent slab/structure (Khazanovich et al. 2001; Korenev & Chernigovskaya 1962). By analyzing similar systems, a smaller number finite element factorial is needed to analyze a large number of pavements.

Chapter 3. Challenges of Modelling Longitudinal Cracks in Mechanistic Empirical Design

3.1 Introduction

Stress analysis in the MEPDG is conducted only on uncracked slabs, which implies the assumption made that transverse cracks in different slabs occur independently of each other. This is a fairly intuitive assumption for transverse cracks because the crack in one slab would not be expected to significantly affect stress distributions in adjacent slabs. However, this may not be the case for longitudinal cracks. Finite element modeling was used to determine the influence on stress distribution in a slab when a crack is present in an adjacent slab. The effect of a crack in an adjacent slab was investigated for both transverse and longitudinal cracks. The potential for erosion to occur due to increased deflections between adjacent slabs when a longitudinal crack is present was also investigated.

3.2 Effect of Cracks in Adjacent Slabs

3.2.1 Modeling Cracks

ISLAB2000 models cracks and joints spanning across all slabs and does not permit simulation of longitudinal crack in one slab but not in the adjacent slab. However, ISLAB2000 does have provisions to include an exception area in the model which has different properties that the remainder of the slab. Using this exception area, a crack can be simulated using weak elements by defining a small area of the slab which has very low stiffness.

To determine how the presence of a crack in one slab can influence the stress level in an adjacent, uncracked slab subjected to traffic and environmental loads, a finite element model was created to investigate this situation. The pavement considered was a standard 10 inch thick concrete pavement with an elastic modulus of 4 million psi and a modulus of subgrade reaction of 100psi/in. A “crack” was defined in one slab and a load placed on an adjacent slab. The location of the applied load was varied and thermal loads were

also applied. The finite element modeling program ISLAB2000 (Khazanovich et al. 2000b) used in the creation of the neural networks was also used for this model.

A 3 inch square mesh was used everywhere except the exception area, so that the exception area could be defined as a 1 inch wide strip containing only full elements. Within the exception area, the mesh was refined to be 0.2 inches high. The refinement was continued for several elements on either side of the exception area for as many elements as necessary to resume the typical 3 inch spacing. This is illustrated in Figure 3.1, which shows a zoomed in view of the mesh, exception area, and refined mesh in and around the exception area. While this is not an accurate representation of a typical crack width, it was determined to be the width necessary for the program to function properly and produce realistic results. It should also be noted that the main concern of this study is how the presence of a crack in one slab affects the global behavior and stress response of an adjacent slab separated by a joint but with some amount of load transfer. The intricacies of the crack itself are not the subject of the study and therefore, an unrealistic crack which produces realistic behavior can be used. This meshing and exception area configuration was used for both the 12 foot and 14 foot width slabs studied.

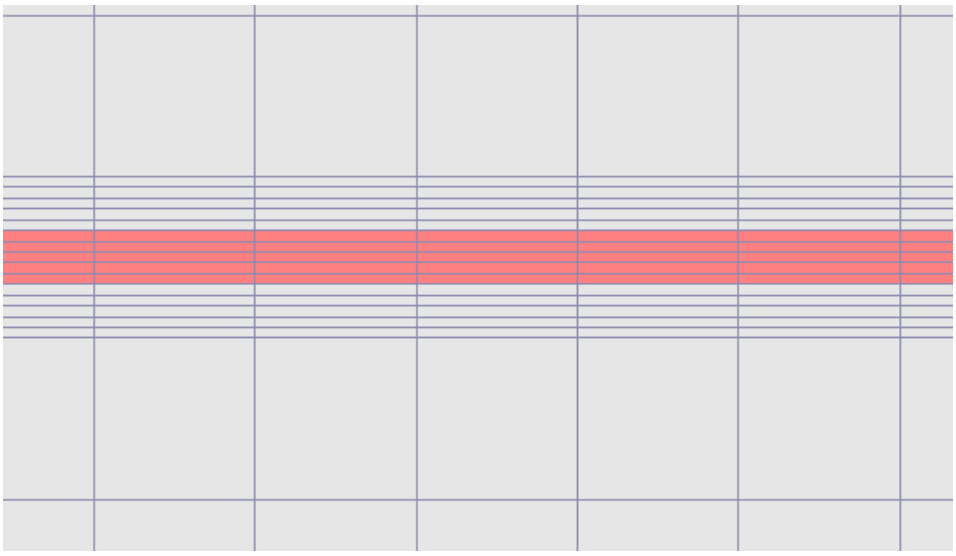

Figure 3.1: Mesh refinement within and around the exception area (pink)

This model was validated extensively to ensure that the presence of the weak elements did not interfere with the meshing in the finite element model, and that an exception area behaved as, and accurately represented, a crack. First, mesh and an exception area were defined as they were in the structural model, but the elements in the exception area were not replaced with weak elements. This model was compared with a standard model with no changes to the mesh and without an exception area. Both cases were found to have the same deflections and stress distributions. Second, weak element "crack" were defined along the entire length of both slabs, allowing for comparison with an actual joint. It was found that slabs with a joint and a line of weak elements exhibited the same behavior.

3.2.2 Effect of Transverse Cracks in Adjacent Slabs

Independence means that the presence of a crack in one slab does not affect the stress distribution in adjacent, uncracked slabs. The independence of transverse cracks is shown in Figure 3.2. This image shows the result of finite element analyses conducted for a load placed on an uncracked slab adjacent to both a cracked and uncracked slab. The results of the analyses show identical stress distributions in the loaded slab in both cases, indicating that the presence of a crack in an adjacent slab has no effect on the stresses in an adjacent slab. This was not found to be the case when longitudinal cracks were considered.

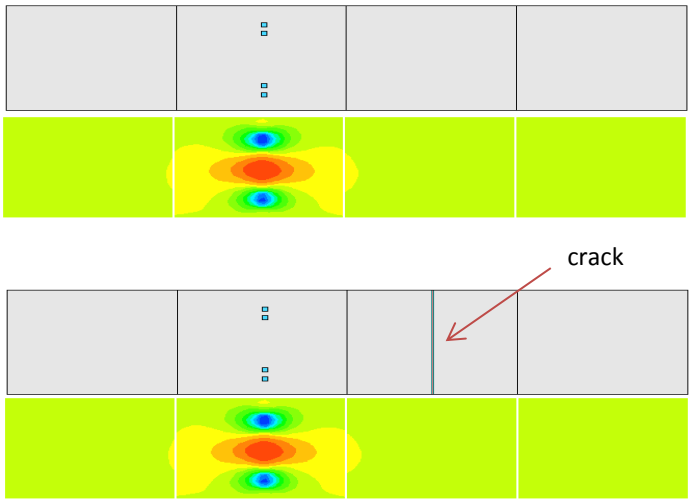

Figure 3.2: Stress distributions are the same when the load is placed next to an uncracked slab (top) and a cracked slab (bottom)

3.2.3 Influence of a Longitudinal Crack on Stresses in an Adjacent Slab

To study the influence of a longitudinal crack in one slab on stresses in an adjacent slab, a structural model was defined consisting of two adjacent slabs with an influence area used to simulate a longitudinal crack in one of the slabs. As previously discussed, the crack was simulated by assigning the influence area to have a stiffness of 1 psi while all other properties of the influence area were the same as those of the surrounding concrete.

Two different locations of crack and wheel load were considered. The most critical case for longitudinal crack formation is when the load is applied at the midslab edge. Loads at this location are fairly rare however, because this would involve driving partially in another lane. To determine the closest location to the midslab edge which could be frequently attained, the distribution of vehicle wander assumed by the MEPDG was examined (NCHRP 2004). The MEPDG assumes vehicle wander to be normally distributed with a mean value of 18 inches. Because vehicle wander is normally distributed, it is equally likely for a wheel to be placed at the edge of the slab (18 inches from the mean wheel path for a standard width slab) as it is for a wheel to be placed 18 inches from the mean wheel path in the other direction (towards midslab). Given that the MEPDG computes damage for transverse cracking at the edge of the slab, it was deemed reasonable to examine longitudinal cracking for a load with equal likelihood of occurring.

Therefore, the closest a load would be placed to midslab would be at 36 inches from the slab edge for the standard width slab and 60 in for the widened slab. The case of the load placed in the wheel path was also considered because this is where most traffic travels.

It is known that the crack will have the largest influence when it is directly under the wheel load. However, one of the limitations of the finite element modeling program used was that the load could not be located within the crack. Therefore, the load was located at the edge of the crack without actually being commensurate with the crack.

The effects of temperature on maximum stress in the uncrack slab as a function of load transfer efficiency with the cracked slab were investigated. To do this, a factorial was run in ISLAB2000 consisting of a control case (with no crack in either slab) and the case of interest, a cracked slab adjacent to a loaded slab. Temperature and load transfer efficiency across the transverse joint were varied; temperatures were considered in increments of 10°F from -20°F to 20°F while load transfer efficiency was considered in increments of 5% varying form 1-99.9% (0% and 100% cannot be input into the program, thus 1 and 99.9% were used instead). This factorial was run once for each slab width for both the control case and the case with a longitudinal crack for both load locations. Only positive values of temperature gradient were considered because bottom-up cracking was the distress of interest in this study; negative temperature gradients are more associated with top-down longitudinal cracking, which is less common.

For each case considered, the maximum stress was determined in the loaded slab. In this discussion, the case with two intact slabs is called the control or uncracked case, while the case with a crack in the slab adjacent to the loaded slab will be called the cracked case (noting that the crack is not actually in the slab whose stresses are being discussed). The results of this investigation will be discussed separately for each load location.

3.2.3.1 *Structural Model*

To study the effects of the presence of a longitudinal crack in one slab on the stresses in an adjacent slab, a structural model was defined in ISLAB2000. This model consisted of

two adjacent slabs of typical dimensions, 12x15ft or 14x15ft, representing a standard width slab and a widened slab, respectively. In the left slab, a series of weak elements was introduced in an exception area to model the crack. The load was placed at various locations on the right slab, along the left edge. An example structural model is shown in Figure 3.3.

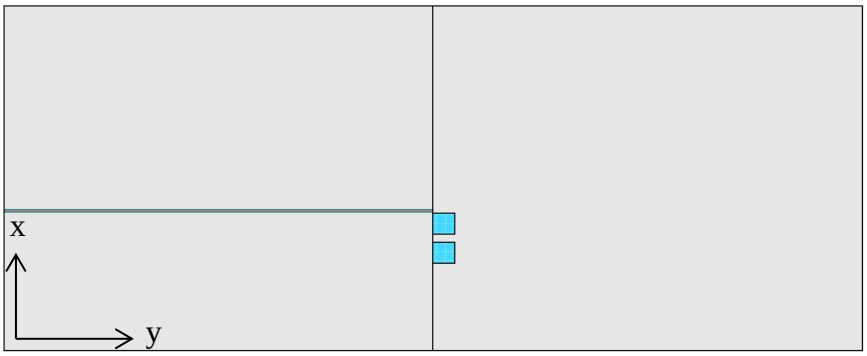

Figure 3.3: Two slab system with a cracked slab (exception area) and with load (blue squares) on the uncracked slab. Mesh is omitted from the figure for clarity

3.2.3.2 *Crack at Midslab*

The structural model used to investigate the case of the crack at midslab is shown in Figure 3.4.

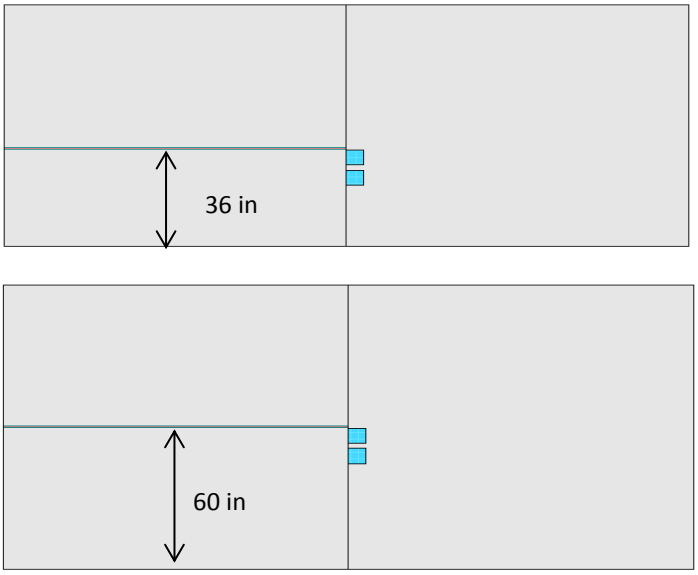

Figure 3.4: Load and crack locations for case of crack at "midslab" for the standard width (top) and widened slab (bottom)

Figure 3.5 and Figure 3.6 show the stresses in the x-direction on the bottom surface of the slab versus load transfer efficiency for the standard width and widened slabs, respectively. From these figures, it can be seen that the presence of a crack in a slab adjacent to the loaded slab causes a decrease in the benefits of load transfer efficiency. For higher values of load transfer efficiency, stresses in the uncracked case are lower than those at lower values of load transfer efficiency. This would be expected; load transfer efficiency shares the load with other slabs to reduce stresses. In the cracked case, however, the stress level remains fairly constant, regardless of the amount of load transfer efficiency provided. Thus added load transfer efficiency will not reduce stresses in a loaded slab if the adjacent slab is cracked. This makes it more likely for the crack to propagate to the loaded slab. The large increase in stress seen at very high values of load transfer efficiency (greater than 95%) are not represented well by the model, as will be discussed later.

By comparing Figure 3.5 and Figure 3.6, it can be seen that both the standard width and widened slabs behave in a similar manner. This is because the load is placed close enough to midslab in both cases that the slabs are behaving as would be expected for Westergaard's edge loading case. However, the stresses in the widened slab are higher because the load is closer to midslab in that case. The stresses in the widened slab are also higher than those in the standard width slab for the cases with applied temperature gradients because larger slabs are more affected by curling.

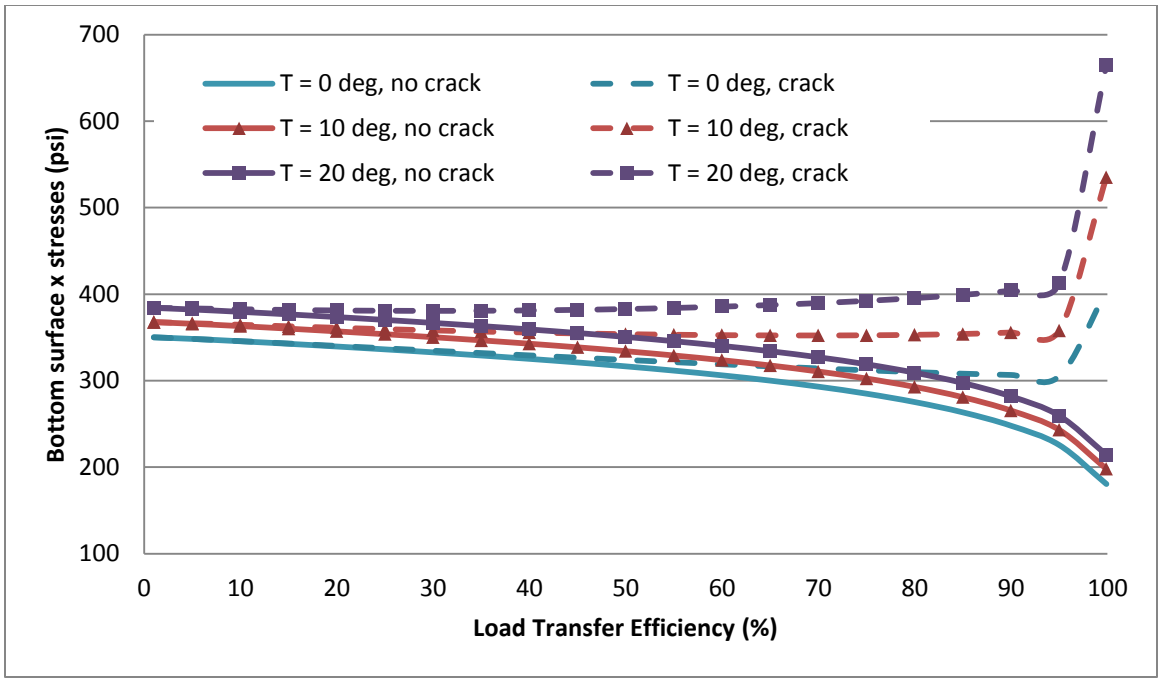

Figure 3.5: Stresses in the x direction at the bottom surface of the loaded slab versus load transfer efficiency for the standard width slab for the "midslab" load case.

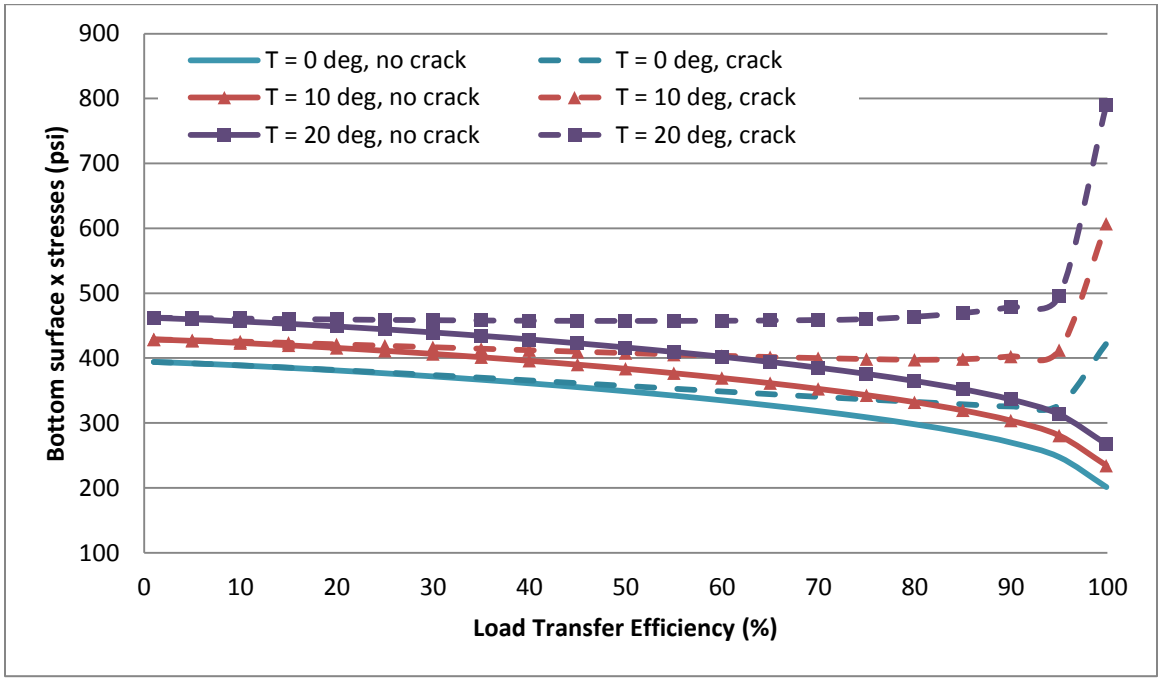

Figure 3.6: Stresses in the x direction at the bottom surface of the loaded slab versus load transfer efficiency for the widened slab for the "midslab" load case.

At high values of load transfer efficiency (greater than 95%), the stresses determine through the finite element analysis do not follow the trends seen in the rest of the analyses. Up until values of load transfer efficiency equal to about 95%, the two adjacent slabs are behaving independently with some measure of load sharing. At the next value of load transfer efficiency considered, 99.9%, the joint is essentially closed and the two adjacent slabs are behaving as one large slab. In this case, the crack tip is acting as a stress concentrator in the middle of one large slab. This case is different than what is being considered in all the rest of the study, and is not what the finite element model was designed to simulate. A large slab with a stress concentrator should be modeled using fracture mechanics and is outside the scope of this project.

3.2.3.3 *Crack in Wheel Path*

The structural model used to investigate the case of the load in the wheel path is shown in Figure 3.7.

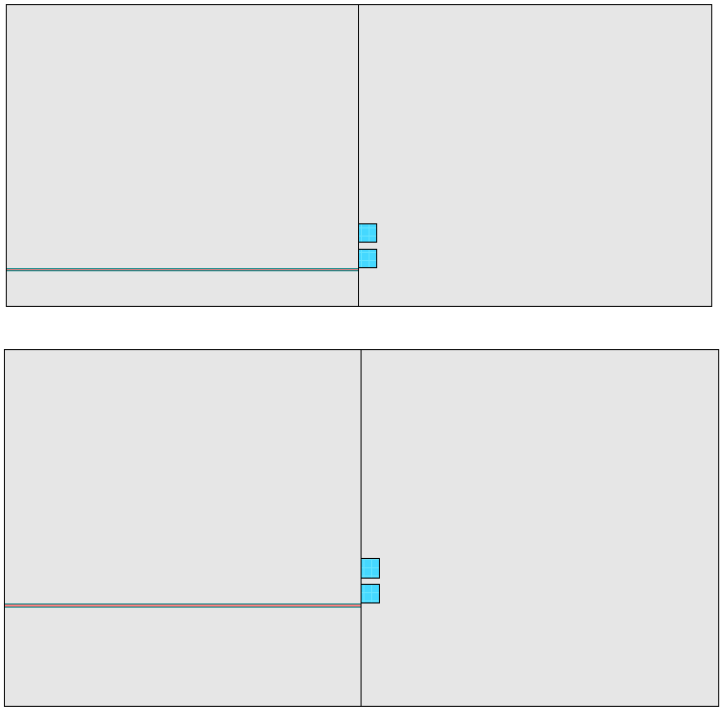

Figure 3.7: Load and crack locations for case of crack in the wheel path for the standard width (top) and widened slab (bottom)

Figure 3.8 and Figure 3.9 show the stresses in the x-direction on the bottom surface of the slab versus load transfer efficiency for the standard width and widened slabs, respectively. While both slab widths show some loss of benefit of load transfer efficiency between the cracked and uncracked cases, this is much more pronounced in the widened slab case. This is because the load is far enough from the midslab edge for the standard slab that the stress distribution is more similar to Westergaard's corner cracking loading case than the edge loading case. For the widened slab, the load is still far enough from the longitudinal edge that the slab is behaving more like an edge loading case. Due to this, the stresses in the widened slab are much higher than those in the standard width slab.

For the standard width slab, stresses are lower for higher values of load transfer efficiency for both the cracked and uncracked cases. The stresses in the cracked case are still slightly higher than those in the uncracked case when a positive temperature gradient is present, indicating that there is still some loss of the benefits of load transfer efficiency. At higher values of load transfer efficiency, there was more loss of benefit of load transfer efficiency when a crack was present. This was not found to be the case when no temperature gradient was present, likely because curling effects corners more than edges and the load is closer to the corner than the midslab edge in this case. At very high values of load transfer efficiency, the behavior became erratic, for reasons previously discussed.

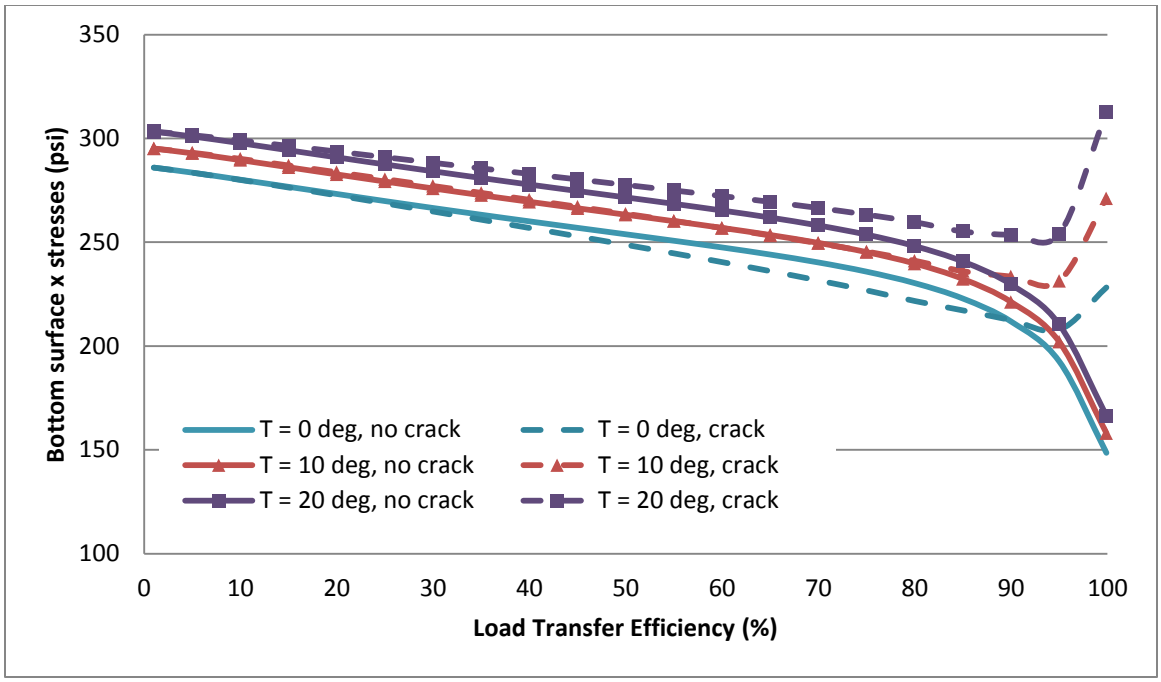

Figure 3.8: Stresses in the x direction at the bottom surface of the loaded slab versus load transfer efficiency for the standard width slab for the wheel path load case.

The widened slab behaved much more like an edge loading case than the standard width slab and therefore closely resembles the behavior seen when the load was placed at midslab (Figure 3.6). For all temperature gradients considered, there was loss of the benefits of load transfer efficiency, though this was more pronounced for larger temperature gradients. Larger values of load transfer efficiency are associated with a larger loss of benefit of load transfer efficiency when the adjacent slab is cracked. Again, the behavior at very high levels of load transfer efficiency should not be considered using this model. The greater loss of benefit of load transfer efficiency coupled with higher stresses in the widened slab case illustrates why widened slabs are of greater concern when longitudinal cracking is considered.

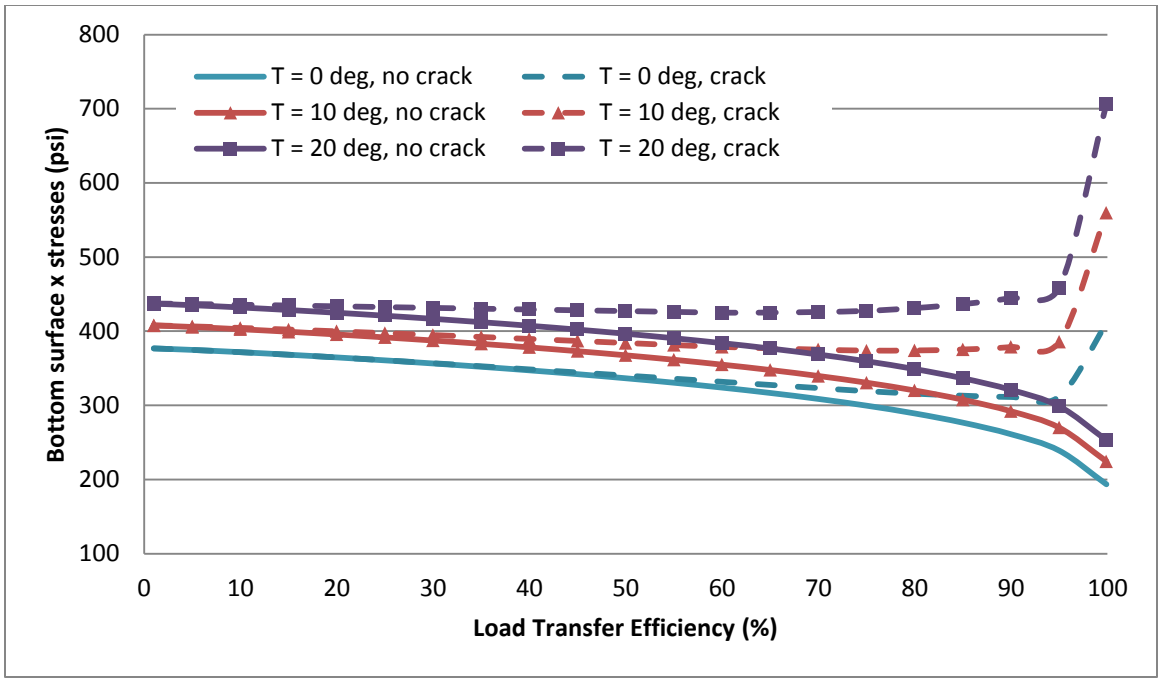

Figure 3.9: Stresses in the x direction at the bottom surface of the loaded slab versus load transfer efficiency for the widened slab for the wheel path load case.

3.2.3.4 *Discussion*

From these figures, it can be seen that the slab width plays an important role in determining the behavior of the system when the load is placed in the mean wheel path. This is in contrast with the case of the crack at "midslab" where the standard width and widened slabs behaved similarly. These results further illustrate how the use of widened slabs is problematic when considering longitudinal cracking. For widened slabs, the stresses will be higher than for standard width slabs.

If a crack is present in an adjacent slab, the loaded slab will experience an increase in stress and lose much of the benefit of load transfer efficiency, which increases the likelihood of crack propagation. While this can happen in the standard width slab, it is more likely to occur with a widened slab. The loss of benefit of load transfer efficiency was much more pronounced in the standard width slab when the load was placed at "midslab" than when it was placed in the wheel path. More loads occur in the wheel

path, which has less loss of benefit of load transfer efficiency and therefore less chance of crack propagation. For the widened slab however, the location of the load was much less of a factor in the amount of benefit of load transfer efficiency lost due to the presence of a crack in an adjacent slab. Loads in the wheel path are almost as likely to cause crack propagation as those at midslab.

The effect of the presences of a crack in an adjacent slab is more pronounced for doweled pavements. An undoweled pavement will have lower load transfer efficiency and therefore higher stresses and higher likelihood of a longitudinal crack forming. Once that crack forms however, stresses will not increase significantly. Dowels, however, are more likely to prevent a crack from forming in the first place.

3.3 Effect of Subgrade Erosion on Longitudinal Crack Development

It was determined above that the presence of an adjacent slab can increase stresses at the transverse joint, and can also increase deflections at that joint. Such an increase in deflections may increase the likelihood of subgrade erosion under the transverse joint. The increase in erosion potential was explored by examining deflections and differential energy in a two slab system with and without a longitudinal crack present. The effects of erosion on stress distribution were also investigated.

3.3.1 Erosion Potential

To investigate the erosion potential of a slab containing a longitudinal crack, the structural models used for investigating the effects of a crack at "midslab" was selected (see Section 3.2.3.2), but this time the load was placed on the cracked slab instead of the uncracked slab, as shown in Figure 3.10. The pavement considered was a standard 10 inch thick concrete pavement with an elastic modulus of 4 million psi and a modulus of subgrade reaction of 100psi/in. Load transfer efficiency between the adjacent slabs was set at 50%.

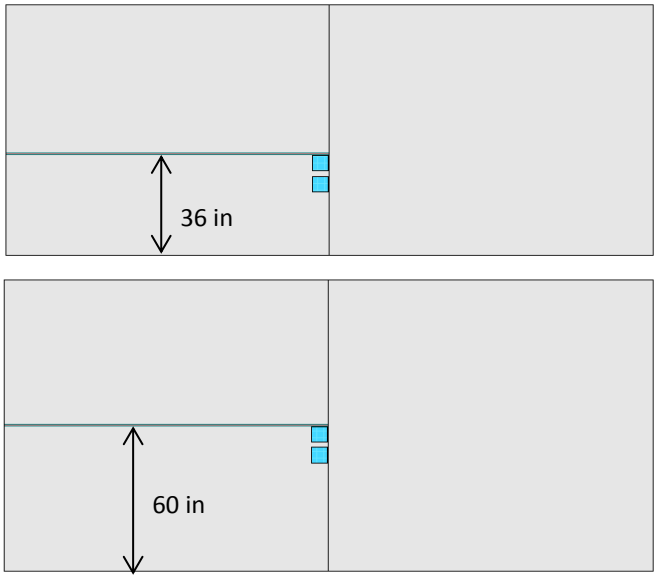

Figure 3.10: Load and crack locations for determining erosion potential for the standard width (top) and widened slab (bottom).

For both the standard width and widened slab cases, the deflections were computed along the transverse joint on both the loaded and unloaded slabs using finite element analysis. The results of the analysis are given in Figure 3.11 for the standard width slab and in Figure 3.12 for the widened slab. These figures show the large increase in deflections on the loaded slab in the cracked case as compared with those in the uncracked case. This indicates that an increase in pumping and erosion potential under the joint after a longitudinal crack forms.

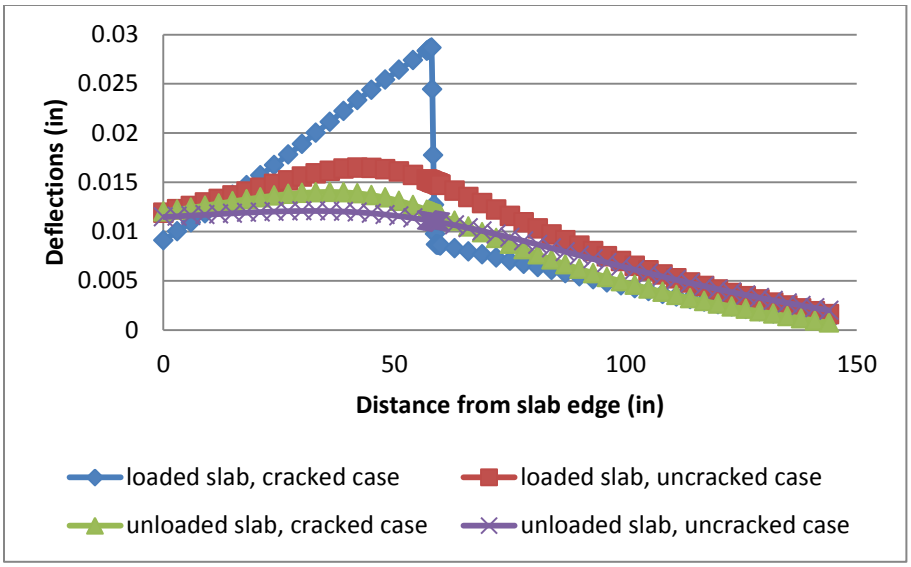

Figure 3.11: Deflections along the transverse joint for the standard width slab

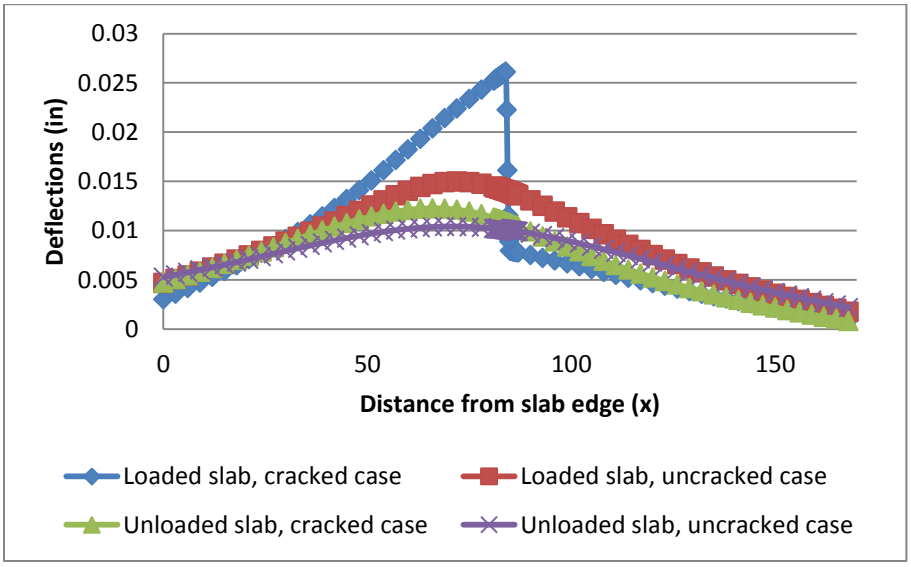

Figure 3.12: Deflections along the transverse joint for the widened width slab

Another measure of erosion potential is differential energy (Khazanovich et al. 2004), which is computed as:

$$DE = \frac{k}{2}(\delta_L^2 - \delta_U^2)$$

Where:

DE = differential energy, lbs/in

k = modulus of subgrade reaction, pci

δ_L^2 = deflection of the loaded slab, in

δ_U^2 = deflection of the loaded slab, in

The differential energy was computed for both the cracked and uncracked cases, see Figure 3.13 and Figure 3.14 for the standard width and widened slabs, respectively. For both slab widths, it can be seen that the cracked cases has a much higher differential energy than the uncracked case, confirming higher erosion potential when a longitudinal crack is present.

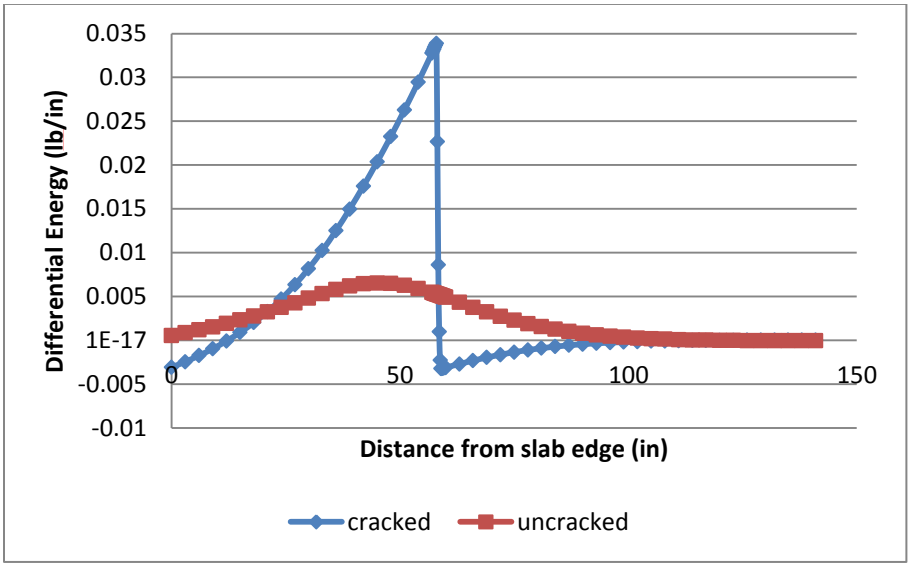

Figure 3.13: Differential energy for the standard width slab

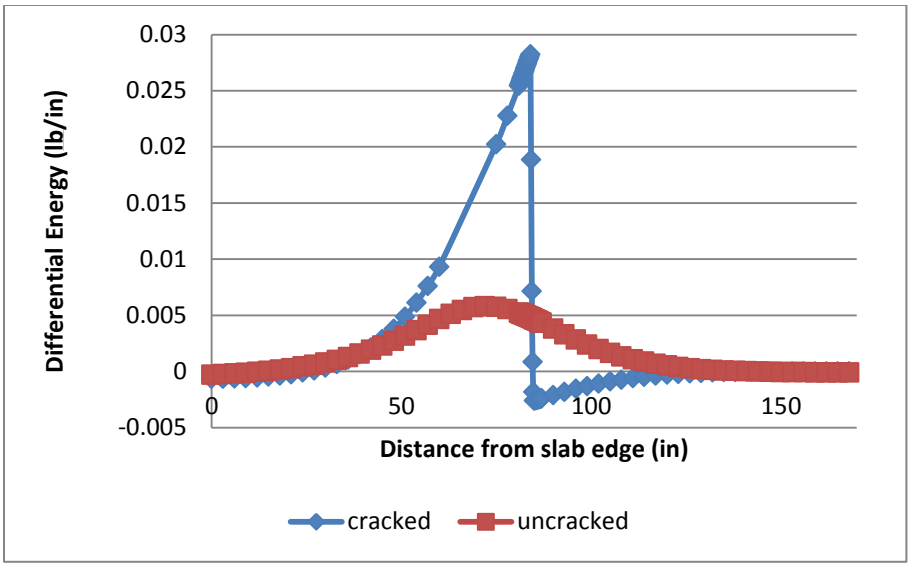

Figure 3.14: Differential energy for the widened slab

3.3.2 Effect of Erosion on Critical Stresses

Once the potential for increased erosion when a longitudinal crack is present was established, the effects of such erosion were further investigated. To simulate subgrade erosion, an exception area was defined near the crack, as shown in Figure 3.15. The modulus of subgrade reaction in the exception area was taken as 1 lb/in^3 to simulate a void with essentially no stiffness; this exception area was 36 inches by 36 inches centered on the load. The load was placed on the uncracked slab.

The effects of temperature gradient on the maximum stress in the cracked, uneroded slab as a function of load transfer efficiency with the cracked, eroded slab were investigated. To do this, a factorial was run in ISLAB2000 consisting of a control case (with a crack in the left slab, but no subgrade erosion) and the case of interest, a cracked slab adjacent to a loaded slab and subgrade erosion near the joint. Temperature and load transfer efficiency across the transverse joint were varied as in the previous cases. This factorial was run once for each slab width for both the case with only a crack and the case with both a longitudinal crack and an eroded subgrade.

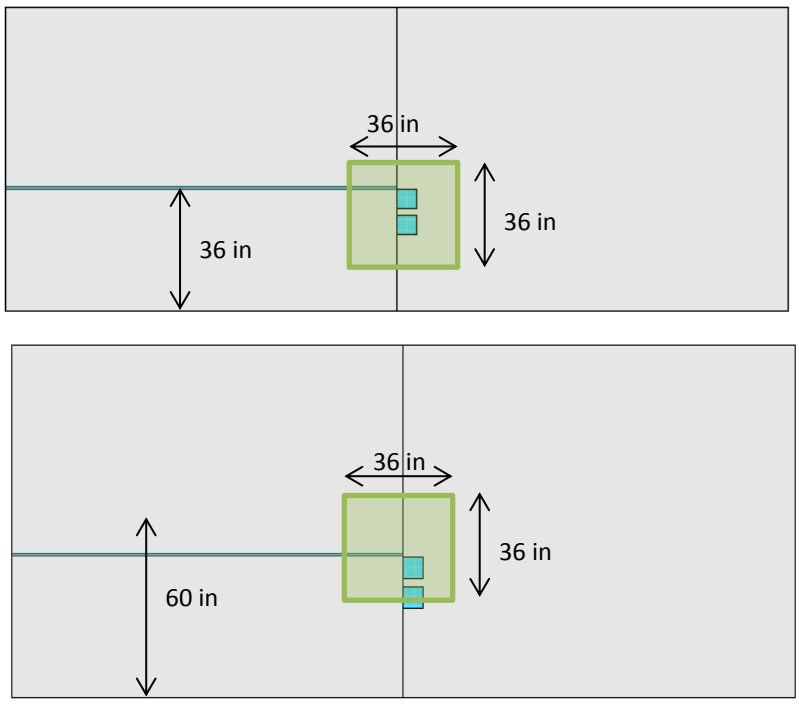

Figure 3.15: Structural models used to investigate the effects of erosion in a standard width slab (top) and a widened slab (bottom).

For each case considered, the maximum stress was determined in the loaded slab. In this discussion, the case without erosion was called the uneroded case while the case with subgrade erosion near the load was called the eroded case. Both cases contained a crack in the slab adjacent to the loaded slab.

Figure 3.16 and Figure 3.17 show a comparison the stresses in the x-direction on the bottom surface of the slab versus load transfer efficiency for the standard width and widened slabs, respectively, when erosion is or is not present. From these figures, it can be seen that erosion leads to an increase in stresses. The presence of the crack does not affect the stresses in this case because both the control and test cases contained the same crack, only the presence of erosion was varied in this case. While load transfer efficiency did not appear to have a significant effect on stress, higher load transfer efficiency did appear to decrease stresses slightly, particularly for lower temperature gradients. Higher levels of load transfer efficiency are also known to reduce erosion potential by decreasing deflections.

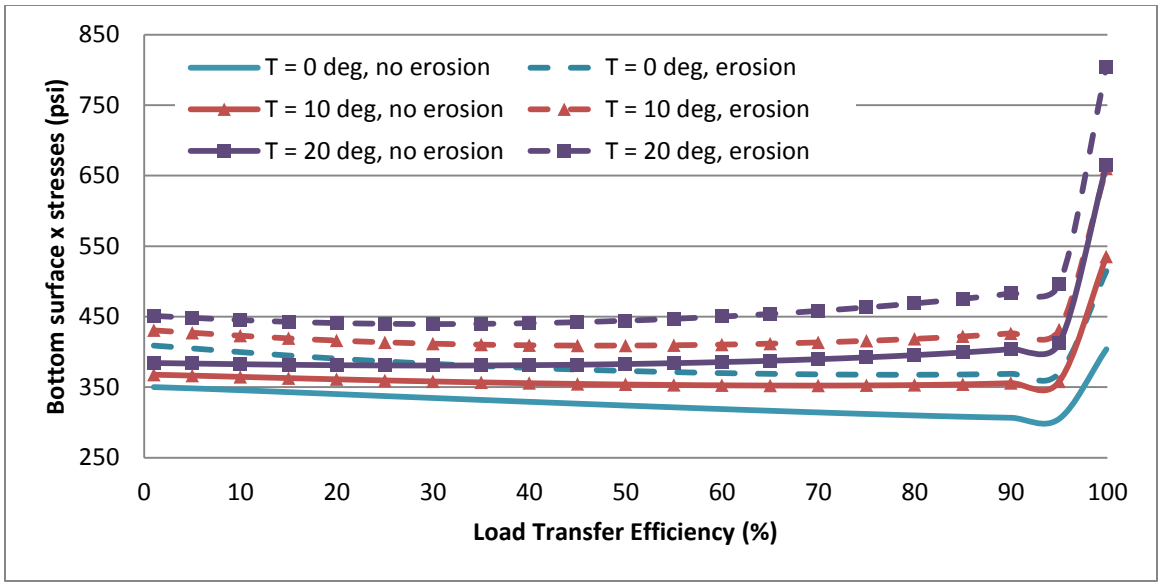

Figure 3.16: Stresses in the x direction at the bottom surface of the loaded slab versus load transfer efficiency for the standard width slab when erosion is present.

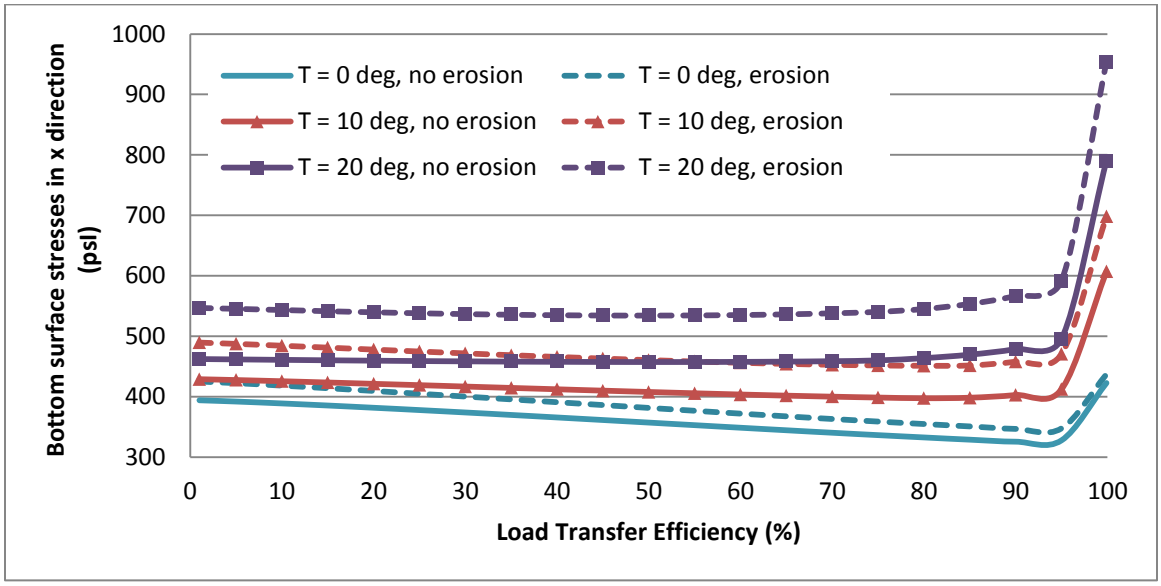

Figure 3.17: Stresses in the x direction at the bottom surface of the loaded slab versus load transfer efficiency for the widened slab when erosion is present.

The presence of a longitudinal crack can increase the potential for pumping and erosion in a pavement. This can be seen by an increase in deflections when comparing pavement systems with and without a longitudinal crack in one of the slabs. The increase in deflections leads to an increase in differential energy, which can cause pumping and erosion. A comparison of longitudinally cracked pavements with and without eroded areas showed that if pumping and erosion occur, there can be a further loss of benefit of load transfer efficiency beyond the loss associated with the presence of a crack alone. While the increase in erosion potential itself is not dramatically different for the standard width slab versus the widened slab, the widened slab will experience higher stresses and therefore an increase in cracking potential.

3.4 Conclusions

This research has shown that the effects of a crack in an adjacent slab on stresses in the slab of interest are very complex and cannot be easily quantified. Because of this observation, prediction of the amount of longitudinal cracking was not feasible in this study. An alternative approach of predicting damage using an uncracked structural model was used. When using this approach in design, it is recommended to limit the damage associated with longitudinal cracking in the mechanistic portion of the design process. Limiting damage accumulation assures that stresses are low enough that cracks will not form in the first place without the need to account for the presence of cracks in adjacent slabs. To determine an appropriate limit on damage, it is recommended to use the transverse cracking and fatigue damage relationship used in the MEPDG as a known underestimate of longitudinal cracking from longitudinal fatigue damage. Based on this relationship and the knowledge that this relationship is an overestimate, the ratio of longitudinal cracking fatigue damage to transverse cracking fatigue damage should be less than some number which is less than one. What this limit should be will need to be determined with engineering judgment until further research can be conducted. A discussion of this approach is presented in Chapter 7.

Chapter 4. Rapid Solutions for Stress Analysis

When the MEPDG was created, only transverse cracking was considered and therefore, stresses were only computed at the critical location for transverse cracking. The critical load and stress locations for longitudinal cracking are different than those for transverse cracking, necessitating new analyses if longitudinal cracking is to be considered. These new analyses need to consider different load positions and compute stresses at different locations; however, to ensure that the longitudinal cracking model is MEPDG compatible, it must span the same scope of possible pavement structures as the MEPDG.

The goal of this chapter was to develop computationally efficient stress analysis tools to compute the critical stresses on the transverse joint. These tools had to cover a wide range of pavement structures and loading conditions. While the stress analysis tools developed by the MEPDG were not applicable when considering longitudinal cracking, the methods used to develop those tools can be used.

Any program which includes an embedded finite element model would run too slowly to be user friendly based on the number of analyses still necessary. To avoid embedding a finite element model in the program, stress analysis in the MEPDG is conducted using neural networks (as was discussed in Section 2.4.4). Because a new model must be MEPDG compatible, it too will use neural networks to compute stresses. This will also eliminate all issues associated with embedded finite element models that the MEPDG avoided. The concepts of similarity were used in the development of the current MEPDG transverse cracking model for both CRCP (Khazanovich et al. 2001) and JPCP pavements (NCHRP 2003b) to reduce the size of the factorial of pavements considered without reducing error. By implementing the principles of similarity differently than was done in the MEPDG, it was possible to avoid some of the difficulties encountered by the MEPDG developers. The reduced factorial was analyzed using finite element analysis and the results were used to develop neural networks in similar space.

To analyze a pavement with the program being developed in this research, it will be necessary to transform that pavement into similar space, compute stresses using neural

networks, and then transform the stresses back into real space. Full details on this procedure are outlined.

4.1 Locations of Stresses Considered

In order to predict longitudinal cracking fatigue damage, it is necessary to compute stresses at the critical location for longitudinal cracking. As was discussed in Chapter 2, the locations where a longitudinal crack could begin to form are along the transverse joint due; this is different than transverse cracking, where the critical location is along the longitudinal edge. Similarly, the critical load location for longitudinal cracking is along the transverse joint while it is at midslab of the longitudinal edge for transverse cracking.

While the finite element analysis computes stresses and deflections at every node in the finite element model, only stresses at certain locations are pertinent to determine cracking. To compute longitudinal cracking damage, stresses were considered at the transverse joint from the lane edge to mid width for the standard width slab and from the wheel path to midslab for the widened slab because this is where the highest stresses will occur. For the standard width slab, the lane edge corresponds with the slab edge, while, for the widened slab, the lane edge is 24 inches from the slab edge. Stresses were determined approximately every 4 inches along the transverse joint. The location of stresses used to determine longitudinal cracking is shown in Figure 4.1.

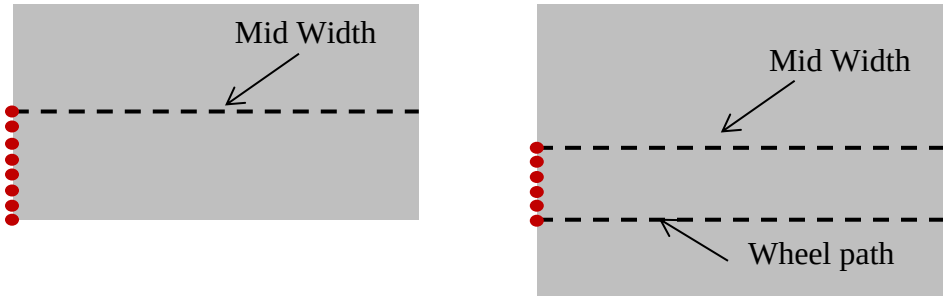

Figure 4.1: Location of stress analysis points used to compute longitudinal cracking for standard width (left) and widened slabs

While stresses along the longitudinal edge were not used in the development of the longitudinal cracking fatigue damage model, they were computed for use in the

longitudinal cracking potential study detailed in Chapter 5. Because they were computed in the same manner as stresses along the transverse joint, details are provided here. To compute transverse cracking, stresses were considered at the mid-slab edge for the standard width slab and the widened slabs; this matches with the procedure used in the MEPDG transverse cracking model for JPCPs (NCHRP 2003a). The location of the stresses used to determine transverse cracking are shown in Figure 4.2.

Figure 4.2: Location of stress analysis points used to compute transverse cracking for standard width (left) and widened slabs

4.2 Finite Element Modeling

Stress analysis of the final reduced factorial was conducted in the concrete pavement specific finite element modeling program ISLAB2000 (Khazanovich et al. 2000b). This program allows factorials to be run in batches provided that the slab configuration and mesh geometry are the same for all cases in the batch. For all cases, the driving and passing lanes and the shoulder were modeled for three slab lengths. Three slabs lengths were needed in order to be able to place the truck at all intervals required for the influence line analysis.

For each batch in the factorial, a base file was developed with slab geometry and meshing unique to that batch. The batches were divided based on slab geometry into two main categories: standard width slabs and widened slabs. The standard slab width was assumed to be 12 ft, while the widened slab was modeled as 14 ft wide. Both models had an 8 ft shoulder. The option of performing a temperature analysis was selected in all cases, and a Winkler subgrade model was used. The base finite element model used to

generate all files for the standard width slab is shown in Figure 4.3, while the base file for the widened slab is shown in Figure 4.4.

Mesh for both models was selected to be both refined and computationally efficient. The default node spacing for a "fine" mesh in ISLAB2000 is 6 in. This spacing was considered to be acceptable for most areas in the model; however refinement was desired in the slab of interest. To accomplish this, the node spacing was decreased to 2.4 in across the slab width and 3 in across the slab length. These dimensions were selected to ensure that a whole number of nodes at a constant spacing could cover the desired slab dimension, and to ensure that the aspect ratio of the elements was no greater than 4:1. Because both the slab and the loading are symmetrical, it was determined that the mesh needed to be made finer on only half of the slab width, which allowed for greater computational efficiency. Across the length of the slab, the node spacing was increased to 7.5 inches on the first and third slabs (not the slab of interest), again to increase computational efficiency. Further reduction in run times was achieved by making the mesh coarser on the shoulder.

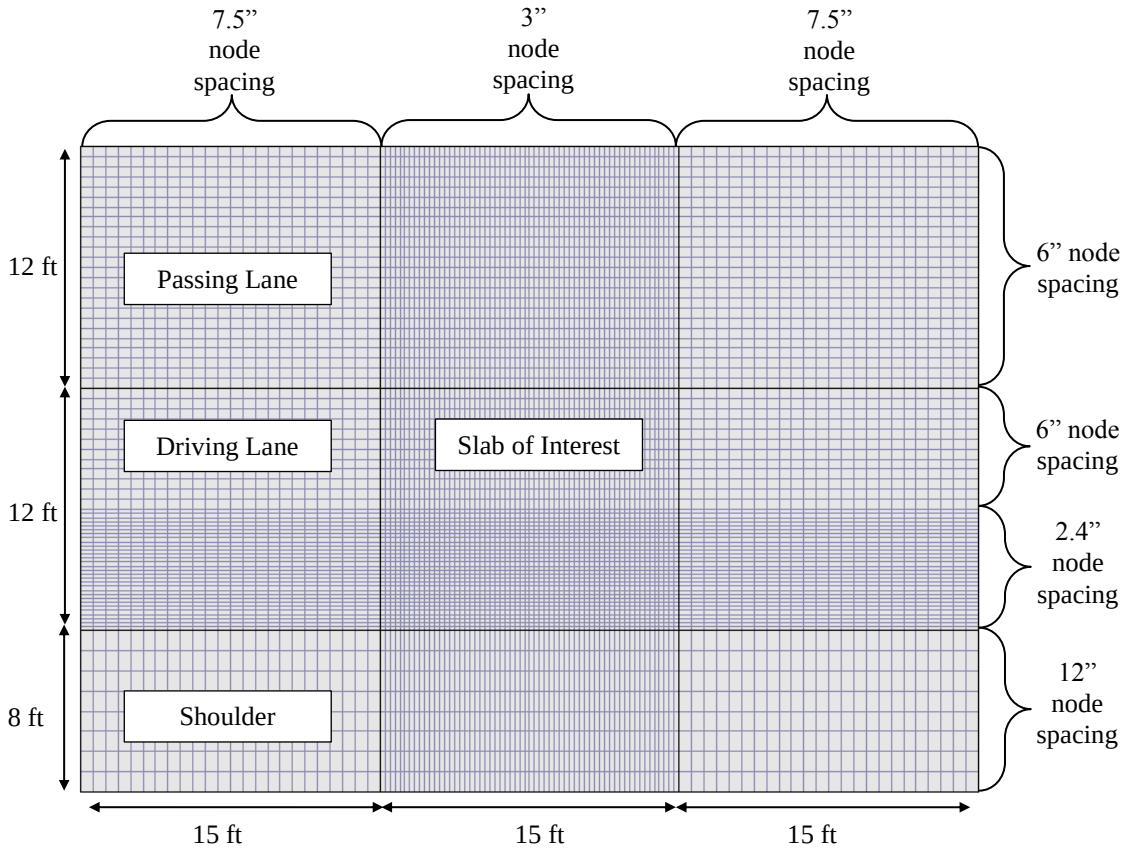

Figure 4.3: Base finite element model for a standard width slab

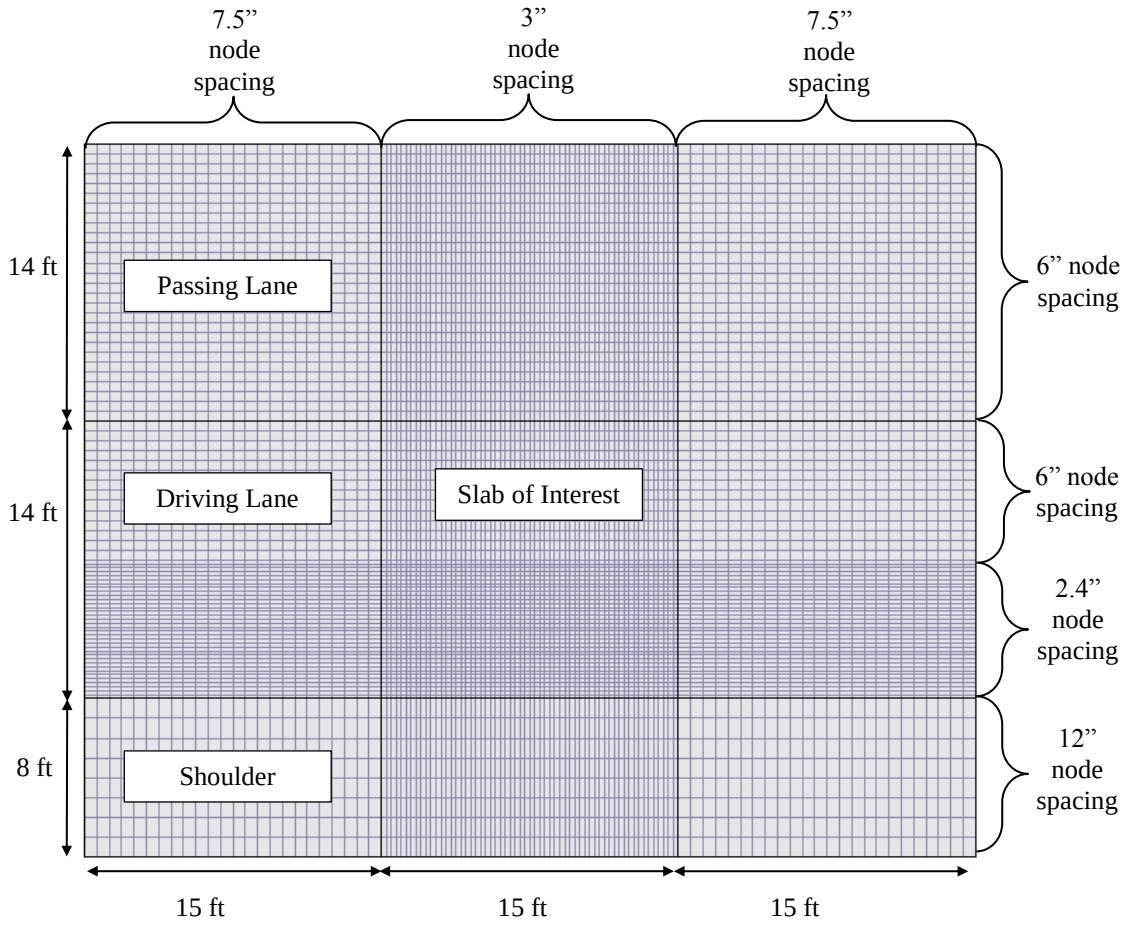

Figure 4.4: Base finite element model for a widened slab

Both single and tandem axel loads were considered in the reduced factorial. The dimensions and configurations of these loads are given in Table 4.1. Standard axles can be used because the MEPDG converts all traffic loading into equivalent loads from standardized axles. The vehicle wander specified in the factorial refers to the location of the lower left corner of the lower left tire, see Figure 4.5. For tandem axles, the factorial was run twice, once for the load location refereeing to the lower left corner of the lower left tire on the front axle, and once for the load location referring to the lower left corner of the lower left tire of the rear axle.

Table 4.1: Axle load configurations

Single Axle		
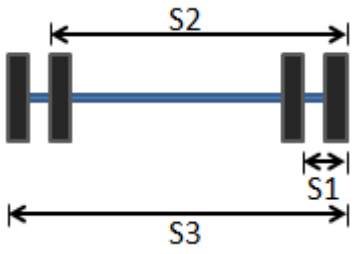	Parameter	
	S1	13 in
	S2	84 in
	S3	97 in
	Tire footprint	6.75in square
Tandem Axle		
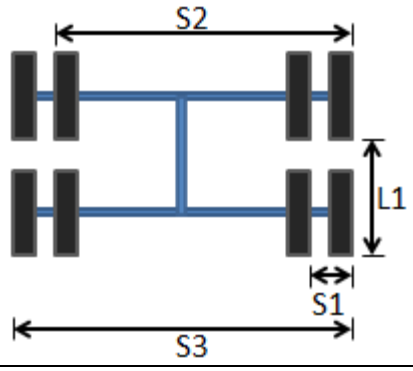	Parameter	
	S1	13 in
	S2	84 in
	S3	97 in
	L1	39 in
	Tire footprint	6.75in square

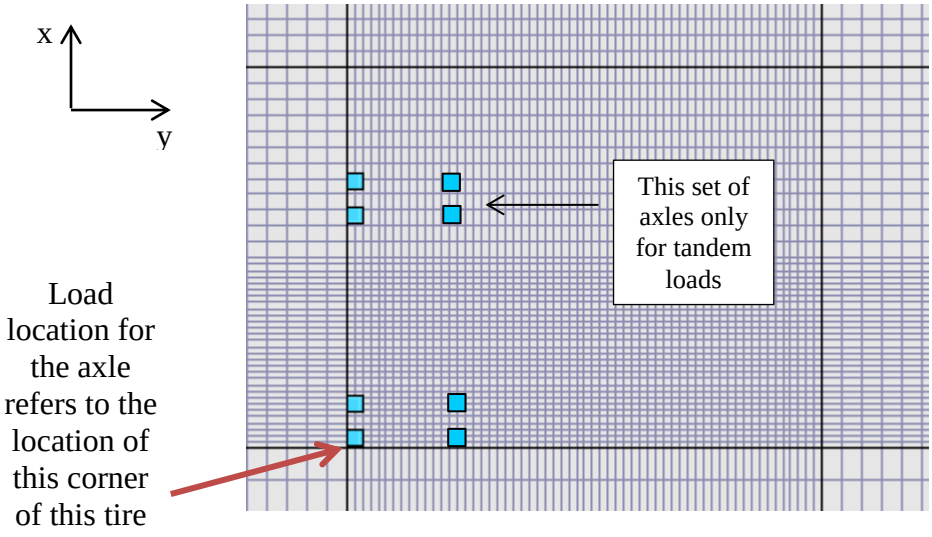

Figure 4.5: Vehicle wander of the axle refers to the location of the lower left corner of the lower left tire

Tandem axle loads were considered as two different loading cases, one with front axle at the joint and one with the rear axle at the joint (as pictured). While neural networks were developed for both cases, currently only the case with the rear axle at the joint is considered in design.

The load transfer efficiency across the longitudinal joints, transverse joints, and between the pavement and shoulder all must be considered in analysis. However, it is conventionally assumed that the load transfer efficiency across the longitudinal joint does not have a large influence on the magnitude of stresses computed in analysis, and a constant value of 50% for the load transfer efficiency across the longitudinal joint between slabs was deemed sufficient to obtain the required accuracy in analysis (Hiller 2007; NCHRP 2003b). Therefore, the value of load transfer efficiency across the longitudinal joint was set at a constant value of 50%, effectively eliminating one variable from the reduced factorial. Load transfer efficiency across the transverse joint and between the pavement and shoulder were left as variables in the reduced factorial.

Some of the assumptions made in the MEPDG concerning materials properties were also made in this program. The coefficients of thermal expansion of both the concrete and the base layer were assumed to be equal, as was Poisson's ratio. Temperature gradients were assumed to vary linearly within the concrete layer and then be constant in the base layer. While the MEPDG assumes that the concrete layer and the base layer can be either fully bonded or completely unbonded, at this time the program only works for the unbonded case, though it could be easily expanded for the bonded case.

The factorial reduction process was used to determine the range of each variable which must be considered. However, to run the factorial in ISLAB2000, values for each variable must be entered, rather than a range. To solve the problem of needing a factorial to create neural networks, but needing a neural network to determine how many values of each variable are needed in the factorial, an initial factorial was created and run in ISLAB2000. The results of this factorial were used to create neural networks and

sensitivity analysis was conducted to determine how many values of each variable were needed to create accurate neural networks.

Table 4.2 shows the unreduced factorial which would be required to cover the range of cases which would be analyzed by the MEPDG. Within the analysis of a single pavement, some of these inputs will not change while others will. For example, in the analysis of a single pavement, the thickness does not change. However, the load transfer efficiency of the joints degrades over time. Therefore, the MEPDG will consider several different values of load transfer efficiency over the life of the pavement. Examining all of the inputs in Table 4.2 shows how large the factorial is for even a single pavement and why a reduced factorial is necessary. If the factorial were not reduced, its size would be truly staggering. If each variable considered in design were given only 5 values (which would not be enough train the neural networks), then the resulting factorial would consist of $1.5*10^{13}$ cases.

Table 4.2: Unreduced Factorial

Ranges of Inputs	Minimum Value	Maximum Value
Concrete Thickness (inches)	4	15
Concrete Elastic Modulus (psi)	2,500,000	8,000,000
Concrete Poisson's Ratio	0.1	0.2
Concrete Coefficient of Thermal Expansion (in/in/°F)	4.10E-06	8.00E-06
Concrete Unit Weight (lbs/in^3)	0.072	0.095
Base Thickness (in)	5	25
Base Elastic Modulus (psi)	12,000	100,000
Base Poisson's Ratio	0.1	0.2
Base Coefficient of Thermal Expansion (in/in/°F)	4.10E-06	7.30E-06
Base Unit Weight (lbs/in^3)	0.072	0.095
Built-in Curl (°F)	-50	10
Slab Width	Standard Width	Widened Slab
Friction Between Layers	Unbonded or Fully bonded	
Modulus of Subgrade Reaction (psi/in)	50	600
Temperature Gradient (°F)	-50	50
Moisture Warping (°F)	-25	0
Load Weight (lbs)	0	120,000
Vehicle wander in x-direction (in)	0	48
Transverse Load Transfer Efficiency (%)	1	95

4.3 Factorial Reduction Method

To reduce the factorial, the original system is transformed into an equivalent single layer system. This equivalent system is similar to the original system and was used to define the range of values considered in the factorial used to train the neural networks. In order to fully realize the benefits of the factorial reduction process, stress analysis was conducted on a third system, the neural network system. This system is defined in similar space. The majority of the properties in this system were held constant, which greatly reduced the number of cases the factorial had to consider. To ensure that the reduced factorial would cover all possible cases of the original system that the program

could consider, the equivalent system was used to define the range of values covered by the variables used to define the neural network system. The solutions to analysis of the neural network system will be used to calculate the solutions in the original system (a process discussed in Chapter 6.

4.3.1 Equivalent Single Layer System

Two systems are considered to be similar if their deflection basins are proportional. The equivalent single layer system of a concrete pavement system is the single layer system with the properties necessary to ensure that it is similar to the original concrete pavement system (further details given in 2.6.2). To define the equivalent system, an equivalent concrete thickness and equivalent unit weight are determined using equations (2.23) through (2.25). By changing to an equivalent system, the base layer is eliminated. This also eliminates the need to vary all variables associated with the base layer.

If a temperature gradient is present, it must be converted to equivalent linear temperature gradients. The equivalent linear temperature gradient applied to the equivalent single layer system is a linear temperature gradient which causes the same bending moment distribution as the non-linear gradient induces in the original two layer system. This temperature gradient is computed using equations (2.33) and (2.34) for the unbonded and bonded cases, respectively.

4.3.2 Neural Network System

The neural network system is the system which will be used to conduct the finite element analysis in similar space. Results from this analysis will be used to create the neural networks, also in similar space. The program will use the results from the neural network to compute stresses in the original system by transforming them from similar space back into real space, as will be discussed in Chapter 6. The neural network system differs from the equivalent system in that it has constant values for most its defining variables, regardless of which original system it is similar to.

4.3.3 Variable Elimination

Each of the variables in the unreduced factorial was examined in turn to determine which were suitable for variation in the reduced factorial, and which should be held constant. The criteria considered included how the variable is used in the MEPDG and in ISLAB2000, and if it was possible to eliminate the variable during the factorial reduction process. By converting the two layer slab system in to an equivalent single layer slab system, the need to vary all properties associated with the base layer was eliminated. For the remaining parameters, it was determined that concrete thickness, unit weight, coefficient of thermal expansion and Poisson's ratio would be held constant, as would the modulus of subgrade reaction and load transfer efficiency across the longitudinal joint. The values used for each of these variables are shown in Table 4.3. These variables will be used to define the neural network system, as discussed in Section 4.4. Concrete modulus of elasticity and temperature gradient would be varied in order to analyze systems with a variety of radii of relative stiffness and Korenev's non-dimensional temperature gradients. Slab geometry, load transfer efficiency across the transverse and shoulder joints, and load weight and location must remain variable either because of how the ISLAB2000 works or because they are not included in any equivalencies and therefore cannot be eliminated.

Table 4.3: Values of Variables Held Constant in Reduced Factorial

Variable Held Constant	**Value**
Concrete Thickness	10 in
Concrete Unit Weight	0.087 lbs/in^3
Concrete Coefficient of Thermal Expansion	$4.4*10^{-6}$
Concrete Poisson's Ratio	0.15
Modulus of Subgrade Reaction	250 psi/in

Variables from the unreduced factorial defining the neural network system are eliminated by examining each of the equivalencies in turn and determining the theoretical range of one variable necessary to ensure that the same range of all parameters is considered while

holding all other variables constant as it would be if all variables were varied. It should be noted that this theoretical range of variables defining the neural network system in similar space is not always a practical range for the variable, but is a mathematically necessary one. The parameters considered during variable elimination are the radius of relative stiffness ℓ, Korenev's non-dimensional temperature gradient ϕ, the equivalent linear temperature gradient ΔT_{equiv}, and the equivalent unit weight γ_{equiv}.

4.3.3.1 *Equivalent Thickness*

As was discussed in Section 4.3, the original two layer system is converted to an equivalent single layer system. A minimum and maximum value for h_{eq} is computed using equations (2.23) and (2.24) for the unbonded and bonded cases, respectively. The values for all of the variables needed for this are taken from the unreduced factorial, as given in Table 4.2. Similarly, minimum and maximum values for γ_{eq} are determined using equation (2.25). As long as the entire range of h_{eq} and γ_{eq} is considered in the factorial, there will be an equivalent slab which corresponds to all possible combinations of concrete layer and base layer properties. This eliminates the need to vary the base thickness, elastic modulus, unit weight, coefficient of thermal expansion, Poisson's ratio, and the friction coefficient between layers.

The parameter equivalent unit weight is examined to determine if the range on h_{eq} as computed using equations (2.23) and (2.24) is sufficient to ensure that all cases considered in the unreduced factorial will be captured by the reduced factorial. The range of γ_{eq} ($\gamma_{eq,min}$ and $\gamma_{eq,max}$) was calculated using (2.25) using all possible combinations of the input variables given in Table 4.2. As long as this range of γ_{eq} is achieved, there will be an equivalent slab which corresponds to all possible combinations in the unreduced factorial.

It was previously determined that, in the reduced factorial, h and γ would be held constant. However, because h_{eq} and γ_{eq} are equal to h_{const} and γ_{const}, respectively, in the equivalent single layer system, the only way to ensure that the appreciate range of γ_{eq} is

achieved is to ensure that a wide enough range of h_{eq} is used in the remainder of the factorial reduction process. This range of h_{eq} was calculated as:

$$h_{eq} = \frac{\gamma_{const} h_{const}}{\gamma_{eq}} \tag{4.1}$$

Where:

γ_{eq} = equivalent unit weight

γ_{const} = constant value of unit weight in the reduced factorial

h_{const} = constant value of concrete thickness in the reduced factorial

The values of γ_{const} and h_{const} for the reduced factorial are given in Table 4.3. The range of h_{eq} computed is used when determining the reduced factorial. This eliminates the need to vary the unit weight of the concrete in the reduced factorial.

4.3.3.2 *Korenev's Equivalent Slab*

The principles of Korenev's equivalent slab concept (Khazanovich et al. 2001; Korenev & Chernigovskaya 1962) are applied to the previously determined equivalent single layer system. To use Korenev's equivalent slab, it is necessary that the radius of relative stiffness and Korenev's equivalent temperature gradient of the equivalent single layer system equal those of the original system. Therefore, both of these parameters can be used to eliminate variables for the factorial.

The possible range on ℓ was calculated using equation (2.15), the values from the unreduced factorial given in Table 4.2 for E_{PCC}, $\mu_{PCC,}$ and k, and using h_{eq} as determined from equations (2.23) and (2.24) for the unbonded and bonded cases, respectively. As long as this range of ℓ is achieved, there will be an equivalent slab which corresponds to all possible combinations in the unreduced factorial.

It was previously decided that, in the reduced factorial, h, μ, and k would be held constant. Therefore, the range of E_{PCC} necessary to achieve the required range of ℓ was determined:

$$E = \frac{12\ell^4\ (1-\mu_{const}^2)k_{const}}{h_{const}^3} \tag{4.2}$$

Where:

E = modulus of elasticity in the reduced factorial

ℓ = radius of relative stiffness calculated from the unreduced factorial

μ_{const} = constant value of Poisson's ratio in the reduced factorial

k_{const} = constant value of modulus of subgrade reaction in the reduced factorial

h_{const} = constant value of concrete thickness in the reduced factorial

The values of μ_{const}, k_{const}, and h_{const} for the reduced factorial are given in Table 4.3. The range of E as determined using (4.2) is not necessarily a practical range of modulus of elasticity that would be seen for a concrete pavement, but it is a range which will account for all cases of ℓ in the unreduced factorial while varying only one variable instead of four.

The possible range on ϕ was calculated using Korenev's non-dimensional temperature gradient, ϕ, as given by equation (2.37). The values from the unreduced factorial given in Table 4.2 for α_{PCC}, μ_{PCC} and k, and h_{eq} as determined from equations (2.23) and (2.24) for the unbonded and bonded cases, respectively were used in this computation. As long as this range of ϕ is achieved, there will be an equivalent slab which corresponds to all possible combinations in the unreduced factorial.

It was previously decided that, in the reduced factorial, h, μ, and k would be held constant. Therefore, the range of ΔT necessary to achieve the required range of ϕ must be determined. However, this is complicated by the fact that ϕ is a function of ℓ, which will vary as E_{PCC} is varied in the reduced factorial. This can be overcome by

demonstrating that variation in E_{PCC} does not cause variation in ϕ. However, further complications arise from the fact that ϕ for the similar system is dependent on the original temperature gradient ΔT, as well as the equivalent temperature gradient due to built-in curl ΔT_{BIC} and warping ΔT_{warp}, while ϕ for the original system is only dependent on the original temperature gradient ΔT. Accounting for this, the range of temperature gradients which must be considered is computed using:

$$\Delta T_{NN} = \frac{\alpha_{eq}(1+\mu_{eq})k_{eq}h_{NN}^2\gamma_{NN}}{\alpha_{NN}(1+\mu_{NN})k_{NN}h_{eq}^2\gamma_{eq}} * (\Delta T_{BIC} + \Delta T_{warp}) + \frac{\alpha_{orig}(1+\mu_{orig})\sqrt{\frac{E_{orig}h_{orig}^3}{12(1-\mu_{orig}^2)k_{orig}}}k_{orig}h_{NN}^2\gamma_{NN}}{\alpha_{NN}(1+\mu_{NN})\sqrt{\frac{E_{eq}h_{eq}^3}{12(1-\mu_{eq}^2)k_{eq}}}k_{NN}h_{orig}^2\gamma_{orig}}\Delta T_{orig} \quad (4.3)$$

Where:

α_{orig} = the coefficient of thermal expansion of the concrete for the original system

μ_{orig} = Poisson's ratio of the concrete in the original system

k_{orig} = the modulus of subgrade reaction of the original system

ΔT_{orig} = the temperature gradient applied to the original system

h_{orig} = the thickness of the concrete layer in the original system

γ_{orig} = the unit weight of the concrete in the original system

α_{eq} = the coefficient of thermal expansion of the concrete for the equivalent system

μ_{eq} = Poisson's ratio of the concrete in the equivalent system

k_{eq} = the modulus of subgrade reaction of the equivalent system

h_{eq} = the thickness of the concrete layer in the equivalent system

γ_{eq} = the unit weight of the concrete in the equivalent system

α_{NN} = the coefficient of thermal expansion of the concrete for the neural network system

μ_{NN} = Poisson's ratio of the concrete in the neural network system

k_{NN} = the modulus of subgrade reaction of the neural network system

ΔT_{NN} = the temperature gradient applied to the neural network system

h_{NN} = the thickness of the concrete layer in the neural network system

γ_{NN} = the unit weight of the concrete in the neural network system

Recalling from the definition of the equivalent system that the moduli of elasticity in the equivalent system and the original system are equal, it can be seen that though the temperature gradient in the neural network system is dependent on the modulus of elasticity in the original system, it does not vary with changes in E_{orig}. This means that while ΔT_{NN} must be varied in the reduced factorial in order to ensure that a proper range of values of ϕ are considered, ϕ varies only with ΔT_{NN}, and not also with E_{PCC}. This also eliminates the need to vary several variables in the reduced factorial.

4.3.3.3 *Summary of Variable Elimination*

Using these equivalencies, a factorial can be designed which varies only nine ISLAB2000 inputs, but is comparable to changing all 20 required inputs, see Table 4.4. This table also shows the ranges of each variable for which the finite element factorial will be run. The ISLAB2000 analysis will be run for an equivalent single layer system with the properties given in Table 4.4. With the exception of elastic modulus, all material properties will be held constant.

Table 4.4: Factorial in Similar Space

Variable Inputs			**Constant Inputs**	
Variable	Min value	Max value	Variable	Value
E pcc (psi)	51,290	153,078,333	h eq (in)	10
ΔT (°F)	-92	92	mu	0.15
load (lbs)	0	121k	CTE (in/in/°F)	$4.40*10^{-6}$
load x (in)	0	midslab	γ (lb/in^3)	0.087
load y (in)	At transverse joint or longitudinal edge		subgrade k (psi/in)	250
LTE transverse (%)	20	95	LTE long (%)	50

4.4 Neural Network Development

The factorial of equivalent variables determined in Chapter 4was run in ISLAB2000 to create a database from which neural networks were trained in similar space using Monte Carlo Random Hierarchical Partitioning. The neural networks output stresses at different nodes in the finite element model. From these stresses, both the maximum stress and the stress range can be determined, and transfer functions can be used to convert these stresses into damage using transfer functions.

4.4.1 Neural Network Construction

The factorial of cases considered was divided into sub categories for ease of creating neural networks. While a large number of variables can be considered in a neural network, adding more variables increases the complexity of the system. It was therefore determined that the number of variables considered by each neural network would be limited to considering the five variables necessary to describe the neural network system, as determined in Section 4.3.3: modulus of elasticity of the concrete E, aggregate interlock factor, tire pressure, temperature gradient, and lateral vehicle wander.

When creating the finite element models in ISLAB2000, natural divisions in the factorial resulted based on the types of considered. For example, ISLAB2000 does not allow the slab sized to be changed within a batch file; therefore the standard width and widened lane cases were considered separately. These natural divisions resulted in creating separate neural networks for each combination of slab width, shoulder type, and axle type considered.

Limiting the neural networks to only considering five variables each also mean that each neural network considered only one analysis point (see Section 4.1). Creating more neural networks had the added advantage of making small batch files, which were more manageable and did not push the limits of the computer programs needed to process the data.

The factorial reduction process and variable elimination discussed in Section 4.3.3 used the intermediate variables of radius of relative stiffness, ℓ, and Korenev's non-dimensional temperature gradient, ϕ, to determine the required values of modulus of elasticity E and temperature gradient ΔT, respectively. When determining the distribution of the values of modulus of elasticity and temperature gradient used in the factorials, better agreement in the neural networks was found when evenly distributed values of ℓ and ϕ were used to computed E and ΔT for the factorial, rather than simply evenly distributing the required number of values for E and ΔT across their respective ranges.

The values of radius of relative stiffness and associated values of modulus of elasticity used in the factorial are given in Table 4.5. The distribution of values of radius of relative stiffness was selected to have more values ion the standard range seen in typical pavements, and fewer outlying values. This is because, for very high values of radius of relative stiffness, the pavement becomes so stiff that stresses due to load and temperature variation no longer change significantly with changes in stiffness. In contrast, at low values of stiffness, stress in the pavement is highly sensitive to changes in the radius of relative stiffness.

Table 4.5: Values of Radius of Relative Stiffness and Associated Values of Elastic Modulus used in the Reduced Factorial

Radius of Relative Stiffness (in)	Elastic Modulus (psi)
11.5	51,290
15	148,458
18	307,842
21	570,316
25	1,145,508
28	1,802,479
33	3,477,713
38	6,114,661
45	12,025,083
50	18,328,125
60	38,005,200
85	153,078,333

The values of Korenev's non-dimensional temperature gradient and associated values of temperature gradient used in the factorial are shown in Table 4.6. The distribution of values of Korenev's non-dimensional temperature gradient was selected to be evenly distributed across the entire range of potential values and to include a value of zero. It is particularly important that analysis be conducted for the case of no temperature gradient because the slab will respond differently to the case of axle loads only than it will to combined axle and thermal loads and it is important that the neural network be able to accurately capture this behavior. Additionally, the case of zero temperature gradient is often an inflection point in the curve of stress versus temperature, which is important in neural network development.

Table 4.6: Values of Korenev's Non-Dimensional Temperature Gradient and Associated Values of Temperature Gradient used in the Reduced Factorial

Korenev's Non-Dimensional Temperature Gradient ϕ	**Temperature Gradient ΔT (°F)**
-193.298	-92
-128.865	-60
-64.4326	-30
0	0
64.43261	30
128.8652	60
193.2978	92

Unlike temperature gradient and elastic modulus, load transfer efficiency across the transverse joint is a parameter that was not used in the factorial reduction process. However, the values of load transfer efficiency used in the factorial must be carefully considered because they must be inputted into the finite element program as aggregate interlock factors. This is made complicated by the fact that load transfer efficiency and aggregate interlock are not linearly related. The values of load transfer efficiency and associated values of aggregate interlock factor used in the reduced factorial are shown in Table 4.7. The distribution of values of load transfer efficiency was selected to be fairly even across the range of potential values. However, because of the non-linear relation between load transfer efficiency and aggregate interlock factor, it was necessary to have a distribution of values of load transfer efficiency that was slightly skewed towards higher values to ensure that the range of values of aggregate interlock factor was adequately represented. This is discussed in further detail in Section 4.4.3.3.

Table 4.7: Values of Load Transfer Efficiency and Associated Values of Aggregate Interlock Factor used in the Reduced Factorial

Load Transfer Efficiency (%)	Aggregate Interlock Factor
20.0	2069
40.0	6569
60.0	17073
75.0	38627
87.1	100000
92.4	200000
95.0	339702

Once all values of the variables in the reduced factorial were selected, the factorial was run. The factorial is given in Table 4.8 for the standard width slabs, and Table 4.9 for the widened slabs. Recall from Section 4.3.3 that the values used in the reduced factorial are not representative of typical values for material properties seen in the field. Instead, they are mathematically necessary values needed to ensure that all cases in the unreduced factorial are properly considered in the reduced factorial. The main difference between the factorials for the standard and widened slab cases is the location of the load in the x-direction. This is because wider slabs required that the load be placed at more locations before reaching mid-slab. For both the standard width and the widened slabs, symmetry eliminated the need to place the load further from the shoulder than mid-slab.

Table 4.8: Reduced ISLAB2000 Factorial for Standard Width Slabs

Concrete Elastic Modulus (psi)	**Transverse Joint Aggregate Interlock Factor**	**Tire Pressure (psi)**	**Temperature Gradient (°F)**	**Vehicle wander in the x-Direction from Longitudinal Edge (in)[+]**	**Shoulder Aggregate Interlock Factor**	**Axle Type**
51,920	2069.045	0	-92	0	2069.045 (AC Shoulder)	Single Axle
148,458	6569.001	21.481	-60	6		
307,842	17073.41	42.963	-30	12		Tandem Axle (reference front axle)
570,316	38626.95	66.831	0	18	10590.333 (PCC Shoulder)	
1,145,508	100000	131.687	30	24		
1,802,479	200000	197.531	60	30		Tandem Axle (reference rear axle)
3,477,713	339702	329.218	92	36		
6,114,661		663.923		42		
12,025,083				48		
18,328,125						
38,005,200						
153,078,333						

[+] Vehicle wander is refers to the location of the lower left corner of the lower left tire on the axle

Table 4.9 Reduced ISLAB2000 Factorial for Widened Slabs

Concrete Elastic Modulus (psi)	Transverse Joint Aggregate Interlock Factor	Tire Pressure (psi)	Temperature Gradient (°F)	Vehicle wander in the x-direction from Longitudinal Edge (in)[+]	Shoulder Aggregate Interlock Factor	Axle Type
51,920	2069.045	0	-92	0	2069.045 (AC Shoulder)	Single Axle
148,458	6569.001	21.481	-60	6		
307,842	17073.41	42.963	-30	12		Tandem Axle (reference front axle)
570,316	38626.95	66.831	0	18	10590.333 (PCC Shoulder)	
1,145,508	100000	131.687	30	24		
1,802,479	200000	197.531	60	30		
3,477,713	339702	329.218	92	36		Tandem Axle (reference rear axle)
6,114,661		663.923		42		
12,025,083				48		
18,328,125				54		
38,005,200				60		
153,078,333				66		
				72		
				78		
				84		

[+] Vehicle wander is refers to the location of the lower left corner of the lower left tire on the axle

An additional set of factorials was created to analyze the stresses in the y-direction when the load was placed at mid-slab (y = 90 in from transverse edge). This factorial was used to for comparison purposes and to determine cracking potential, as will be discussed in Chapter 5. These factorials are shown in Table 4.10 for the standard width slab and Table 4.11 for the widened slab. In these factorial, the location of the load in the x-direction correspond to evaluation points used in Gauss integration; this method was used in the development of the JPCP transverse cracking model (NCHRP 2003a). Additionally, loads were placed at x = 0 and x = 18 inches from the lane edge. For the

standard width slabs, the lane edge corresponds to the slab edge, while, for the widened slabs, the lane edge is 24 inches from the slab edge.

Table 4.10: Reduced ISLAB2000 Factorial for Standard Width Slabs with Load at Mid-Slab

Concrete Elastic Modulus (psi)	**Transverse Joint Aggregate Interlock Factor**	**Tire Pressure (psi)**	**Temperature Gradient (°F)**	**Vehicle wander in the x-Direction from Longitudinal Edge (in)[+]**	**Shoulder Aggregate Interlock Factor**	**Axle Type**
51,920	2069.045	0	-92	0	2069.045 (AC Shoulder)	Single Axle
148,458	6569.001	21.481	-60	2.64		
307,842	17073.41	42.963	-30	5.36		Tandem Axle (reference front axle)
570,316	38626.95	66.831	0	7.445	10590.333 (PCC Shoulder)	
1,145,508	100000	131.687	30	10.45		
1,802,479	200000	197.531	60	18		
3,477,713	339702	329.218	92			
6,114,661		663.923				
12,025,083						
18,328,125						
38,005,200						
153,078,333						

[+] Vehicle wander is refers to the location of the lower left corner of the lower left tire on the axle

Table 4.11: Reduced ISLAB2000 Factorial for Widened Slabs with Load at Mid-Slab

Concrete Elastic Modulus (psi)	Transverse Joint Aggregate Interlock Factor	Tire Pressure (psi)	Temperature Gradient (°F)	Vehicle wander in the x-Direction from Longitudinal Edge (in)[+]	Shoulder Aggregate Interlock Factor	Axle Type
51,920	2069.045	0	-92	24	2069.045 (AC Shoulder)	Single Axle
148,458	6569.001	21.481	-60	26.64		
307,842	17073.41	42.963	-30	29.36		Tandem Axle (reference front axle)
570,316	38626.95	66.831	0	31.445	10590.333 (PCC Shoulder)	
1,145,508	100000	131.687	30	34.45		
1,802,479	200000	197.531	60	42		
3,477,713	339702	329.218	92			
6,114,661		663.923				
12,025,083						
18,328,125						
38,005,200						
153,078,333						

[+] Vehicle wander is refers to the location of the lower left corner of the lower left tire on the axle

4.4.2 Neural Network Validation

Validating the neural networks is a multi-step process. First the data which was used to train the networks is run through them to ensure that they can predict solutions which they are guaranteed to know. This mainly tests that the neural networks were built correctly. Then, the predictive abilities of the neural networks are tested by presenting them with cases which are different from the training data; these cases are called testing data. For both the training and testing data, the neural network solutions are compared to finite element solutions. This testing is performed in similar space because the neural networks were trained in similar space. To determine how the neural networks predictions compare with results in real space and the ensure that neither under- nor over-fitting has occurred, sensitivity analysis. Data was still presented to the neural networks

in similar space, but the results were transformed back into real space to conduct the sensitivity analysis.

4.4.2.1 *Validation with Training Data*

The first step in ensuring that the neural networks are functioning properly is to create plots of the stresses predicted by the neural networks compared with the actual stresses observed in the pavement. Initially, the same cases used to train the neural network are presented to the again, though without the solution. A sample predicted versus measured plot for the training data are shown in Figure 4.6. From this plot, it can be seen that the neural networks can predict the training data quite accurately. Similar results were found for the other neural networks created.

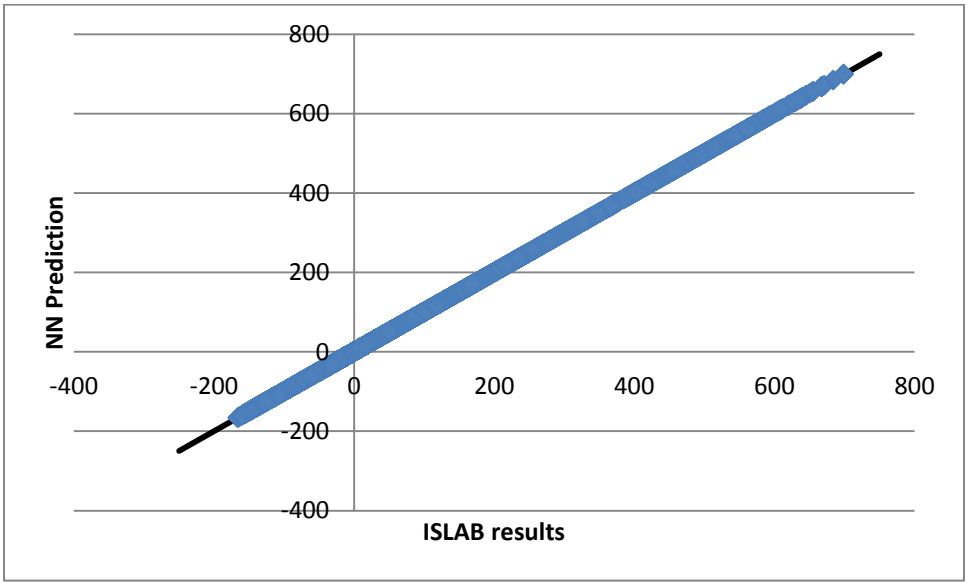

Figure 4.6:Comparison of stresses in similar space predicted for training data by the neural network versus the actual value of those stresses from finite element modeling for neural network 12x15AC_SAy0node1940.

4.4.2.2 *Validation with Testing Data*

Predicted versus measured plots for the training data show that the neural networks are functioning properly, however, for neural networks to be usable in the design program, they must have the ability to predict stresses for cases not included in the training data. To test this ability, many cases different than those used in training were analyzed in

ISLAB2000; these testing cases were also presented to the neural networks. A sample predicted versus measured plot for the testing data is shown in Figure 4.7. From this plots, it can be seen that there is good agreement between the stresses predicted by the neural networks and the actual stresses. This shows that the neural networks can accurately predicted stresses for cases not included in the training set. Similar results were found for the other neural networks created.

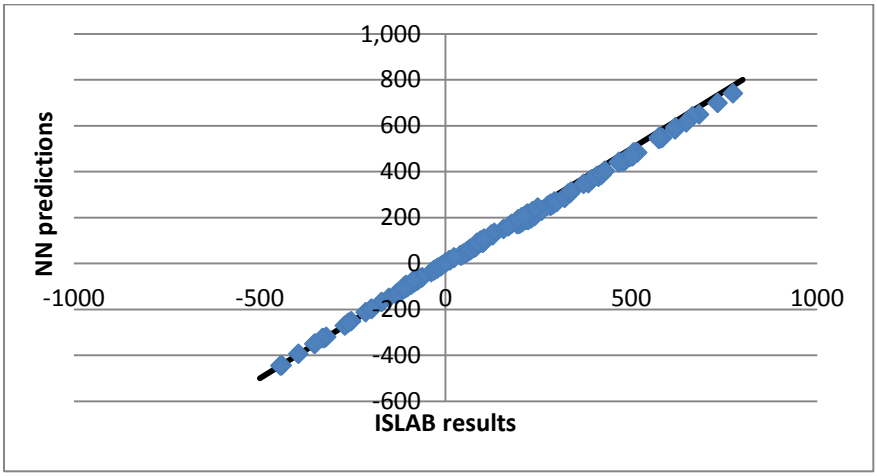

Figure 4.7 Comparison of stresses in similar space predicted for testing data by the neural network versus the actual value of those stresses from finite element modeling for neural network 12x15AC_TAy0y51node1950.

4.4.3 Sensitivity Analysis

The factorial reduction process was used to determine the range of each variable which must be considered. However, to run the factorial in ISLAB2000, values for each variable must be entered, rather than a range. The process used to determine how many values for a given variable are needed to cover the entire range of that variable is related to the functionality of the neural networks. For properly functional neural networks, enough training values are needed to capture variation within the data. For each variable considered, the required number of data points was determined via trial and error. Sensitivity analysis was conducted to ensure that enough data points were used. The final results of these analyses are presented for each variable in turn.

4.4.3.1 *Modulus of Elasticity*

For the modulus of elasticity, it was determined that 12 data points were needed to train the neural networks. Because the magnitude of the range of values of E is much larger than that of the other variables in the reduced factorial, the possibility of manipulating the range of values of E presented to the neural network was explored. Rather than training the neural networks using the values of E for which the ISLAB2000 runs were conducted, the value of log (E) was used instead. The sensitivity analyses conducted for the neural network developed with 12 data points and trained using values of E were repeated for the neural network trained with values of log (E). The results of these analyses are shown in Figure 4.8 and Figure 4.9. From these figures, it can be seen that a good fit was achieved. Training the neural networks on value of log (E) instead of E improved the fit of the neural network slightly over the neural networks trained only on E. This is particularly noticeable for smaller values of E.

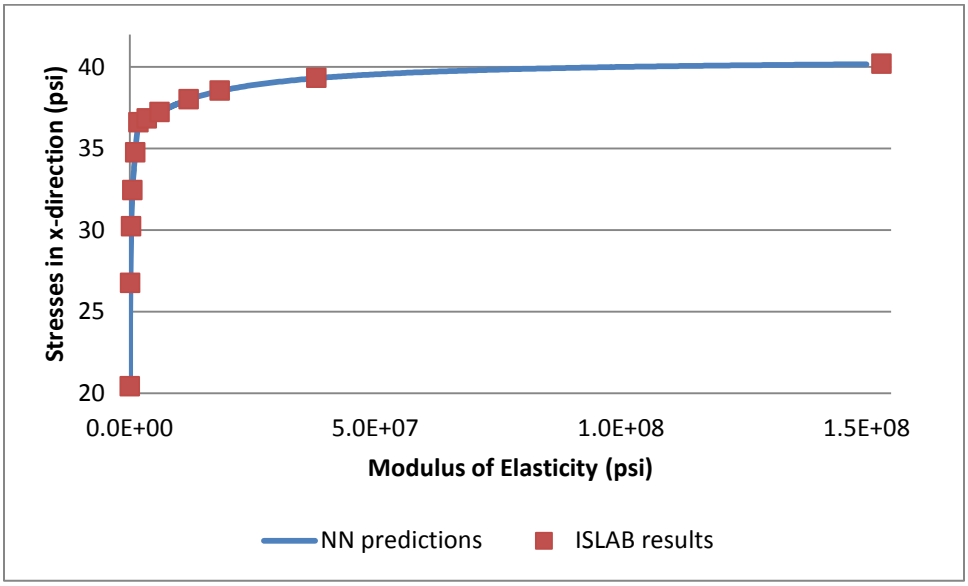

Figure 4.8: Sensitivity analysis for variation in E for a neural network trained with twelve values of Log (E). Constants used for the analysis were: T = -30°F, aggregate interlock factor across the transverse joint = 2070, tire pressure = 52.51 psi, and load reference location in x = 12 in from shoulder joint

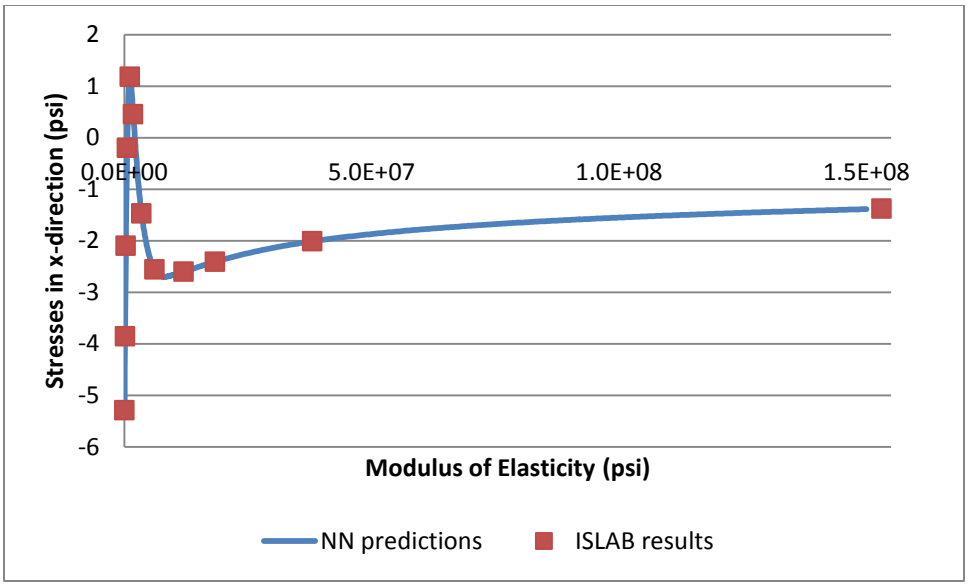

Figure 4.9: Sensitivity analysis for variation in E for a neural network trained with twelve values of Log (E). Constants used for the analysis were: T = 30°F, aggregate interlock factor across the transverse joint = 6569, tire pressure = 42.96 psi, and load reference location in x = 24 in from shoulder joint

4.4.3.2 *Temperature*

Seven values of temperature gradient were used to train the neural network. The results of sensitivity analyses for variation in temperature gradient with two different sets of variables are shown in Figure 4.10 and Figure 4.11. From these figures, it can be seen that neither over- nor under-fitting seem to be occurring. While it appears from Figure 4.10 that the variation in stress with temperature is fairly linear and could possibly be characterized with fewer points, it can be seen in Figure 4.11 that all of the training points are necessary to ensure a proper fit. This also illustrates the importance of considering several cases in the sensitivity analysis, as some cases may indicate that fewer training points are necessary than other cases require.

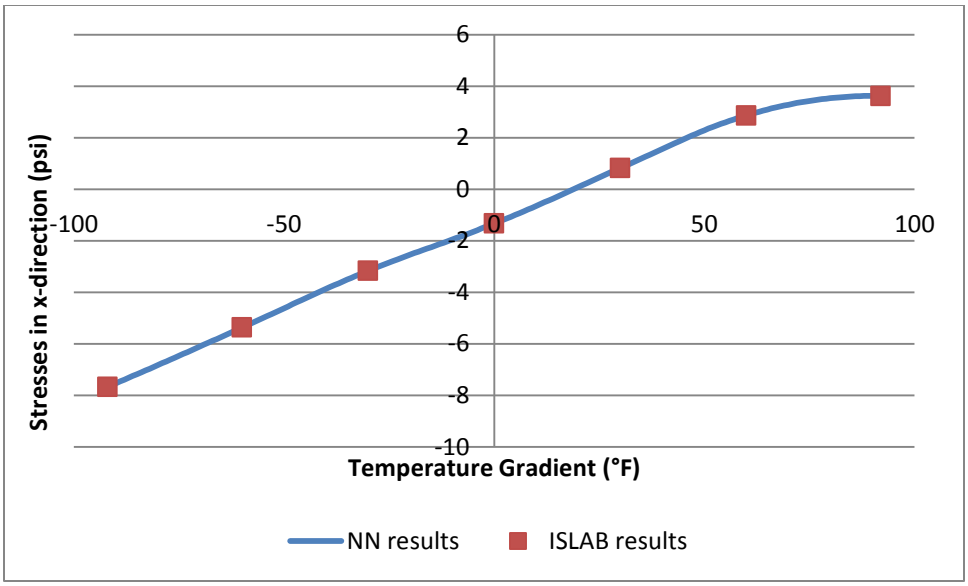

Figure 4.10: Sensitivity analysis for variation in temperature gradient for a neural network trained with seven values of temperature gradient. Constants used for the analysis were: E = 307842 psi, aggregate interlock factor across the transverse joint = 38627, tire pressure = 14.32 psi, and load reference location in x = 48 in from shoulder joint

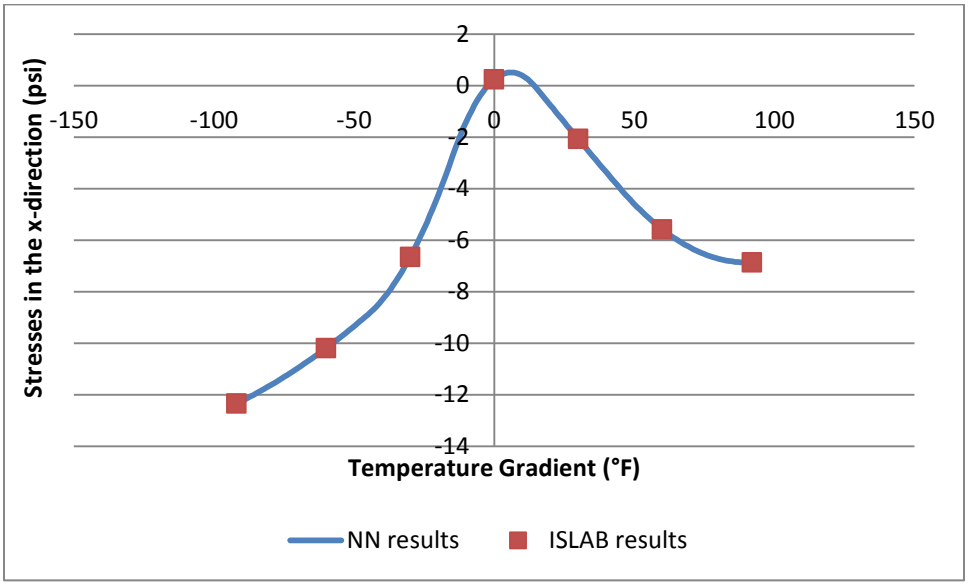

Figure 4.11: Sensitivity analysis for variation in temperature gradient for a neural network trained with seven values of temperature gradient. Constants used for the analysis were: E = 6114661 psi, aggregate interlock factor across the transverse joint = 6569, tire pressure = 66.83 psi, and load reference location in x = 24 in from shoulder joint

4.4.3.3 *Load Transfer Efficiency*

Load transfer efficiency is quantified in ISLAB2000 using the aggregate interlock factor (AGG) given by (Crovetti 1994):

$$AGG = \frac{0.00546 * k * \ell}{\left(\frac{1}{LTE} - 0.01\right)^{1.178}} \tag{4.4}$$

Initially, five values of AGG were used to train the neural networks, however, it was determined that this was not enough data points. Therefore, additional data points were added in areas where the sensitivity analysis showed poor performance. This resulted in using 7 data points to train the neural networks. The results of the sensitivity analysis conducted on neural networks trained with 7 values of AGG are shown in Figure 4.12 and Figure 4.13. From these figures, it can be seen that a good fit was achieved.

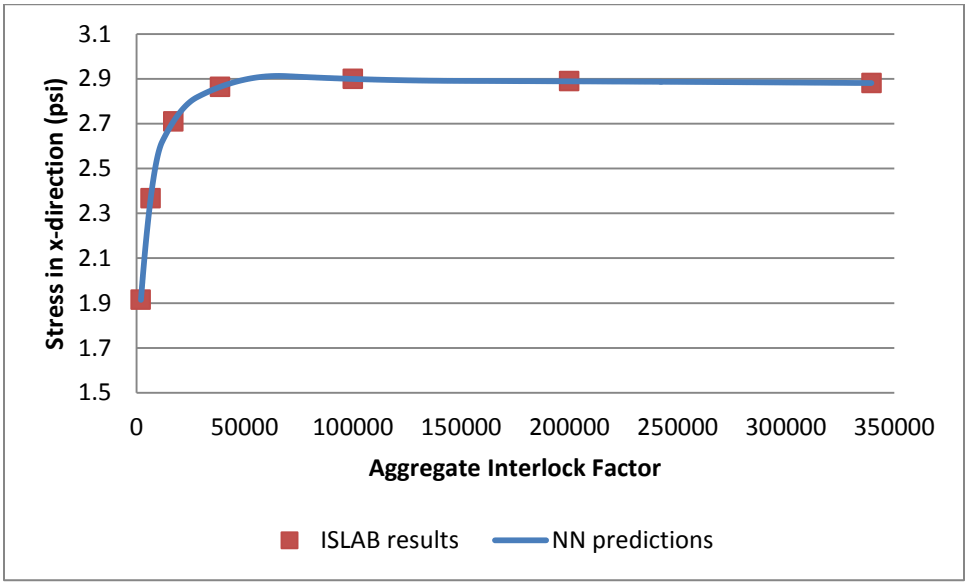

Figure 4.12: Sensitivity analysis for variation in load transfer efficiency for a neural network trained with seven values of aggregate interlock factor. Constants used for the analysis were: E = 307842 psi, temperature gradient =60°F, tire pressure = 14.32 psi, and load reference location in x = 48 in from shoulder joint.

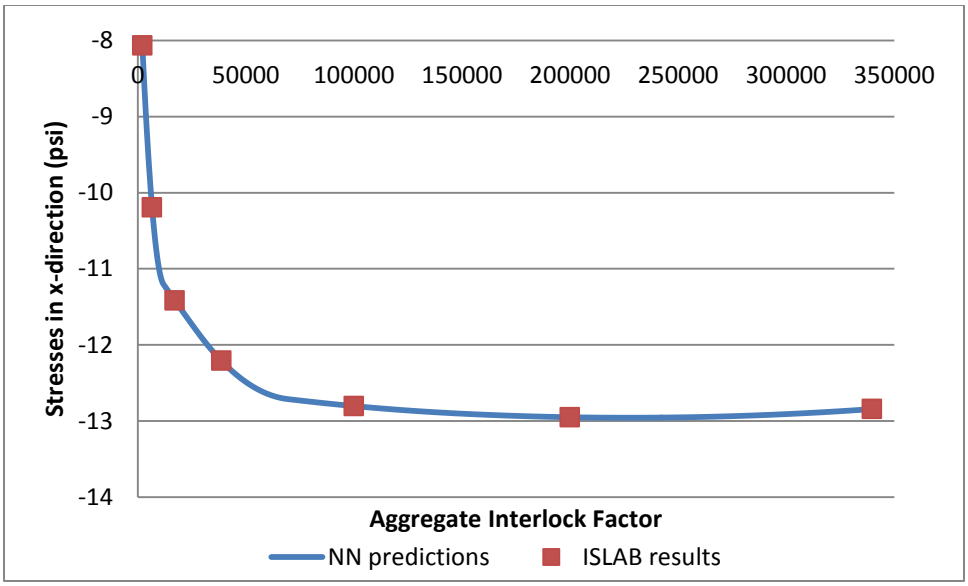

Figure 4.13: Sensitivity analysis for variation in load transfer efficiency for a neural network trained with seven values of aggregate interlock factor. Constants used for the analysis were: E = 6114664 psi, temperature gradient = -60°F, tire pressure = 66.83 psi, and load reference location in x = 24 in from shoulder joint.

4.4.3.4 *Load*

Within the factorial, loads are input as a tire pressure distributed over a tire footprint. Given that the same tire footprint was used for all cases, only tire pressure varied as the load varied. Initially, six values of tire pressure were used to train the neural networks and results were found to be quite linear in all cases. It was determined that the number of data points could be reduced to four while maintaining quality of fit.

After stress analysis had been conducted for the four values of tire pressure identified, it was determined that a unit conversion error had been made when determining the values of tire pressure to use, and that they all should have been ten times larger. Rather than disregarding the already conducted stress analysis, new analyses were conducted over a wider range of tire pressure and the finite element data for the two data sets were merged. The sensitivity analysis was repeated for the new data set containing seven points to ensure that this number of points produced acceptable neural networks. Results of this analysis are shown in figures Figure 4.14 and Figure 4.15. From these figures, it can be

seen that a good level of accuracy was achieved. It was determined from these figures that merging the two training data sets (and thereby providing more data than is necessary for very low ranges of tire pressure) did not in any way decrease the predictive capabilities of the neural networks.

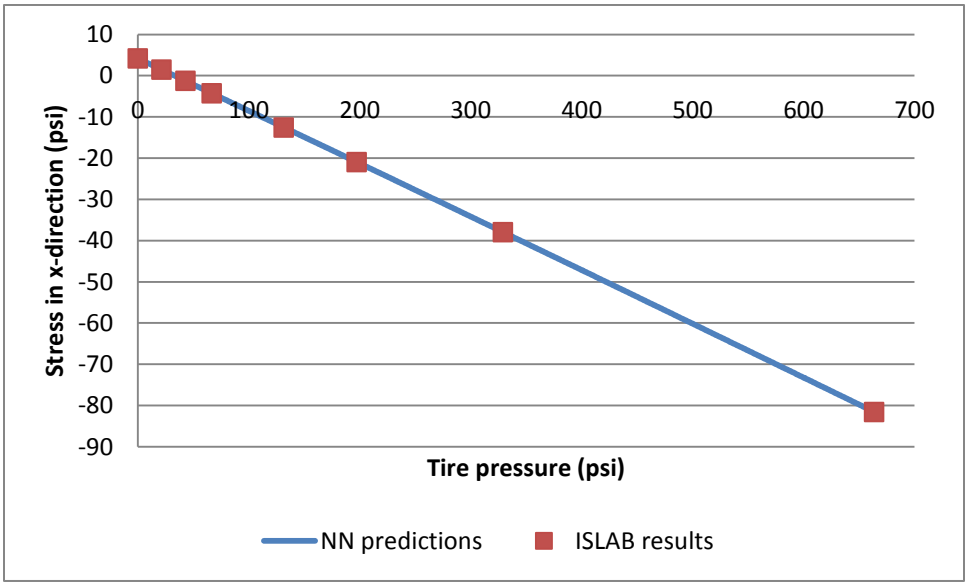

Figure 4.14: Sensitivity analysis for variation in load for a neural network trained with eight values of tire pressure. Constants used for the analysis were: E = 307842 psi, temperature gradient =60°F, aggregate interlock factor =6569, and load reference location in x = 48 in from shoulder joint.

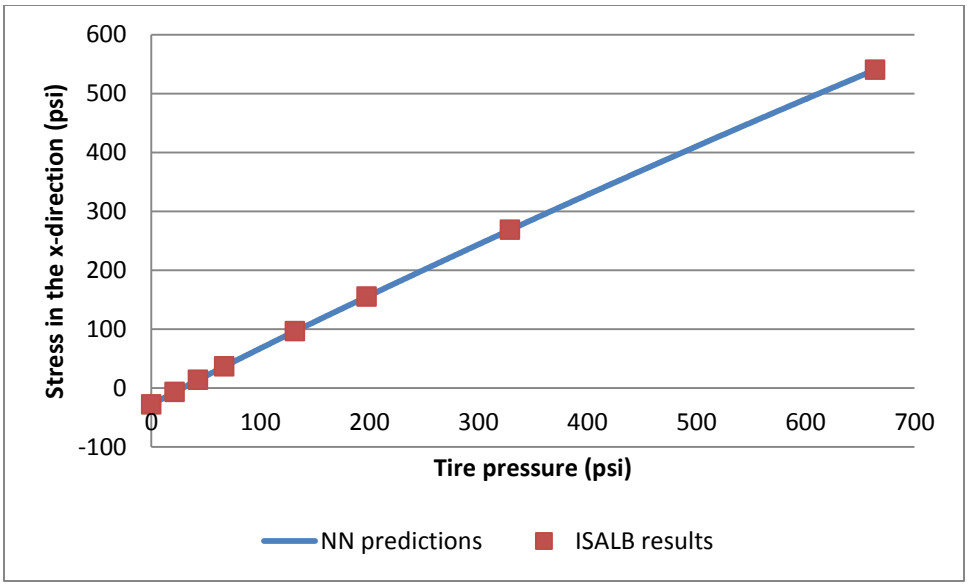

Figure 4.15: Sensitivity analysis for variation in load for a neural network trained with eight values of tire pressure. Constants used for the analysis were: E = 6114664 psi, temperature gradient = -60°F, aggregate interlock factor = 38627, and load reference location in x = 24 in from shoulder joint.

4.4.3.5 *Vehicle Wander*

Initially, a spacing of 12 inches was considered between values of the vehicle wander in the x-direction. This translated into five values of vehicle wander in the x-direction for the standard width slab and eight values for the widened slab being used to train the neural networks. The results of sensitivity analyses for neural networks created with these values of vehicle wander showed that the variation was not well captured.

To improve the performance of the neural networks, they were retrained using a six inch spacing for the load locations in the x-direction. This translated into nine values of vehicle wander in the x-direction for the standard width slab and 15 values for the widened slab. The sensitivity analyses conducted for the neural network developed with five data points for the standard width slab were repeated for the neural network developed with nine data points. The results of these analyses are shown in Figure 4.16 and Figure 4.17; from these figures, it can be seen that a good fit was achieved.

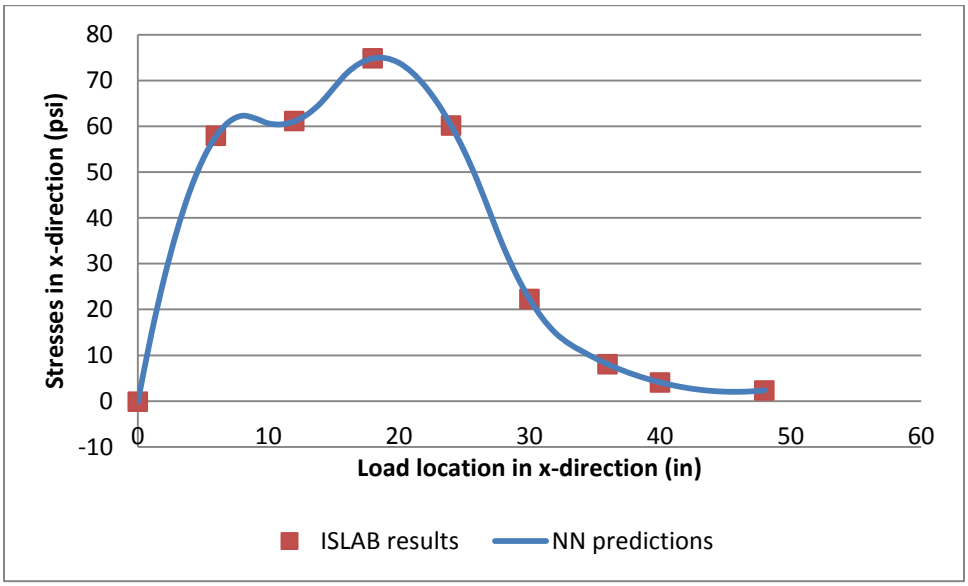

Figure 4.16: Sensitivity analysis for variation in vehicle wander in the x-direction for a neural network trained with nine values of vehicle wander. Constants used for the analysis were: E = 307842 psi, temperature gradient =60°F, aggregate interlock factor =6569, and tire pressure = 66.83 psi.

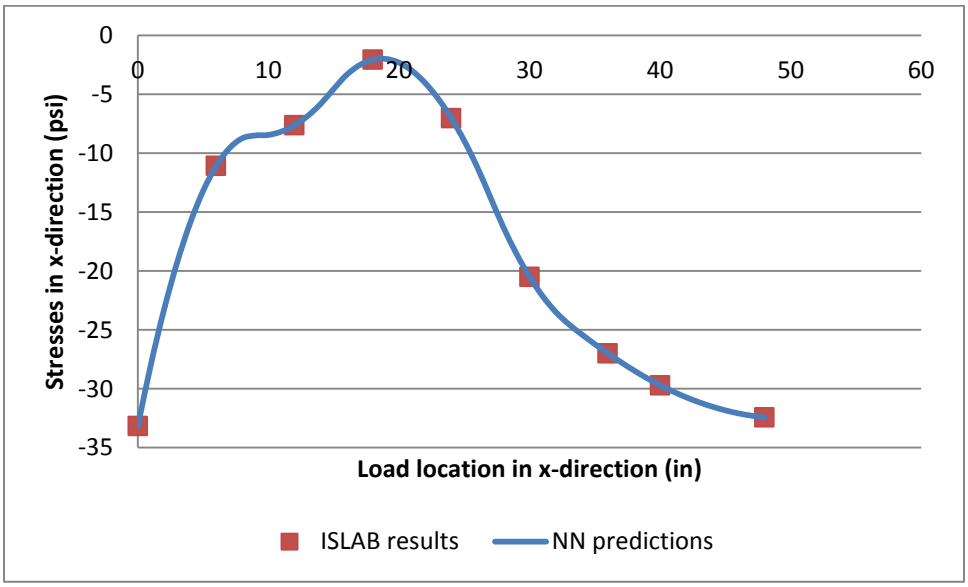

Figure 4.17: Sensitivity analysis for variation in vehicle wander in the x-direction for a neural network trained with nine values of vehicle wander. Constants used for the analysis were: E = 6114664 psi, temperature gradient = -60°F, aggregate interlock factor = 38627, and tire pressure = 21.48 psi.

4.5 Stress Analysis Procedure

When stress analysis is conducted in the program, neural networks will be used to provide stresses in similar space in a computationally efficient manner. The following stress computation method follows the same procedure as wad outlined in the MEPDG (as detailed in NCHRP 2003b).

1. The first step in determining stresses in a given system using the neural networks is to transform the problem into similar space. To transform the problem into similar space, the original system must first be transformed into its equivalent single layer system using equations (2.23) through (2.25). The equivalent linear temperature gradients for the equivalent system are computed using equations (2.29) and (2.30) for the unbonded and bonded cases, respectively.

   To use the neural networks, values of modulus of elasticity, tire pressure, temperature gradient, aggregate interlock factor and traffic wander must be computed for the neural network system defined in Table 4.4 from the equivalent system. The original system and the equivalent system must satisfy the following conditions for the equivalent system concept to apply (Khazanovich et al. 2001):

   $L_1 = L_2$

   $\ell_1 = \ell_2$

   $\phi_1 = \phi_2$

   $$\frac{AGG_1}{k_1 \ell_1} = \frac{AGG_2}{k_2 \ell_2}$$

   $$\frac{P_1}{h_1 \gamma_1} = \frac{P_2}{h_2 \gamma_2}$$

   $s_1 = s_2$

   $f_1 = f_2$

Compute the linear component of stress in the original system $\sigma_{orig,linear}$ by scaling the linear component of stress in the neural network system σ_{NN} using the appropriate scaling factor λ, as given in Table 4.12.

$$\sigma_{orig,linear} = \lambda \sigma_{NN} \tag{4.5}$$

2. Compute the non-linear component of stress in the original system, $\sigma_{orig,nonlinear}$.

$$\sigma_{orig,nonlinear} = \frac{-E_{PCC}\alpha_{PCC}}{(1-\mu_{PCC})}\left[\frac{\Delta T_{equiv}}{2h_{equiv}}h_{PCC} - \frac{\sum_{i=1}^{10} T_i}{10} + \frac{T_1}{20} + \frac{21T_{11}}{10}\right] \tag{4.6}$$

Where:

$\sigma_{orig,nonlinear}$ = nonlinear component of stress at the bottom of the slab in the unknown original system

T_1 = temperature at the top surface of the slab

T_{11} = temperature at the bottom surface of the slab

T_i = temperature at evenly spaced pointes from the top to the bottom of the slab

3. Compute the total stress in the original system $\sigma_{orig,total}$ by summing the linear and non-linear components of stress

$$\sigma_{orig,total} = \sigma_{orig,linear} + \sigma_{orig,nonlinear} \tag{4.7}$$

Table 4.12: Scaling factors for calculating stresses in a two layer system from those in a similar single layer system

Case	Unbonded	Bonded	
	Top and Bottom Surface	**Top Surface**	**Bottom Surface**
Two layer to effective one layer	$\lambda = \frac{h_1}{h_{equiv}}$ (4.8)	$\lambda = \frac{2x}{h_{equiv}}$ (4.9)	$\lambda = \frac{2(h_1 - x)}{h_{equiv}}$ (4.10)
Two layer to one layer	$\lambda = \frac{h_1^2 h_2 \gamma_1}{h_{1,equiv}^3 \gamma_2}$ (4.11)	$\lambda = \frac{2x\gamma_{1,equiv} h_2}{h_{1,equiv}^2 \gamma_2}$ (4.12)	$\lambda = \frac{2(h_1 - x)\gamma_{1,equiv} h_2}{h_{1,equiv}^2 \gamma_2}$ (4.13)

Where:

γ = unit weight

x = distance from the top surface to the neutral axis

subscript eq = the equivalent single layer system

Once stresses in the original system have been determined, they can then be used in damage computations. Examples of stress computations are given in Appendix A.

4.6 Summary

To develop a longitudinal cracking model, it is necessary to compute stresses at the critical location for longitudinal cracking. The critical stress and load locations for longitudinal cracking are different from those for transverse cracking, therefore the analysis needed is different from that used in the MEPDG transverse cracking model. The number of combinations of different pavement structures and loading types which must be considered created a staggeringly large factorial.

To reduce the size of this factorial without introducing error, the principles of similarity were used to map the problem from real space to similar space. Each variable in the original factorial was individually considered to determine which variables should be held constant in the reduced factorial and which should be varied. Consideration was

given to how the principles of similarity were applied in the creation of the MEPDG transverse cracking model in order to avoid some of the difficulties experienced by the MEPDG creators.

Based on the stress analysis of the factorial of various pavement structures and loading conditions defined, neural networks were developed to rapidly compute stresses within the longitudinal cracking program. By using neural networks, the need to embed a finite element analysis program within the longitudinal cracking program was eliminated. The neural networks were tested with both training and testing data to ensure their ability to accurately predict solutions. Sensitivity analysis was also conducted to confirm that the neural networks were neither over- nor under-trained. Within the program, the stresses computed using the neural networks are converted back into real space and used to compute fatigue damage, as discussed in Chapter 6.

Chapter 5. Using Similarity to Determine Transverse versus Longitudinal Cracking Potential

In traditional pavement design, transverse cracking has always been considered as the primary failure mode. As was discussed in Chapter 2, widened lanes are often used to mitigate transverse cracking. It has been observed that the use of widened lanes can change the failure mechanism to longitudinal cracking, as was discussed in Section 2.2. While widened slabs are one pavement characteristic which is thought to cause longitudinal cracking, it would be helpful to pavement engineers to identify other characteristics which pavements prone to longitudinal cracking share.

Hiller (2007) examined 2160 cases in an attempt to characterize types of pavements prone to longitudinal cracking. While Hiller's study was able to find some general trends of characteristics which can make a pavement more susceptible to transverse cracking (such as the use of a widened slab), it was not able to characterize more than a limited subset of pavements. To avoid the limitations of the size of the factorial Hiller encountered, similarity was used to analyze a wide range of pavement design parameters. Examining more pavements and using parameters in similar space to characterize pavements prone to longitudinal cracking allows for much more specific characteristics to be defined.

Similarity is a powerful concept used to reduce the dimensions of a problem without introducing error. As was discussed in Chapter 2, the principle of similarity states that if the stress state in one system is known, the stresses in any similar slab can be computed from the known solution. To be considered similar, the two systems must have proportional deflection basins. Thus, to analyze a large number of pavements, it is only necessary to analyze a select subset of pavements. As long as each pavement in the overall set is similar to one pavement in the subset, it will be possible to compute the solution to all of the pavements in the overall set by analyzing only the pavements in the subset.

As part of developing the longitudinal cracking model in this research, a large factorial of finite element runs was performed as discussed in Chapter 4. This analysis was performed in a similar space, i.e. for a single layers lab with the fixed thickness and fixed coefficient of subgrade reaction. Having many parameters fixed (for example base properties) significantly reduced the scale of the problem. However, the ranges other system parameters, such us slab elastic modulus, temperature gradients, and applied tire pressure, were selected such so the solution for a wide range of the pavement systems with various slab and base properties could be obtained.

In this chapter, the stresses occurring at the critical locations for both transverse and longitudinal cracking in the similar space were compared. This allowed determination of the conditions favorable for transverse of longitudinal cracking; only bottom-up cracking was considered in this study. The similarity principle was used to demonstrate the validity of the results in the original space. This information will allow pavement engineers to determine when longitudinal cracking needs to be considered in design.

5.1 Background

While the concepts of similarity were discussed in detail in Section 2.6, they are summarized here for the reader's convenience. The two systems can be considered as similar as long as their deflection basins are scalable. Similarity allows for the stresses in one system to be computed from those in a different system as long as the two systems have scalable deflection basins. Thus, if system 1 is subjected to axle loading and a linear temperature gradient is applied, the stresses in system 1 can be found from those in system 2 using the following relationship, provided the stresses in system 2 are known:

$$\sigma_{1,total} = \lambda_{stress}\sigma_{2,linear} + \sigma_{1,nonlinear} \qquad (2)$$

Where:

σ_{total} = total stress at the surface of the slab (top or bottom), independent of coordinates

σ_{linear} = linear component of stress due to traffic and thermal loading at the surface of the slab, independent of coordinates

λ_{stress} = scaling factor for stress, dependent only on properties of the pavement structure

$\sigma_{nonlinear}$ = non-linear component of stress due to thermal loading only at the surface of the slab independent of coordinates.

Of the three equivalencies discussed in Section 2.6.1, the equivalent slab concept will be the main concept used in this research. The equivalent slab concept allows the stresses in a single, circular slab to be calculated based on those in a similar slab (Korenev & Chernigovskaya 1962). The equivalent structure concept extended this principle to rectangular, multi-slab systems (Khazanovich et al. 2001). Two intermediate parameters needed in the equivalent structure method are the radius of relative stiffness ℓ, and Korenev's non-dimensional temperature gradient ϕ, which are given in equations (2.15) and (2.37), respectively.

From the equivalent structure concept (Khazanovich et al. 2001), the stresses in one pavement system can be computed from those in the other if the following conditions are fulfilled:

- $\ell_1 = \ell_2$
- $L_1 = L_2$
- $\phi_1 = \phi_2$
- $\frac{AGG_1}{k_1 \ell_1} = \frac{AGG_2}{k_2 \ell_2}$
- $\frac{P_{a,1}}{h_{pcc,1} \gamma_{pcc,1}} = \frac{P_{a,2}}{h_{pcc,2} \gamma_{pcc,2}}$
- $s_1 = s_2$

Where:

ℓ = radius of relative stiffness

L = slab length (joint spacing)

ϕ = Korenev's non-dimensional temperature gradient

AGG = aggregate interlock factor

P_a = axle load

γ_{pcc} = concrete unit weight

s = distance between the pavement shoulder and the outer wheel tire edge

subscripts 1 and 2 indicate the two slab systems

An example is provided in Section 5.2 to better illustrate similar pavements are defined and how their stresses are calculated.

5.2 Using Similarity to Determine Transverse versus Longitudinal Cracking Potential

To determine which mode of cracking will control, it is necessary to compare the stresses at the critical location for transverse cracking are compared to the stresses at the critical location for longitudinal cracking. In order to make such a comparison for the entire range of typical pavement designs, the reduced factorial determined in Section 4.3 was considered. This smaller factorial was defined using the principles of similarity and still considers all of the original cases, but in a much more efficient manner. Because not every pavement defined in the reduced factorial could be analyzed due to time and data space constraints, a representative range of values for each variable in the reduced factorial had to be considered. This was accomplished by using the values previously used for neural network training, as discussed in Section 4.4.1.

The critical load and stress locations for transverse cracking are at midslab along the longitudinal edge, while the critical and stress locations for longitudinal cracking are at midslab along with transverse joint, see Figure 5.1 and Figure 5.2 for the standard width and widened slab cases respectively. The stresses in similar space were computed at the critical location for both types of cracking for loads placed at the respective critical locations, see Table 5.1. Analysis was conducted for the entire reduced factorial, which includes a variety of pavement types under a variety of loads. It was assumed that there was no erosion present and only bottom-up cracking was considered.

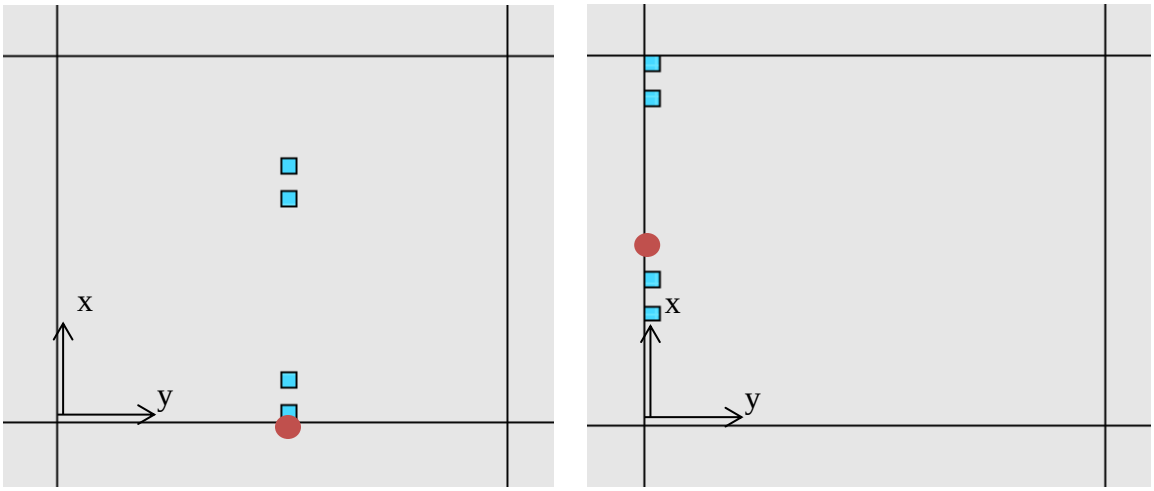

Figure 5.1: Critical location of load (blue squares) and stress (red dot) for transverse (left) and longitudinal (right) cracking of the standard width slab.

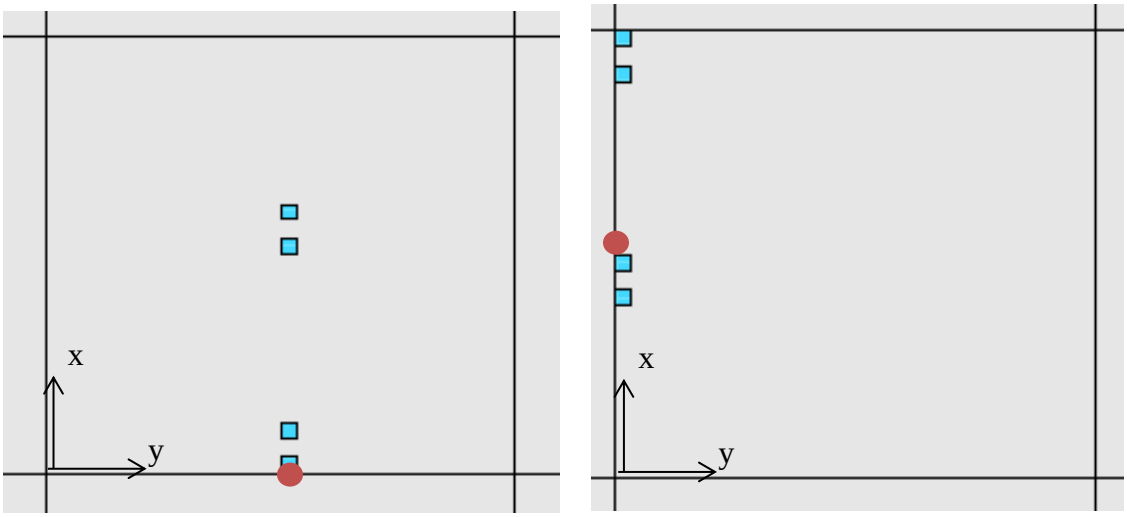

Figure 5.2 Critical location of load (blue squares) and stress (red dot) for transverse (left) and longitudinal (right) cracking of the widened slab.

Table 5.1: Load and Stress Locations for Cracking Potential Study

Slab width	Cracking type	Load x*[+]	Load y*[+]	Stress x[+]	Stress y[+]
Standard Width	Transverse	0 in	90 in	0 in	90 in
	Longitudinal	48 in	0 in	72 in	0 in
Widened Slab	Transverse	0 in	90 in	0 in	90 in
	Longitudinal	72 in	0 in	84 in	0 in

* load coordinates are specified for the lower left corner of the lowest wheel

[+] origin at the lower left hand corner of the slab

To better illustrate how similarity works to compare stresses which cause transverse and longitudinal cracking, an example is provided. Table 5.2 gives the properties of three different pavement structures (A, B, and C) which are all similar, despite having very different properties. It can be determined that the pavements are all similar by observing that the values of radius of relative stiffness, Korenev's non-dimensional temperature gradient, $\frac{AGG}{k\ell}$, and $\frac{p}{h\gamma}$ (also shown in Table 5.2) are equal for all three pavements. These pavements are also similar to a single layer pavement, whose properties are given in Table 5.2 as well. By analyzing the equivalent single layer system, it is possible to compute the stresses in Cases A, B, and C.

Table 5.2: Properties of Example Similar Pavements

	Case A	**Case B**	**Case C**	**Equivalent Single Layer System for Stress Computation**
Concrete Thickness (in)	12	10	10	10
Concrete Elastic Modulus (psi)	4,000,000	5,030,811	6,012,212	5,108,571
Concrete Unit Weight (lb/in^3)	0.087	0.07	0.08	.087
Concrete Coefficient of Thermal Expansion (in/in/°F)	$4.40*10^{-6}$	$4.40*10^{-6}$	$5.50*10^{-6}$	$4.4*10^{-6}$
Concrete Poisson's Ratio	0.15	0.15	0.15	.15
Base Thickness (in)	20	12	15	-
Base Elastic Modulus (psi)	30000	45000	35000	-
Base Unit Weight (lb/in^3)	0	0	0	-
Base Coefficient of Thermal Expansion (in/in/°F)	4.40E-06	4.40E-06	5.50E-06	-
Modulus of Subgrade Reaction (psi/in)	350	250	300	-
Bond Condition	unbonded	unbonded	unbonded	-
Temperature Gradient (°F)	15	11.515	8.81	14.094
Load (lbs)	18,000	12,069	13,793	15,000
Load Transfer Efficiency (%)	70	70	70	70
Computed Parameters for Similarity				
Radius of Relative Stiffness (in)	36.330	36.330	36.330	36.330
Korenev's Non-dimensional Temperature Gradient	5.4096	5.4096	5.4096	5.4096
$\frac{AGG}{k\ell}$	3.3627	3.3627	3.3627	3.3627
$\frac{p}{h\gamma}$	94.60	94.60	94.60	94.60

For the pavements with properties given in Table 5.2, stresses were computed along the longitudinal edge and at the transverse joint for loads placed at those locations, as shown in Figure 5.1 and Figure 5.2. These stresses are given in Table 5.3. The stress induced along the transverse joint σ_J is the stress that could cause longitudinal cracking while the stress along the longitudinal edge σ_E is the stress of concern when considering transverse cracking. This analysis was conducted for standard width and widened slabs.

Since the bending stresses at the bottom of the PCC slab in systems A, B, and C can be obtained by scaling the stresses in the same equivalent system, the ratio of the bending stresses from two locations in these systems are equal to the ratio of the bending stresses in equivalent system from the same locations. Therefore, if the joint stress is greater (or smaller) than the longitudinal edge stress for the equivalent system, it is greater (or smaller) for any of the systems A, B, or C. Although the temperature distributions throughout the PCC layer thickness in systems A, B, and C were linear, presence of the base layers caused that a portion of the temperature distribution caused non-linear (self-equilibrating) stresses, which have to be added to the bending stresses. These self-equilibrating stresses, however, are the same at any PCC depth for the given system. Therefore, addition of these stresses does not change the relative value (which is greater or smaller) of the longitudinal edge and transverse joint stresses.

Table 5.3: Stresses in the Example Cases

		Standard width			**Widened slab**		
		Case A	**Case B**	**Case C**	**Case A**	**Case B**	**Case C**
stress in similar space	$\sigma_{J,similar}$	75.81	75.81	75.81	174.80	174.80	174.80
	$\sigma_{E,similar}$	223.60	223.60	223.60	148.29	148.29	148.29
linear component of stress in real space	$\sigma_{J,linear\ temp}$	61.06	60.07	68.37	140.78	138.50	157.64
	$\sigma_{E,linear\ temp}$	180.08	177.17	201.64	119.43	117.50	133.73
	$\frac{\sigma_{j,linear\ te}}{\sigma_{e,linea}}$	0.3391	0.3391	0.3391	1.1788	1.1788	1.1788
nonlinear stress in real space	$\sigma_{nonlinear\ temp}$	5.21	2.28	3.30	5.21	2.28	3.30
total stress	$\sigma_{J,total}$	66.27	62.35	71.67	145.99	140.79	160.94
	$\sigma_{E,total}$	185.29	179.45	204.95	124.64	119.78	137.03

From Table 5.3, it can also be seen that the ratio of stress at the transverse joint to stress at the longitudinal edge is less than one for all of the standard width slabs, while it is greater than one for the widened slabs. This shows that longitudinal cracking would

potentially be a concern for the widened slab cases, but transverse cracking is likely the dominant failure mode for the standard width cases.

5.3 Comparison of Edge and Joint Stresses for the Entire Reduced Factorial

By plotting the stress at the critical location for longitudinal cracking against the stresses at the critical location for transverse cracking, it is very easy to visually determine which type of cracking will likely control by simply comparing the point representative of each case to the equality line. The critical locations were selected for bottom -up cracking only. Only cases with non-negative temperature gradients were considered because negative temperature gradients would cause top-down cracking. Figure 5.3 and Figure 5.4 show the graphs of stresses at the critical location for longitudinal cracking σ_J (joint stresses) plotted against the stresses at the critical location for transverse cracking σ_E (edge stresses) for single and tandem axle loads, respectively for the standard width case obtained from the results of the ISLAB analysis discussed in Chapter 4. Figure 5.5 and Figure 5.6 show the same for the widened slab case, and Figure 5.7 and Figure 5.8 again show the same, but for a standard width slab with a tied PCC shoulder. A tied PCC should was not considered in conjunction with a widened slab because these transverse cracking mitigation members are not typically used together.

Although each point on the graph represents the stresses in a specific pavement structure in similar space with a given combination of axle load and temperature gradient, it also represents the bending stresses for the equivalent pavement systems with corresponding temperature and axle loadings. However, the relative magnitude of the stresses in similar space is the same as that in real space. For example, if the edge stresses are higher than joint stresses in similar space, they will also be higher in real space. To use these figures, the relative magnitudes of edge stresses should be compared with joint stresses

At the same time, it is important to remember that a pavement experiences many different combinations of axle load and temperature gradient throughout its life; in addition, the properties of a pavement change as it ages. Therefore, a pavement is not represented by any one point on the graph; instead a specific case of loading for a pavement at a specific

point in time is given. In addition, the amount of damage depends on the absolute magnitude of the stresses in the real (not similar) space. It is important to note that high stresses in similar space do not necessarily imply high stresses in real space and low stresses in similar space do not necessarily imply low stresses in real space due to scaling and the effects of the nonlinear temperature gradient. Thus, the graph cannot be used to say at a specific pavement will fail in either longitudinal or transverse cracking. Instead, it can be used to determine if a certain combination of pavement structure and loading characteristics prone to more longitudinal or transverse cracking damage accumulation.

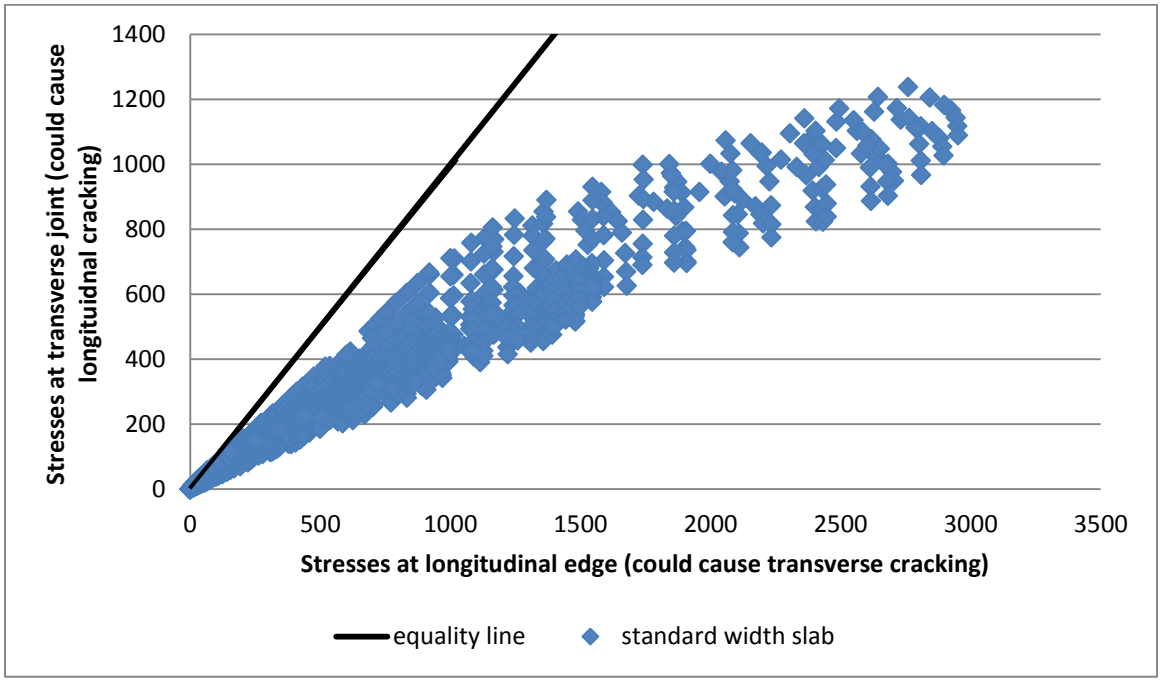

Figure 5.3: Stresses at the longitudinal edge versus stress at the transverse joint for the reduced factorial for single axle loads, standard width case with asphalt shoulder.

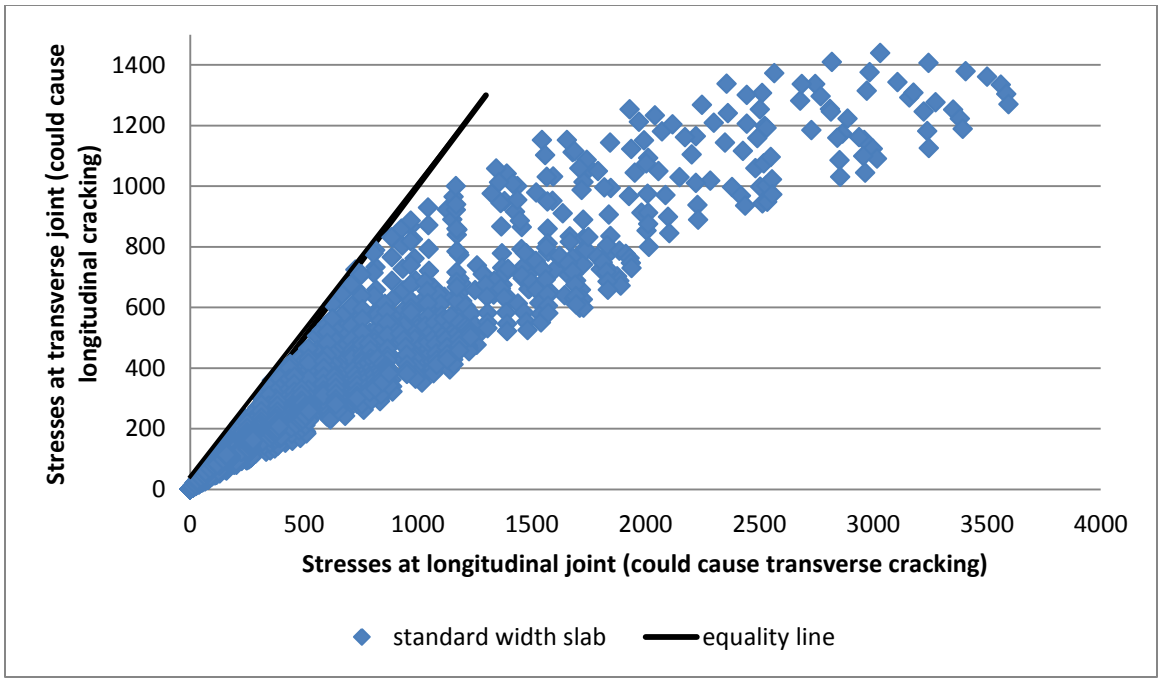

Figure 5.4: Stresses at the longitudinal edge versus stress at the transverse joint for the reduced factorial for tandem axle loads, standard width case with asphalt shoulder.

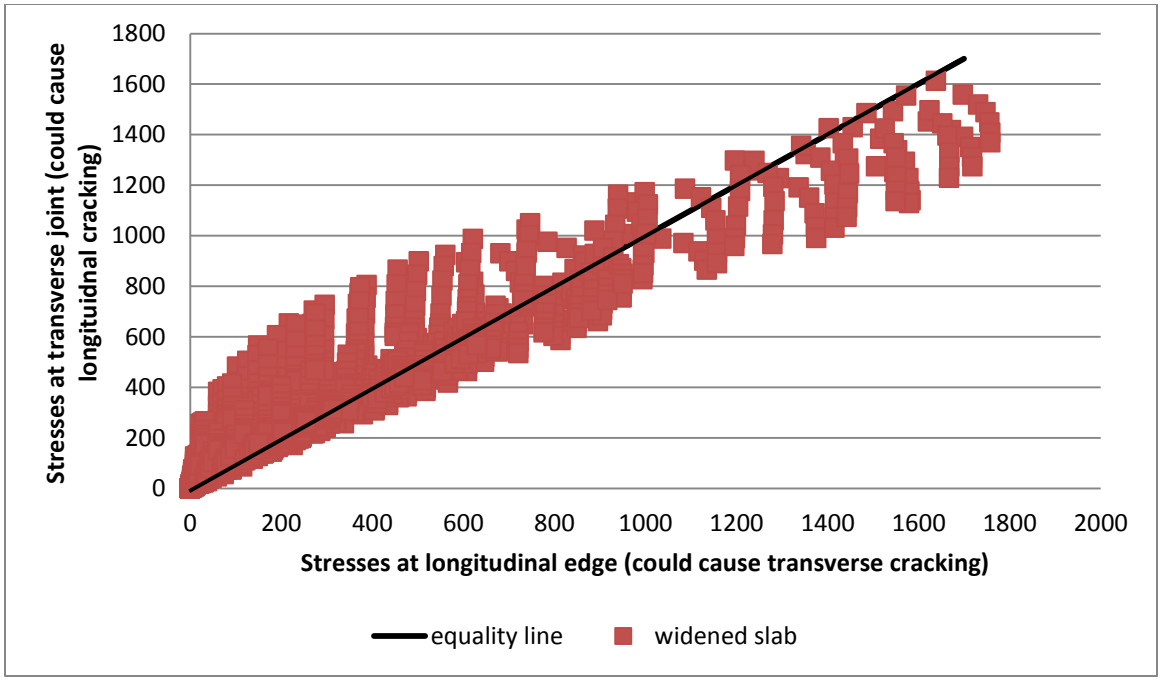

Figure 5.5: Stresses at the longitudinal edge versus stress at the transverse joint for the reduced factorial for single axle loads, widened slab case.

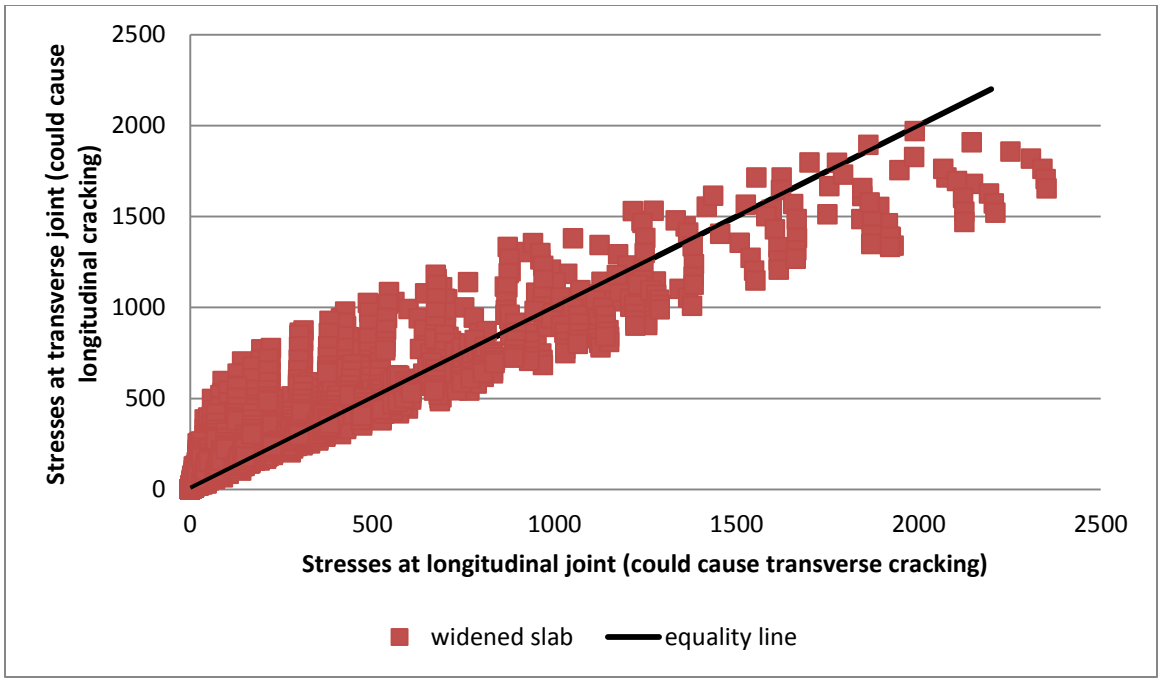

Figure 5.6: Stresses at the longitudinal edge versus stress at the transverse joint for the reduced factorial for tandem axle loads, widened slab case.

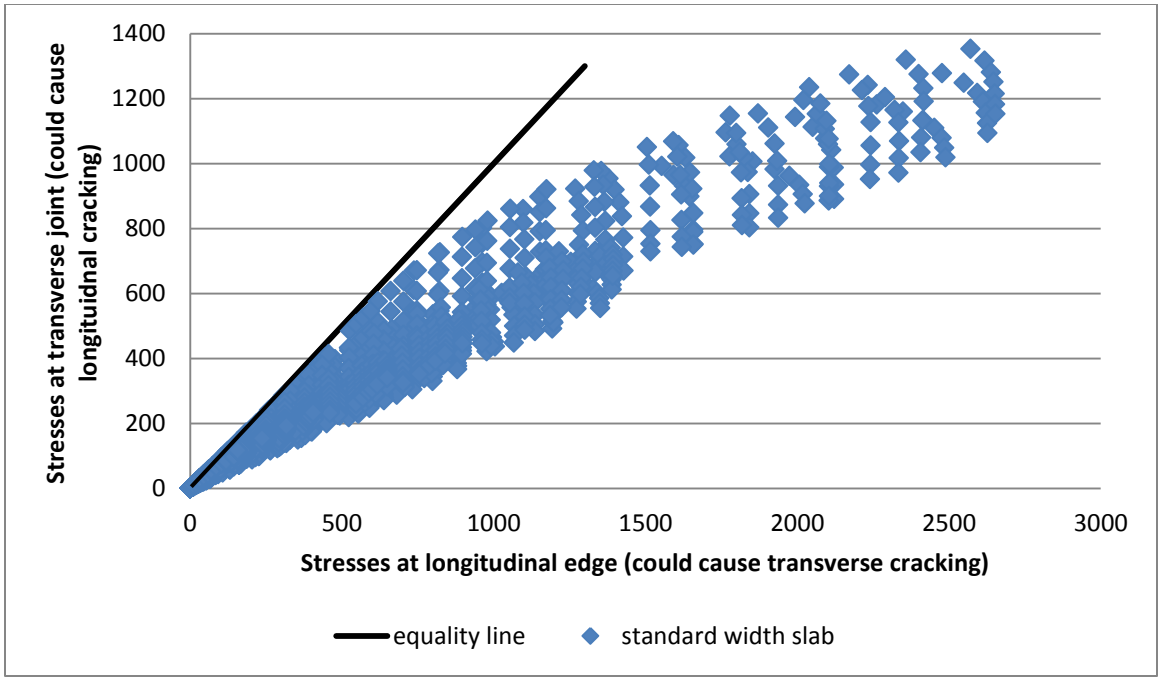

Figure 5.7: Stresses at the longitudinal edge versus stress at the transverse joint for the reduced factorial for single axle loads, standard width case with a tied PCC shoulder.

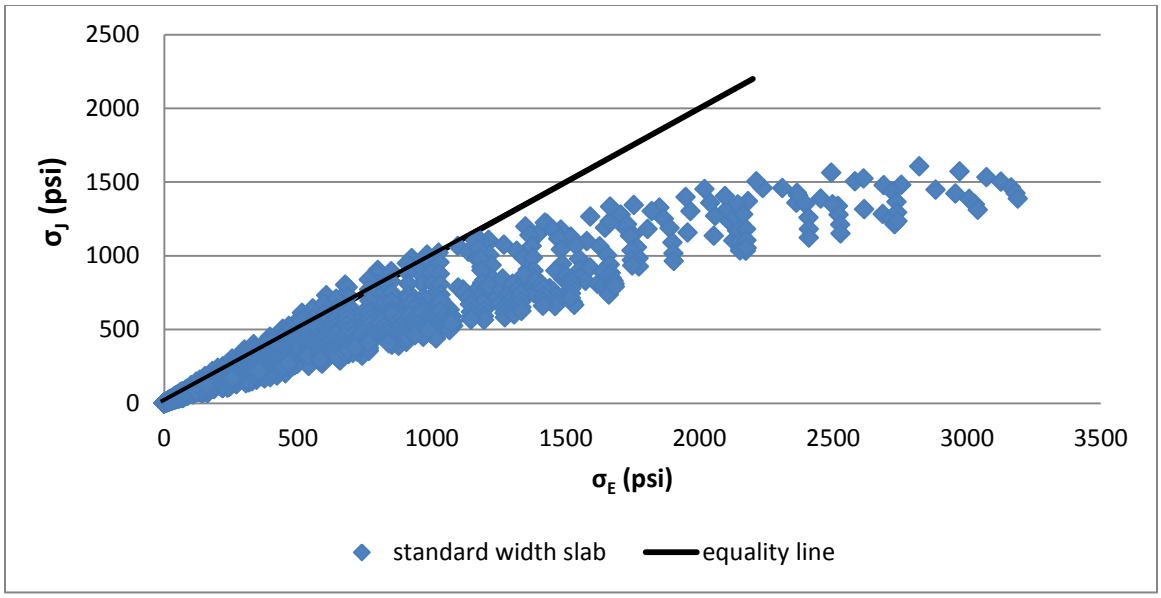

Figure 5.8: Stresses at the longitudinal edge versus stress at the transverse joint for the reduced factorial for tandem axle loads, standard width case with a tied PCC shoulder.

5.4 Application of Determining Cracking Potential

The best use of the analysis presented in Figure 5.3 through Figure 5.8 is to determine the characteristics of pavements which are likely to fail in transverse cracking or longitudinal cracking. It is obvious from Figure 5.5 and Figure 5.6 that widened lane pavements experience joint stresses larger than edge stresses for many different combinations of load and pavement structure properties. This is not the case for standard width pavements with an asphalt shoulder as shown in Figure 5.3 and Figure 5.4.

Figure 5.7 and Figure 5.8 show that the presence of a tied-PCC shoulder causes the standard width slab to have a shift in the point cloud more towards the equality line. This makes sense, as the presence of a tied shoulder causes the slab to behave more like a widened slab as there is load sharing between the slab and the shoulder. Indeed, this is why tied PCC shoulders are used to help mitigate transverse cracking, as is shown in Figure 2.3.

Further analysis was conducted to determine which pavement characteristics beyond slab width indicated that longitudinal cracking could be a potential failure mode. This

analysis investigated the longitudinal cracking potential based on the parameters used to ensure similarity:

- ℓ
- ϕ
- $\frac{p}{h\gamma}$
- $\frac{AGG}{k\ell}$

Where:

ℓ = radius of relative stiffness

ϕ = Korenev's non-dimensional temperature gradient

p = tire pressure = load/tire footprint

h = concrete layer thickness

γ = concrete unit weight

AGG = aggregate interlock factor

k = modulus of subgrade reaction

For the widened slabs, all values of all parameters were found to have some cases which failed in longitudinal cracking. Most pavements in the region above the equality line also had standard values of radius of relative stiffness (19-42), which are associated with normal thickness and stiffness pavements (recall that the example pavements had ℓ = 36.33). Pavements below the equality line but with high stresses in similar space were associated with very high values of ℓ, which is not common. This means that most normal, widened lane pavements which would be considered in design will fall above the equality line and could be susceptible to longitudinal cracking. This matches what was found by Hiller for the range of pavements he considered (cases with very high values of ℓ were outside the scope of his study).

For the standard width slabs, very few cases were found to fall above the equality line, which fits with conventional thinking that standard width pavements tend not to experience longitudinal cracking. Pavements with a Korenev's non-dimensional temperature gradient less than 4 and very low values of stiffness (ℓ = 12) were found to

have the potential to fail in longitudinal cracking, but only when there was no load present. For these cases, the thermal loading alone will not produce high enough stresses in real space to induce cracking. It was determined that the radius of relative stiffness, $\frac{p}{h\gamma}$, and $\frac{AGG}{k\ell}$ were not good parameters for indicating which cases of standard width pavements were susceptible to longitudinal cracking because some cases experienced joint stresses higher than edge stresses at all values of radius of relative stiffness, $\frac{p}{h\gamma}$, and $\frac{AGG}{k\ell}$. These findings fit with Hiller's conclusion that bottom-up longitudinal cracking is not a concern for standard width pavements. The few cases which were found to experience joint stresses higher than edge stresses were outside the scope of Hiller's study because of their low stiffness.

The case of the standard width slab with the tied PCC shoulder resembles a cross between the widened slab and standard width pavements. Similar to the standard width slab with an asphalt shoulder, standard width pavements a tied PCC shoulder loaded with single axle loads were found to have no longitudinal cracking except at very low levels of stiffness. With a tied PCC shoulder however, the threshold of Korenev's non-dimensional temperature gradient needed to for longitudinal cracking to be a concern was raised to 19.5 from the value of 4 found for an AC shoulder. This finding fits well with those of Hiller, who found that standard width pavements with a tied PCC shoulder loaded with single axle loads did not experience longitudinal cracking unless negative temperature gradients were present. When tandem axle loads were considered, Figure 5.7 shows that there are a number of points above the equality line. These points were found to correspond to a variety of load levels, though the limit of Korenev's temperature gradient of 19.5 was found to still apply. Hiller found that a tied PCC shoulder in conjunction with tandem axle loads and no temperature gradient could produce longitudinal cracking, but that positive temperature gradients were not a problem. However, Hiller's study considered a much narrower range of pavements than was considered in this study, so these results are not necessarily contradictory. It was also determined that the radius of relative stiffness, $\frac{p}{h\gamma}$, and $\frac{AGG}{k\ell}$ were not good parameters for

indicating which cases of standard width pavements with tied PCC shoulders were susceptible to longitudinal cracking

When considering the types of loading which can cause a pavement to be susceptible to longitudinal cracking, it is important to remember that the factorial considered in this research included loads at levels too small to be of concern when computing damage. Therefore it is important to check the magnitude of the load for points above the equality line to determine if they are truly of concern. For example, in the standard width asphalt shoulder case, pavements with no vehicle loading were found to lie above the equality line, but the stresses caused by thermal loading alone are not great enough to be of concern. This is not always the case, however.

Figure 5.9 shows the ratio of joint stresses to edge stresses for a standard width slab pavement with a tied PCC shoulder. The pavement shown was an 8 inch thick pavement with a concrete modulus of elasticity of 4,000,000 psi subgrade k-value of 310 psi/in. The pavement was subjected to a temperature gradient of 12 degrees. This figure shows that, while standard axle loads have a ratio of joint stresses to edge stresses is less than one, this ratio is greater than one for overloads. These loads can cause sufficient damage to make longitudinal cracking a real concern.

When considering the longitudinal cracking potential by comparing joint and edge stresses, it is important to note that the "equality line" does not always need to be set equal to a ratio of 1:1. As was discussed in Chapter 3, to limit longitudinal cracking in design, the ratio of joint to edge stresses should be set to less than some number which is less than one. Thus the equality line simply represents an upper bound of the design criteria to limit longitudinal cracking. The limiting value of the ratio of joint to edge stresses to be used in design needs to be determined, though what this value should be is beyond the scope of this project.

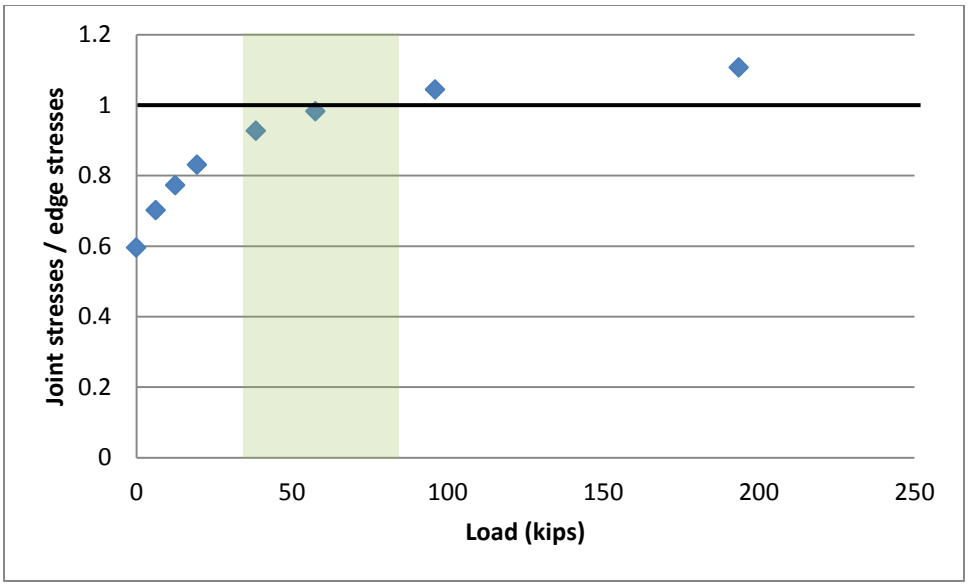

Figure 5.9: Ratio of joint stresses to edge stresses versus tire pressure for a standard width slab with a tied PCC shoulder; range of typical axle loads (36-70 kip) is shaded.

5.5 Accounting for the Number of Load Applications

While the figures of longitudinal versus transverse stress are very useful for identifying pavement structures and load combinations susceptible to longitudinal cracking, they do not account for the fact that most loads do not occur at the critical location for either transverse or longitudinal cracking. Additionally, these plots do not consider the relative damage from different loads at different locations, nor do they consider how many times different loads are applied.

As was discussed previously in Chapter 2, as the load moves further away from the longitudinal edge, the load condition changes from edge loading to interior loading, which results in much lower stresses. This is not the case along the transverse joint however, where most values of vehicle wander will result in an edge loading case, and the remainder will be corner loading cases. Therefore, as the vehicle wander moves away from the longitudinal edge, the failure mode tends to shift from transverse cracking to longitudinal cracking.

In order to account for the fact that all loads will cross over the transverse joint but not many wander close to the longitudinal joint, the number of loads needed at the transverse joint to induce the same damage as the is induced by a load at the transverse edge was computed. Fatigue damage is given by equation (2.9) and is dependent on both the stress produced by a given load and the number of times that load is applied.

For a given value of concrete modulus of rupture, the number of allowable loads at the transverse joint N_J were computed based on stresses at the transverse joint (causing longitudinal cracking). The number of allowable loads at the longitudinal edge N_E were computed based on the stresses at the longitudinal edge (causing transverse cracking). The ratio of these numbers of allowable loads N_J/N_E shows the number of additional loads which would need to be applied at the transverse joint to get the same damage as is caused by loads applied at the longitudinal joint. N_J/N_E was plotted against the normalized quantity of stress at the longitudinal joint (causing transverse cracking) σ_E divided by the modulus of rupture of the concrete. Different curves were plotted for various ratios of stress at the transverse joint σ_J to stress at the longitudinal joint σ_E and are shown in Figure 5.10.

From these figures, it can be seen that as σ_J approaches σ_E, fewer loads at the transverse joint are needed to induce the same amount of damage as is induced at the longitudinal edge. Similarly, the higher the stresses at the transverse joint in comparison with those at the longitudinal edge, more loads at the transverse joint are needed to induce the same damage as is induced at the longitudinal edge. Figure 5.3 through Figure 5.8 showed that widened slabs will often have a higher ratio of stresses at the transverse joint to those at the longitudinal joint, while the reverse is true for standard width slabs. Thus, for the standard width case (lower σ_J/σ_E), more loads at the transverse joint are needed to induce the same damage as a load at the longitudinal edge, while for the widened slab case (higher σ_J/σ_E), fewer loads at the transverse joint are needed to induce the same damage as a load at the longitudinal edge.

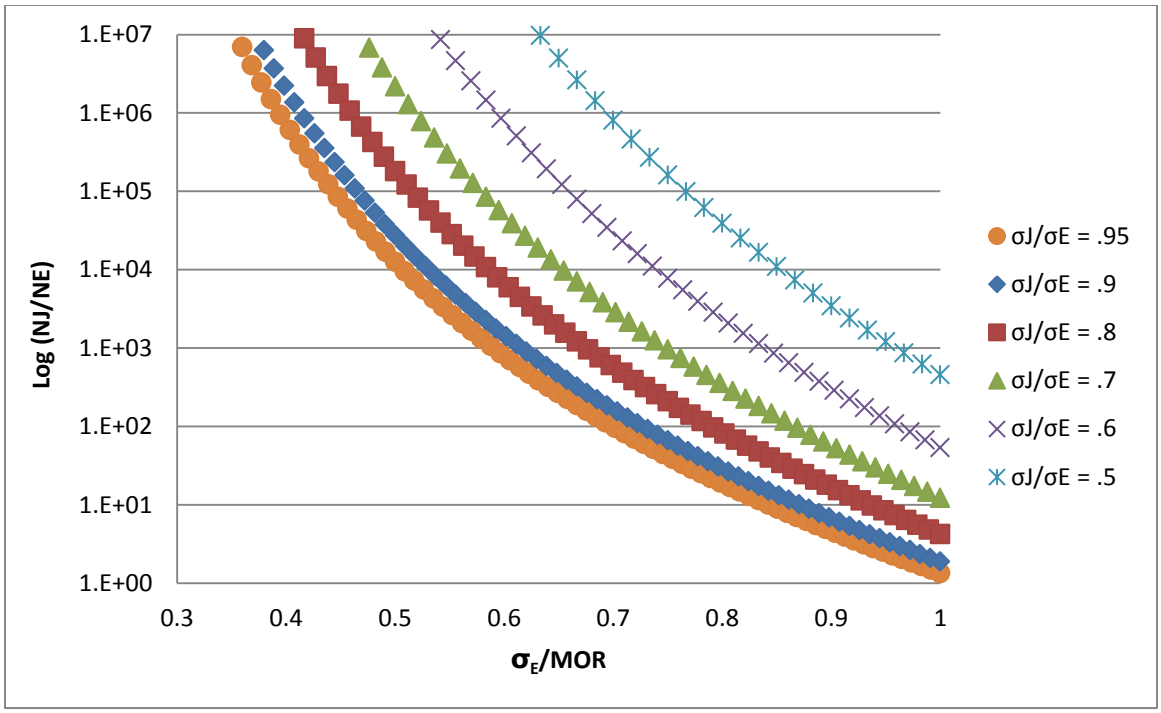

Figure 5.10: Number of loads required to induce the same amount of damage from transverse cracking as from longitudinal cracking.

While loads at the longitudinal edge are rare, all loads must cross over the transverse joint to travel across the slab. In a standard width slab, some loads wander along the longitudinal edge, but in a widened slab, it is assumed that no load has a wander less than 24 inches from the longitudinal edge, which minimizes damage from transverse cracking. In a widened slab, there is also a higher σ_J/σ_E ratio, showing that fewer loads at the transverse joint are needed to induce the same level of damage as would be caused by a load at the longitudinal edge (were a load to travel there).

For example, consider two loading cases. In the first case, a load traveling along the longitudinal edge causes a stress at the critical location for transverse cracking of σ_E = 300 psi. In the second case, a load traveling in the wheel path causes a stress of at the critical location for longitudinal cracking of σ_J = 275 psi. While both of these loads are below the modulus of rupture of the concrete, in this case assume 700 psi, the controlling load case would appear to be the load traveling along the longitudinal edge, because it

causes higher critical stresses. However, this ignores the contribution of the number of load applications to fatigue damage. Say that 1 million loads were going to be applied. From the modified normally distributed traffic loading used in the MEPDG (detailed in Section 2.4.1), only approximately 5% of loads will occur along the longitudinal edge in standard width pavement, while approximately 23% will occur in the wheel path. Using equation (2.9), this results in a value of fatigue damage of 0.128 at the critical location for longitudinal cracking, but only of 0.119 at the critical location for transverse cracking because of the difference in the number of vehicles occurring at each wander. Fatigue damage is then used to compute the percentage of slabs cracked.

Comparing a case representative of a standard width slab to one representative of a widened slab, it can be seen that fewer loads at the transverse joint are necessary in the widened slab case to induce the same amount of damage as in the standard width case. Coupling this with the fact that fewer loads will travel along the longitudinal edge in the widened slab case shows why longitudinal cracking is more of a problem for widened slabs when accounting for traffic wander.

5.6 Summary and Conclusions

In this research, the stresses at the critical locations for longitudinal and transverse cracking were determined and compared for a large number of pavement structures and loading conditions. By comparing the stresses at both locations, it was possible to determine which mode of failure would control for a given pavement structure and loading condition. Performing this computation for many pavements allowed the characteristics of pavement structures and loading conditions susceptible to longitudinal cracking to be identified.

It was determined that the design of any pavement using a widened slab should consider longitudinal cracking because it is a very likely failure mechanism. Some cases of standard width slabs with tied PCC shoulders were also of concern, but almost all cases of standard width slabs with asphalt shoulders were found unlikely to experience longitudinal cracking. In the instances where the joint stresses were found to be higher

than the edge stresses for the standard width pavement with the asphalt shoulder, the load levels were not high enough to be of concern. These findings confirm that the trends identified by Hiller (2007) in a much smaller study are applicable to a much broader range of pavements.

Chapter 6. Damage Computation and Design Procedure

As was discussed in Chapter 2, the current MEPDG pavement design method predicts only transverse cracking. However, longitudinal cracking is an observed distress, and is particularly prevalent when widened slabs are used. It was demonstrated in Chapter 3 that the development of a comprehensive mechanistic-empirical model for longitudinal cracking is a challenging task which requires accounting for the effects of cracking in adjacent slabs and subgrade erosion at the joint on the stress distribution in the slab of interest. Due to these complexities, development of such a model was not feasible in this study. Instead, a simpler and more practical approach was selected to account for longitudinal cracking fatigue damage.

An efficient stress analysis procedure for determining critical PCC stresses along the transverse joint of a JPCP was developed in Chapter 4. Chapter 5 demonstrated that these stresses can be of similar magnitude or higher than the critical stresses along the transverse edge which are responsible for transverse cracking. Repeated applications of stress at the longitudinal joint can cause fatigue damage and result in the development on longitudinal cracks. To quantify this phenomenon, a damage accumulation procedure consistent with that used in the MEPDG transverse damage analysis model was developed.

The longitudinal cracking damage analysis method developed in this research is intended to be used in conjunction with the MEPDG program so that a pavement engineer can account for longitudinal cracking in addition to the distresses already computed by the MEPDG for JPCPs. Documentation of a procedure to combine the longitudinal cracking damage analysis with standard MEPDG analysis is provided, as are several examples of the application of this procedure.

6.1 Incremental Damage Approach and Input Processing

As was discussed in Chapter 2, the MEPDG analysis can consider a wide variety of design parameters and pavement features. Different PCC and base layer thickness and material properties, joint spacing, dowel designs, and support types (AC and tied PCC

shoulders, widened lanes), among other design features, can be considered for site specific conditions including climate, subgrade properties and traffic. The MEPDG predicts performance over time, and allows a designer to modify different parameters until the design achieves satisfactory performance.

When analyzing a pavement, the MEPDG considers each month of pavement life separately, beginning with the moth the pavement is opened to traffic. For each month, the pavement structure properties that change with time and season are determined; these include the concrete modulus and modulus of subgrade reaction, as well as the amount of moisture warping seen by the pavement. These properties are held constant for the month, and stresses induced in the pavement due to axle and thermal loads are computed. Fatigue damage induced for the month can then be calculated based on the stress levels for each load combination and the number of times that load combination was applied.

Because the proposed longitudinal cracking damage model uses the MEPDG framework, many of the inputs for each step in analysis are the same as those used in the transverse cracking analysis. Thus, much of the input processing performed by the MEPDG transverse cracking model can be reused and adapted for the longitudinal cracking analysis. The MEPDG uses the inputs provided by the pavement engineer to determine the inputs needed for the analysis process as follows:

- The average daily number of single, tandem, tridem, and quad axles in each axel weight category are determined for each month in the analysis period. The axle weight categories are in load increments of 1000 lbs for single axles, 2000 lbs for tandem axles, and 3000 lbs for tridem and quad axles.

- The temperature at 11 evenly spaced points in the concrete layer is computed at every hour using the Enhanced Integrated Climatic Model (EICM), which is integrated into the MEPDG software.

- The average month relative humidity for each month in the calendar year is also determined from the EICM and is used to compute an equivalent temperature gradient due to moisture warping.

- The strength and modulus of the PCC are computed for each month to account for strength gain with time.

- The monthly average modulus of the base layer is computed.

- The monthly average effective modulus of subgrade reaction (k-value) is determined based on the soil moisture content and the user provided value of subgrade resilient modulus.

- The load transfer efficiency across joints is determined in the MEPDG faulting model for each month.

These models are all quite advanced and capitalizing on them not only eliminates the need to develop new models, but also ensures that the longitudinal cracking program is compatible with the current MEPDG and therefore can be easily implemented into that program. The inputs listed above are all computed automatically in the MEPDG as part of analyzing a pavement and are output in the MEPG output files. In order to benefit from these models and avoid computing these inputs directly, it is assumed that the user performs an MEPDG analysis of the trial design before running the longitudinal cracking damage program. The longitudinal cracking damage program then accesses the output files of the MEPDG to obtain all of the information required to complete the structural response analysis and damage computations. For consistency with the MEPDG, these calculations are made on a monthly basis.

6.1.1 Critical Stress Analysis

The MEPDG transverse cracking model requires computation of critical stresses at different locations than it is required for the longitudinal damage analysis. For transverse cracking, the critical stress location is at midslab along the longitudinal edge, with the top surface being critical for top-down cracking and the bottom surface being of concern for bottom-up cracking. For longitudinal cracking, the critical stress location is along the transverse joint; the critical load case is an axle placed along the transverse joint in conjunction with a positive temperature gradient through the PCC slab. Theoretically, the highest stress will occur directly under the load when the load is placed at midslab along the joint. However, this is unlikely when typical traffic wander is considered. If the load is placed closer to the slab edge, the magnitude of stresses is slightly reduced but significantly more loads occur at locations close to the slab edge.

Because damage calculation is dependent on both the magnitude of stresses and number of load applications, several evaluation points along the transverse joint should be considered. As in the transverse cracking analysis conducted by the MEPDG, several load positions with respect to the evaluation points should be considered because traffic rarely wanders such that a wheel passes directly over midslab along the transverse joint. Although loads further from midslab will reduce stresses at that point, these lower stresses still contribute to cumulative damage and must be accounted for. The stress analysis procedure in Chapter 4 provides a computationally efficient way to determine the critical stresses at the bottom of the PCC slab for a wide range of evaluation points, temperature gradients and axle load locations along the transverse joint for a variety of pavements. The specific evaluation points considered are detailed in Section 4.1.

6.1.2 Determination of the Number of Load Applications

As previously discussed, the MEPDG computes stresses and accumulates damage for every month of pavement life. Within a given month, all structural properties (ex. material properties, modulus of subgrade reaction, load transfer efficiency) of the pavement are considered to be constant. Therefore, the magnitude of stresses at each evaluation point depends only on the loading of the pavement. Loads can be due to

vehicles, thermal loading, or a combination of the two. These loads are characterized by the axle type, axle weight, axle location, and temperature distribution through the PCC layer thickness.

For damage computation, it is necessary to determine the number of occurrences of each combination of loading factors. The number of times each axle of a specified type and weight passes over the pavement in a given month is provided by the MEPDG. However, to account for the interaction of vehicle and temperature loads, it is necessary to determine how many instances of each load occur for a given wheel path and with a given temperature gradient. The MEPDG makes several simplifying assumptions to perform this analysis, including that traffic wander is independent of axle type, axle weight and time of day. The MEPDG also assumes that the percentage of axles depends on the time of day, but is independent of axle type and weight.

6.1.2.1 *Traffic Loads and Vehicle Wander*

Lateral vehicle wander is a measure of the location of the vehicle in relation to the pavement marking and is an input in determining the stresses in the pavement induced by the vehicle. It is typically assumed that traffic wander within the lane is normally distributed, with a mean value of 18 inches (NCHRP 2003a). The standard deviation for vehicle wander can be taken as 10 inches (Darter 1977; Darter et al. 1985; NCHRP 2003a; Yu et al. 1998).

Using this distribution presents a problem in that some amount of traffic loading is predicted to travel with a negative wander, that is to say with the wheel on the shoulder or an adjacent slab. However, this load will still have an effect on the slab due to load transfer. The MEPDG solved this problem by assuming that the effects of a load located x inches from the pavement edge are the same, regardless of the side of the pavement edge on which the load is located (NCHRP 2004). In other words, a load 5 inches from the pavement edge on the slab was assumed to have the same effect as a load 5 inches from the pavement edge on the shoulder. While this assumption is not particularly realistic, it is conservative and it greatly simplifies the task of predicting damage from

loads located near but not on the slab, therefore, the same assumption was made in this program.

Using this assumption and the normal distribution function, it was determined that the probability of a vehicle having a wander of x was given as:

$$P(x) = \frac{1}{s\sqrt{2\pi}} e^{-\left(\frac{(x-m)^2}{2s^2}\right)} + \frac{1}{s\sqrt{2\pi}} e^{-\left(\frac{(-x-m)^2}{2s^2}\right)} \quad (6.1)$$

Where:

x = vehicle wander

P(x) = probability of a vehicle having wander x

m = mean value of vehicle wander

s = standard deviation of vehicle wander

A graph of this function was shown in Figure 2.7. The probability of a vehicle having a wander x is used when computing fatigue damage, a process that involves summing the damage caused by all loads. This requires integrating the probability curve of vehicle wander.

The MEPDG used Gauss integration to determine the area under the probability curve in the computation of fatigue damage. Gauss points and weight factors were determined separately for top-down and bottom-up damage computations, and were optimized for the one evaluation point considered by the MEPDG. This procedure is not applicable in the proposed model because multiple evaluation points will be used, and instead, standard numerical integration was performed using the trapezoid rule, see Figure 6.1.

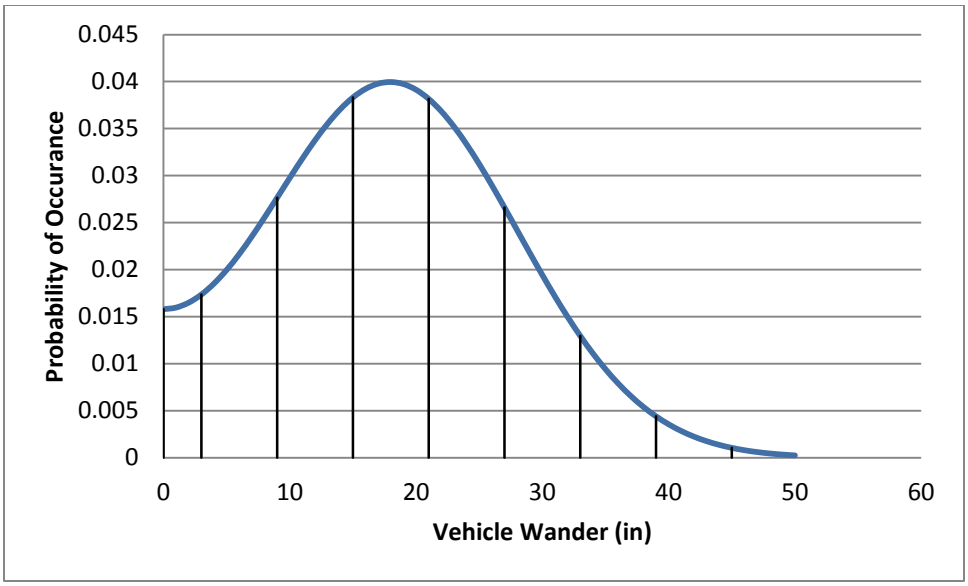

Figure 6.1: Numerical integration of vehicle wander

From this integration, the weights of traffic wander were calculated, results are shown in Table 6.1. The weights used for the widened slab are the same as those used for the standard width slab except the values to which the weights correspond is shifted by 24 inches, which is the amount by which the lane line is shifted away from the slab edge when a widened slab is used. Just as it is assumed for standard width slabs that no vehicles travel with one set of wheels on the shoulder, it is also assumed that no vehicles travel with one set of wheels over the lane line when a widened slab is used. Therefore, the same vehicle distribution applies to both cases when vehicle wander is considered in relation to the lane line. The difference for widened slabs is the location of the lane line in relation to the slab edge.

Table 6.1: Vehicle Wander in the Longitudinal Cracking Model

Standard Width		Widened Slab	
Wander (inches from the slab edge)	**Weight**	**Wander (inches from the slab edge)**	**Weight**
0	4.97%	24	4.97%
6	13.50%	30	13.50%
12	19.79%	36	19.79%
18	22.94%	42	22.94%
24	19.43%	48	19.43%
30	11.87%	54	11.87%
36	5.21%	60	5.21%
42	1.63%	66	1.63%
48	0.36%	72	0.36%
54	0.06%	78	0.06%
60	0.01%	84	0.01%

6.1.2.2 *Temperature*

Temperature gradients in the MEPDG are computed using the EICM, as was discussed above. Both actual temperature gradient and the effects of the other components of differential volume change are accounted for by computing a total equivalent temperature gradient, as discussed in Section 2.3. This temperature gradient was used in the new program for simplicity and compatibility.

To account for the equivalent temperature gradient in the MEPDG, a process called linearization is used, as discussed in Section 2.4.3. This process was selected during the creation of the MEPDG to accommodate limitations in computing power at the time, but involves making simplifying assumptions. In order to avoid making those same assumptions, modifications were made to the procedure used to compute n without using the linearization process.

Instead, the probability of the traffic load occurring at a temperature gradient was computed based on the probability of a specific nonlinear temperature gradient occurring in conjunction with a given linear temperature gradient. The total temperature gradient

was dividing into the equivalent linear temperature component and the nonlinear component. The linear component corresponds to the linear component computed for the neural network system, which includes the contributions of curl and warp. The nonlinear component is computed from the original system parameters. For each hour, and month, the probability of different combinations of linear and nonlinear temperature gradient occurring was computed. Linear temperature gradients were considered in increments of 2°F while nonlinear temperature gradients were considered in increments of 1°F.

6.1.3 Cracking and Damage Prediction

While the transverse cracking model in the MEPDG predicts a percentage of slabs which will experience transverse cracking, such a prediction is not possible for longitudinal cracking. As was discussed in Chapter 3, prediction of the level of longitudinal cracking a pavement will experience is complicated by the lack of independence of longitudinal cracks. While a transverse crack in one slab will not influence the stress distribution in an adjacent slab, the presence of a longitudinal crack in one slab will have a significant impact on the stress distribution in an adjacent slab. When a slab is adjacent to a longitudinally cracked slab, there is a loss of the benefits of load transfer efficiency, which effectively increases the stresses in the uncracked slab and can encourage crack propagation. This creates significant difficulty in determining a relationship between damage and cracking.

The lack of independence associated with longitudinal cracking also illustrates why preventing longitudinal cracks from forming in the first place is so important. While a transverse crack can propagate across the road way, it stops once it has crossed the pavement. Additionally, the presence of a transverse crack does not encourage the formation of other transverse cracks. A longitudinal crack however, can continue to propagate until it reaches a joint too wide to cross. This, coupled with the difficulty of predicting longitudinal cracking levels, prompted the recommendation in Chapter 3 that longitudinal fatigue damage be minimized in design. At this time, the longitudinal cracking program computes only bottom-up fatigue damage but can be expanded in the future to include top-down fatigue damage as well.

6.2 Design Procedure

When designing concrete pavement using both the MEPDG and the longitudinal cracking program developed as part of this research, the following approach should be used:

1. The acceptable level of transverse cracking and longitudinal cracking fatigue damage permitted in design should be established.

2. The MEPDG should be run to determine the level of transverse fatigue damage and cracking. If the level of transverse cracking is not acceptable, the design should be modified until the predicted level of transverse cracking is below the threshold established in Step 1. The amount of both bottom-up and top-down transverse fatigue damage should be compared and the higher value is considered to control; this value should be considered as the level of transverse fatigue damage for comparison purposes later.

3. The program developed as part of this research should be run to determine the level of bottom-up longitudinal fatigue damage at various locations along the transverse joint. It should be noted that because damage is dependent on both the number of applied load and the induced stress level, it is possible for a location other than the critical location for longitudinal cracking to have the highest level of damage. The highest level of damage at any node along the transverse joint should be considered as the level of longitudinal damage.

4. The amount of longitudinal damage should be compared with the amount of transverse damage by computing the damage ratio as:

$$Damage\ Ratio = \frac{longitudinal\ fatigue\ damage}{transverse\ fatigue\ damage} \tag{6.2}$$

   If the damage ratio is less than 1, then transverse fatigue damage will control, though this does not guarantee that the design is acceptable and that longitudinal cracking will not occur. A damage ratio greater than 1 guarantees that

longitudinal cracking will be the dominate failure mode, but does not automatically disqualify the pavement design, as will be discussed below.

5. In order to minimize the amount of longitudinal cracking which will occur, the longitudinal cracking fatigue damage must be below the acceptable threshold established in Step 1. If it is not, steps 2-4 must be repeated as changes to the pavement design are made.

While the damage ratio is a useful tool in the design process, it should not be treated as the only criteria for determining if longitudinal cracking is a problem in a specific pavement design. A damage ratio less than 1 indicates that transverse cracking will be the predominate failure type, but does not indicate that longitudinal cracking will not occur. Indeed, if both transverse and longitudinal fatigue cracking damage are high, both distresses could be seen. Likewise, a damage ratio greater than 1 does not guarentee that longitudinal cracking will be a problem. If both transverse and longitudinal fatigue cracking damage are very low, it is entirely possible that the damage ratio could be greater than one while neither fatigue damage is high enough to result in significant cracking. Therefore, the damage ratio should merely be used as a quick comparison tool to determine the predominate failure mode, but fatigue damage levels should also be examined.

At this time, it is not possible to correlate longitudinal fatigue cracking damage with cracking levels. This is due in part to the lack of independence of longitudinal cracks, as discussed in Chapter 3, and partly due to lack of research into the area. In the future, such a relationship should be investigated.

In the meantime, the relationship between transverse cracking fatigue damage and transverse cracking levels can be used as a minimum estimator of longitudinal cracking levels based on longitudinal cracking fatigue damage. Chapter 3 established that the presence of a longitudinal crack in an adjacent slab increases the stresses in a loaded slab and can cause the crack to propagate. This is not an issue for transverse cracking, thus

the relation between fatigue damage and cracking for transverse cracking will be an underestimate if applied to longitudinal cracking. However, as long as it is known that this is an underestimate, this relation can be used to determine the threshold of longitudinal cracking fatigue damage allowed in design as long as extremely conservative thresholds are established.

6.3 Case Study

To further illustrate how the longitudinal cracking program can be used in conjunction with the MEPDG transverse cracking model for pavement design, several pavements were analyzed in both programs and the damage from each was compared. Four thicknesses of pavement were considered: 6, 8, 10, and 12 inches. All pavements had a 12 inch A-1-a base, and an A-7-6 subgrade. For each pavement thickness, both standard width (12 feet) with both asphalt and tied PCC shoulders, and widened slabs (14 feet) were considered; for each slab width, both doweled and undoweled pavements were analyzed. MEPDG defaults were used for all other properties and the climate was that of Minneapolis-St. Paul.

To determine traffic levels, the annual average daily truck traffic (AADTT) was varied to obtain the same level of transverse fatigue damage for each pavement thickness for the standard width, doweled case (most common). These traffic levels were then applied to all other cases of the same thickness. The MEPDG considers both bottom-up and top-down fatigue cracking, and assumes that a given load combination will only cause one type of cracking (NCHRP 2003a). When selecting a traffic level, the controlling transverse fatigue damage was considered. Traffic was varied until a damage level of approximately 0.20 was reached for whichever type of transverse cracking controlled. This translated to a percentage of slabs cracked at 20 years at 90% reliability of between 12 and 13.5%. For the 8 and 10 inch pavements, the AADTT was within the realm of normal values, but the 6 and 12 inch pavements required unrealistic values of AADTT to ensure the same damage as the 8 and 10 inch thick pavements; this was deemed acceptable for the sake of this exercise because it allowed even comparisons. AADTT levels used for each case are given in Table 6.2.

Table 6.2: Fatigue Damage for Case Studies

Dowels	Width	Slab Thickness (in)	AADTT	Transverse Fatigue Damage		% Slabs Cracked Transversely at 20 years at 90% reliability	Longitudinal Fatigue Damage	Damage Ratio
				Bottom-Up	Top-Down			
Un-doweled	Standard Width Asphalt Shoulder	6	85	0.2037	0.0226	12.3	0.05578	0.27383
		8	1250	0.2065	0.0865	13.4	0.00896	0.04339
		10	18000	0.0750	0.2034	13	0.00311	0.01529
		12	130000	0.0069	0.2001	12	0.00302	0.01509
	Standard Width Tied PCC Shoulder	6	85	0.0822	0.0086	6.7	0.2445	28.4302
		8	1250	0.0593	0.0313	6.1	0.0697	2.22684
		10	18000	0.0135	0.0767	6.5	0.02895	0.37745
		12	130000	0.0007	0.0847	6.8	0.02001	0.23625
	Widened Slab	6	85	0.0251	0.0046	4.8	1.59355	63.4881
		8	1250	0.0181	0.0177	4.8	1.59135	87.9199
		10	18000	0.0040	0.0448	5.4	1.55985	34.8181
		12	130000	0.0002	0.0508	5.6	1.0935	21.5256
Doweled	Standard Width	6	85	0.2037	0.0226	12.3	0.00158	0.00776
		8	1250	0.2043	0.0864	13.3	0.00286	0.01400
		10	18000	0.0754	0.2035	13	0.00178	0.00875
		12	130000	0.0068	0.1999	12	0.00204	0.01021
	Standard Width Tied PCC Shoulder	6	85	0.0822	0.0086	6.7	0.00696	0.80930
		8	1250	0.0586	0.0313	6.1	0.02051	0.65527
		10	18000	0.0135	0.0767	6.5	0.01639	0.21369
		12	130000	0.0007	0.0847	6.8	0.01271	0.15006
	Widened Slab	6	85	0.0251	0.0046	4.8	0.05983	2.38367
		8	1250	0.0181	0.0177	4.8	0.16215	8.95857
		10	18000	0.0041	0.0448	5.4	0.94844	21.1705
		12	130000	0.0002	0.0509	5.6	0.72087	14.1625

The MEPDG computes transverse fatigue damage at the critical location for transverse cracking, which is at midslab along the longitudinal edge. Both top-down and bottom-up cracking damage are computed by the MEPDG; whichever value is higher will control. Longitudinal fatigue damage was computed at various locations along the transverse joint including in the wheel path and at the midslab edge. The highest value of fatigue damage in all cases was found to be in the wheel path. Currently, the longitudinal cracking program computes only bottom-up fatigue damage, though it could be expanded to

include top-down fatigue damage in the future. For comparison purposes, however, the bottom-up cracking damage is sufficient. The computed transvers and longitudinal fatigue damage for each case are show in Table 6.2.

Within the longitudinal cracking fatigue damage program, damage is accumulated at multiple points simultaneously and the largest damage level controls. This is illustrated in Figure 6.2, which shows the damage accumulation with time for three different points analyzed by the longitudinal cracking fatigue damage program for the 8 inch thick, doweled, widened slab case presented in Table 6.2. One analysis point was located in the wheel path, while the others were located at midslab along the transverse joint, and three inches away (towards the load) from midslab. Similar results were obtained for the standard width slab. From this figure, it can be seen that damage in the wheelpath was higher, as would be expected because the majority of the loads occurred in or near the wheel path. Stresses are reduced further from the load, as can be seen by comparing the midslab and near midslab points.

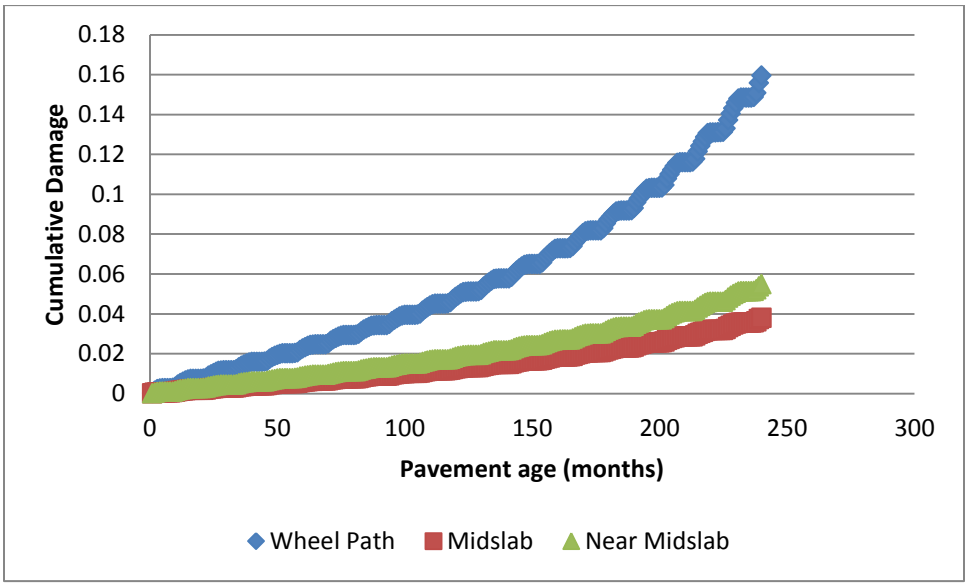

Figure 6.2: Accumulation of longitudinal cracking fatigue damage at various locations.

To further illustrate how damage is accumulated over time in both the MEPDG and the longitudinal fatigue damage cracking model, plots were made for the 8 inch thick pavement described above. Figure 6.3 and Figure 6.4 show the damage accumulation with time for the standard width and widened slab pavements respectively. From these figures, it can be seen that the damage accumulation process is the same between the MEPDG and the longitudinal cracking fatigue damage program. Only damage in the wheel path is shown for longitudinal cracking because this was the case which was found to control. These figures also reiterate that longitudinal cracking controls for the widened slab while transverse cracking controls for the standard width slab, as discussed above.

Figure 6.3: Damage accumulation over time for transverse and longitudinal cracking for the standard width slab.

Figure 6.4: Damage accumulation over time for transverse and longitudinal cracking for the widened slab.

As seen in Table 6.2, the damage ratio was found to be less than one for all of the standard width pavements with asphalt shoulders considered and greater than one for all of the widened slab pavements; the damage ratio of the standard width pavements with tied PCC shoulders were sometimes greater than one and sometimes less. To better visualize the data presented in Table 6.2, these results are also presented graphically in Figure 6.5 through Figure 6.8 for the 6, 8, 10, and 12 inch thick pavements respectively. These graphs show the transverse and longitudinal fatigue damage for a standard width pavements with asphalt and tied PCC shoulders (labeled as standard width and tied PCC repsectively), and widened slab, all with and without dowels.

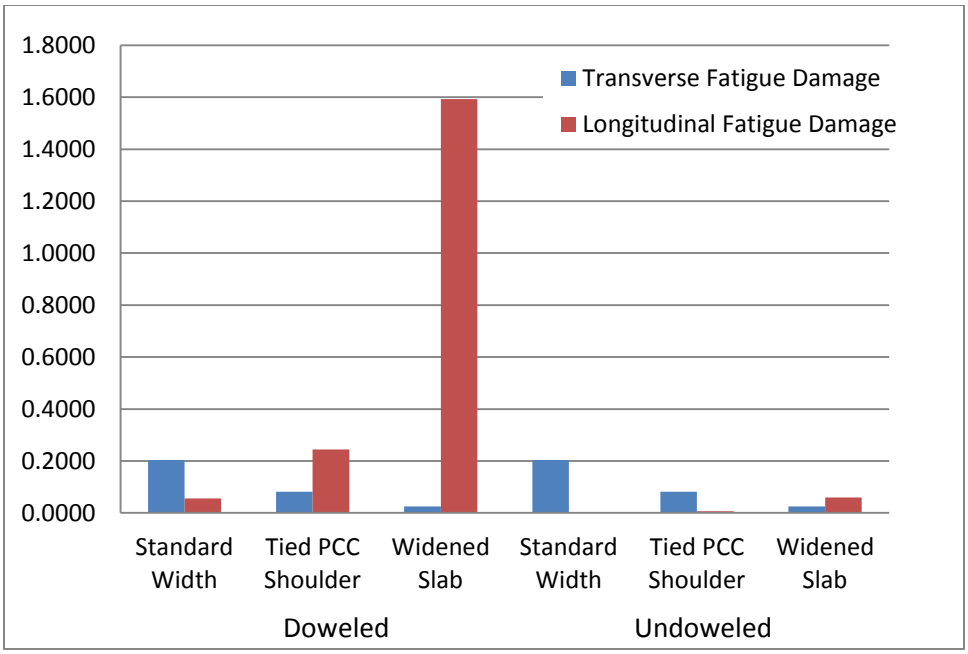

Figure 6.5: Fatigue damage for the 6 inch thick pavement.

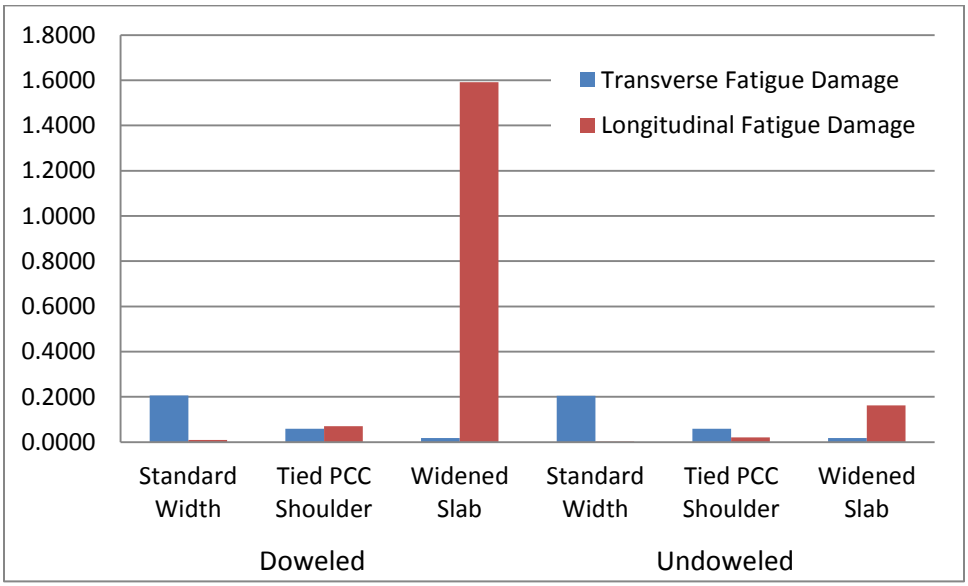

Figure 6.6: Fatigue damage for the 8 inch thick pavement.

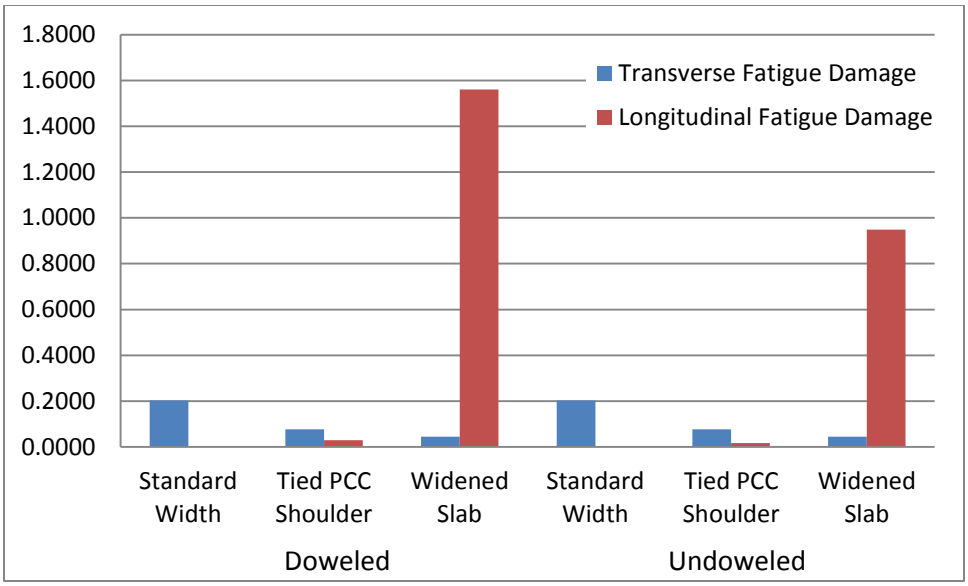

Figure 6.7: Fatigue damage for the 10 inch thick pavement.

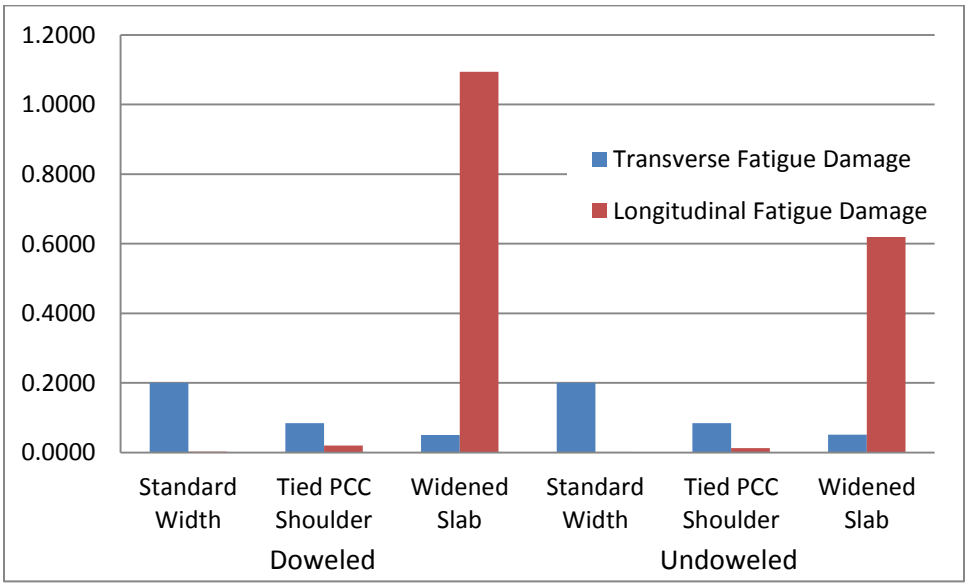

Figure 6.8: Fatigue damage for the 12 inch thick pavement.

From these figures, it can be seen that transverse fatigue damage dominates for the standard width slab with an asphalt shoulder while longitudinal fatigue damage controls for the widened slab case. For the standard width slab with at tied PCC shoulder, transverse cracking controlled for thicker pavements while longitudinal cracking doinated

for thinner pavements. The presence of dowels does not change the amount of transverse fatigue damage expected, but it has a large influence on the magnitude of the longitudinal fatigue damage. Doweled pavements were found to have lower levels of longitudinal fatigue damage, which is consistent with the findings and recommendations of Chapter 7.

If an acceptable level of transverse cracking at 20 years were to be established as 15%, all of the designs would have been considered acceptable designs based on the current MEPDG design practice. However, once longitudinal cracking is considered, not all of the pavement designs remain viable. For example, if longitudinal cracking fatigue damage were limited to 0.1, then all of the undoweled widened slab pavements and the 8, 10, and 12 inch doweled widened slab pavements would be unacceptable.

6.4 Summary and Conclusions

This chapter presented damage accumulation procedure for longitudinal cracking damage for JPCP pavements using the stress analysis procedure developed in Chapter 4. The program developed in this research was used in conjunction with the MEPDG to examine several different pavement designs. Procedure was detailed which will allow a design engineer to modify their current design procedure in order to account for longitudinal cracking as well as transverse cracking in design.

The results of the analyses conducted showed that the fatigue damage for longitudinal cracking controlled for widened slab pavements while transvers fatigue damage was higher for standard width pavements with asphalt shoulders, as would be expected. Longitudinal cracking damage was higher for some but not all standard width pavements with tied PCC shoulders, again as expected. These results agree with the cracking potentials determined in Chapter 5. Dowels were found to reduce the longitudinal fatigue damage and therefore the damage ratio but not to affect transverse fatigue damage. Based on the damage ratio, the widened slab pavements which would have been considered acceptable when only transverse cracking was considered using the current MEPDG were found to be unacceptable.

Chapter 7. Conclusions and Future Work

In this research, a procedure was developed to compute longitudinal fatigue damage in jointed plain concrete pavements. This procedure is MEPDG compatible and will allow pavement engineers to have a better understanding of the potential failure mechanisms of different pavement designs.

Creating an MEPDG-compatible incremental damage analysis of longitudinal cracking damage analysis required computation of stresses the transverse joint of the pavement induced by a large combination of axle loading, temperature gradients, and material properties. To facilitate this stress analysis and avoid embedment of a finite element model, a computationally efficient procedure for determination of these stresses, was developed. The rapid solutions were developed in this study to determine critical stresses for longitudinal damage analysis for a wide range of possible pavement property and load combinations which could be considered in design. The concepts of similarity were used to reduce a dimension of the space of an independent parameters required for training of the rapid solutions. Based on stresses in similar space computed from the neural networks, the program can compute the actual stresses in real space. These stresses are used to determine the amount of damage seen over the course of pavement life.

The results of the stress analysis conducted as part of this research were also used to investigate the characteristics of pavement susceptible to longitudinal cracking. A study was also conducted on the effects of the lack of independence between adjacent slabs when a longitudinal crack is present. Case studies were presented to show how the new longitudinal cracking model can be incorporated into traditional MEPDG design.

7.1 Conclusions

From this research, the following conclusions were drawn:

- By comparing the stresses in similar space at the critical location for longitudinal cracking determined from the reduced factorial with those for transverse cracking, it was possible to determine the most likely failure mode for many different

combinations of pavement parameters and loading. This analysis was used to determine the characteristics of pavement susceptible to longitudinal cracking. Pavements with widened slabs were found to be prone to longitudinal cracking, as were some standard width pavements with tied PCC shoulders. For standard width slabs with asphalt shoulders, longitudinal cracking was not found to be a likely failure mode.

- The longitudinal cracking model developed in this research decmonstrated that longitudinal damage was higher for widened slab pavements and transverse cracking was higher for standard width pavements. These trends fit well with those determined by previous researchers. This was shown using case study examples and matches field observations and classical pavement theory predictions.

- The presence of a longitudinal crack in an adjacent slab influenced the stress distribution in an uncracked slab. It was found that the change in stress distribution in a slab when a crack is introduced to an adjacent slab can lead to loss of benefit of load transfer efficiency, increased probability of crack propagation, and increased potential for pumping and erosion. If erosion did occur, there an increase in stresses as compared with the uneroded case.

- Widened slabs were found to be more affected by the presence of a crack in an adjacent slab than standard width slabs. The loss of benefit of load transfer was greater in widened slabs and the effects of erosion were also more detrimental.

- Using dowels was found to drastically reduce the amount of longitudinal fatigue damage seen in the case studies. This fits with the results of the study on the effect of a longitudinal crack in an adjacent slab, where it was found that dowels reduced stresses by providing load transfer until a crack forms. Once a crack forms however, the benefit of load transfer efficiency between slabs is lost and dowels only encourage crack propagation.

- The principles of similarity proved to be a very valuable tool both for defining a reduced factorial. This reduced factorial was used not only for stress analysis but also determine the characteristics of pavements susceptible to longitudinal versus transverse cracking.

7.2 Design Recommendations

Based on the results of this research, it was possible to identify certain recommendations which designers can implement immediately to improve the designs of their pavements. These recommendations are detailed below:

- Whenever widened slabs are used, longitudinal cracking must be considered. If analysis such as that performed by the program developed in this research cannot be performed to ensure that longitudinal cracking is not a concern, it is recommended that widened slab design be avoided.

- While dowels are recommended in most pavements to reduce stresses and distresses, their use is particularly important when a widened slab is used. This research showed that pavements which higher load transfer efficiency have lower stresses at the transvers joint, which reduces the chances of a longitudinal crack forming. Given the high potential for longitudinal cracks to propagate to adjacent slabs, it is important to stop them from forming in the first place. Therefore, if a widened slab is used, the pavement should be doweled.

- Because of the difficulties associated with predicting longitudinal cracking levels from damage, it is recommended that the design procedure for longitudinal cracking be to choose a pavement design which reduces the longitudinal fatigue damage to below a predetermined threshold. At a minimum, this threshold should be less than the damage due to transverse cracking. This removes any uncertainty associated with the conversion of damage to the percentage of slabs cracked.

Minimizing longitudinal fatigue damage also reduces the risk of having a crack propagate down many slabs in the pavement.

7.3 Future Work

Any research project will answer some questions and produce many more which need to be answered. The areas of future work identified in this research are outlined below:

- It was recommended that longitudinal cracking fatigue damage be limited in design, but currently, it is unknown what the limit on damage should be. Further study will be needed to determine the level of fatigue damage with results in unacceptable performance.

- This research developed a procedure to predict longitudinal fatigue damage. However, to be completely MPEDG compatible and more user friendly, it would be necessary to predict longitudinal cracking itself. This is currently not possible because of the lack of independence between longitudinal cracks and the stress distribution in adjacent slabs. This relationship should be further explored to develop a model for predicting longitudinal cracking amounts from damage which accounts for the presence of a longitudinal crack in an adjacent slab.

- When exploring the effects of a longitudinal crack in an adjacent slab on the slab of interest, it was determine that standard finite element modeling cannot be used to model the case of very high (>95%) load transfer efficiency between adjacent slabs. This case should be further explored using fracture mechanics to determine the behavior of the system when one slab is cracked longitudinally.

- Another issue associated with predicting longitudinal cracking discovered when examining the effects of adjacent longitudinal cracks was that the presence of a longitudinal crack increases the probability of erosion at the joint. Erosion was found to further increase the potential of longitudinal crack propagation by further increasing stresses. Currently, the effects of erosion are not accounted for in the

program because only damage is computed. However, when the program is expanded to predict longitudinal cracking, these erosion effects will have to be accounted for.

References

AASHTO 1993, 'Guide for Design of Pavement Structures', American Association of State Highway and Transportation Officials, Washington DC.

Altoubat, S. A. & Lange, D. A. 2001, 'Creep, Shrinkage, and Cracking of Restrained Concrete at Early Age', *ACI Materials Journal*, vol. 98, no. 4, pp. 323-31.

Ardani, A., Hussain, S. & LaForce, R. 2003, 'Stitching Concrete Pavement Cracks and Joints', Skokie IL.

Armaghani, J. M., Larsen, T. J. & Smith, L. L. 1987, 'Temperature Response of Concrete Pavements', *Transportation Research Record*, no. 1121, pp. 23-33.

Banan, M. R. & Hjelmstad, K. D. 1994, 'Data-Based Mathematical Modeling: Development and Application', University of Illinois at Urbana Champaign, Urbana, Illinois.

Banan, M. R. & Hjelmstad, K. D. 1995, 'A Monte Carlo Strategy of Data-Based Mathematical Modeling', *Mathematical and Computer Modelling*, vol. 22, no. 8, pp. 73-90.

Banan, M. R. & Hjelmstad, K. D. 1996, 'Neural Networks and the AASHO Road Test', *ASCE Journal of Transportation Engineering*, vol. 122, no. 5, pp. 358-66.

Bazant, Z. P. & Baweja, S. 1995, 'Creep and Shrinkage Prediction Model for Analysis and Design of Concrete Structures - Model B3', *Materials and Structurs/Materiaux et Constructions*, vol. 28, no. 6, pp. 357-65.

Beckemeyer, C. A., Khazanovich, L. & Yu, H. T. 2002, 'Determining the Amount of Built-in Curling in JPCP: A Case Study of Pennsylvania I-80', in *Transportation Research Board Annual Meeting*, Washington, D.C.

Bissonnette, B., Attiogbe, E. K., Miltenberger, M. A. & Fortin, C. 2007, 'Drying Shrinkage, Curling, and Joint Opening of Slabs-on-Ground', *ACI Materials Journal*, vol. 104, no. 3, pp. 259-67.

Bradbury, R. D. 1938, *Reinforced Concrete Pavements*, Wire Reinforcement Institute, Washington D.C.

Buch, N., Gilliland, D., Vongchusiri, K. & Van Dam, T. 2004, 'A Preliminary Mechanisitic Evaluation of PCC Cross-Sections Using ISLAB2000 - A Parametric Study', Michigan Department of Transportation, Lansing, MI.

Ceylan, H., Tutumluer, E. & Barenberg, E. J. 1999, 'Artificial Neural Network Analyses of Concrete Airfield Pavements Serving the Boeing B-777 Aircraft', *Transportation Research Record*, no. 1684, pp. 110-7.

Ceylan, H., Tutumluer, E. & Barenberg, E. J. 2000, 'Effects of Combined Temperature and Gear Loading on the Response of Concrete Airfield Pavements Serving the Boeing B-777 Aircraft', in *International Air Transport Conference, 2020 Vision of Air Transportation*, San Francisco, California.

Ceylan, H., Tutumluer, E. & Barenburg, E. J. 1998, 'Artifical Neural Networks As Design Tools in Concrete Airfield Pavement Design', in *25th International Air Transportation Conference*, Austin, Texas, pp. 447-65.

Choubane, B. & Tia, M. 1992, 'Nonlinear Temperature Gradient Effects on Maximum Warping Stresses in Rigid Pavements', *Transportation Research Record*, vol. 1370, pp. 11-9.

Choubane, B. & Tia, M. 1995, 'Analysis and Verification of Thermal-Gradient Effects on Concrete Pavement', *Journal of Transportation Engineering*, vol. 121, no. 1, pp. 75-81.

Corley-Lay, J. & Morrison 2002, 'Thirty-Three-Year Performance of Jointed Concrete Test Sections in North Carolina', *Transportation Research Record*, no. 1806, pp. 88-94.

Crovetti, J. A. 1994, Evaluation of Jointed Concrete Pavement Systems Incorporating Open-Graded Permeable Bases, Dissertation, University of Illinois at Urbana Campaign.

Darter, M. 1977, 'Design of Zero-Maintenance Plain Jointed Pavements', Federal Highway Administration, Washington DC.

Darter, M. I., Beck, J. M., Snyder, M. B. & Smith, R. E. 1985, 'Portland Cement Concrete Pavement Evaluation System - COPES', Transportation Research Board, Washington D.C.

Darter, M. I., Hall, K. T. & Kuo, C. 1995, 'Support Under Portland Cement Concrete Pavements', ed T.R. Board, National Research Council, Washington D.C.

Eisenmann, J. & Leykauf, G. 1990, 'Effect of Paving Temperature on Pavement Performance', in *2nd International Workshop on the Theoretical Design of Concrete Pavements*, Siguenza, Spain, pp. 419-28.

FHWA 2009, 'Long Term Pavement Performance Database', Federal Highway Administration.

Gardner, N. J. & Lockman, M. J. 2001, 'Design Provisions for Drying Shrinkage and Creep of Normal Strength Concrete', *ACI Materials Journal*, vol. 98, no. 2, pp. 159-67.

Granger, L., Torrenti, J.-M. & Diruy, M. 1994, 'Simulation Numerique du Retrait du Beton Sous Hygrometrie Variable', *Bulletin de Liaison de Laboratoires des Ponts et Chaussees*, vol. 190, no. 3881, pp. 57-64.

Guo, E. H. 2001, 'Back-Estimation of Slab Curling and Joint Stiffness', in *7th International Conference on Concrete Pavements*, Orlando, FL.

Harr, M. E. & Leonards, G. A. 1959, 'Warping Stresses and Deflections in Concrete Pavements', *Transportation Research Record*, vol. 38, pp. 286-320.

Haussmann, L. D., Tutumluer, E. & Barenberg, E. J. 1997, 'Neural Network Algorithms for the Correction of Concrete Slab Stresses from Linear Elastic Layered Programs', *Transportation Research Record*, no. 1568, pp. 44-51.

Helmuth, R. A. & Turk, D. H. 1967, 'The Reversible and Irreversible Drying Shrinkage of Hardened Portland Cement and Tricalcium Silicate Pastes', Research and Development Laboratories of the Portland Cement Association, pp. 8-21.

Hiller, J. E. 2007, Development of Mechanistic-Empirical Principles for Jointed Plain Concrete Pavement Fatigue Design, University of Illinois - Urbana Champaign.

Hiller, J. E., Lederle, R. E. & Deshpande, Y. S. 2011, 'Characterization of Recycled Concrete Aggregates for Reuse in Rigid Pavements', in *2011 Australian Society for Concrete Pavements Conference*, West Ryde, New South Wales, Australia.

Hiller, J. E. & Roesler, J. R. 2002, 'Transverse Joint Analysis for Mechanistic–Empirical Design of Rigid Pavements', *Transportation Research Record*, no. 1809, pp. 42-51.

Hiller, J. E. & Roesler, J. R. 2005, 'User's Guide for Rigid Pavement Analysis Design in California (RadiCAL) Software. Version 1.2', UC-Berkeley/Caltrans Partnered Pavement Research Center, Richmond, California.

Hiller, J. E., Signore, J. M., Kannekanti, V., Basheer, I. & Harvey, J. T. 2012, 'Prediction of Longitudinal Fatigue Cracking in Rigid Pavements Using Radical', in *10th International Conference on Concrete Pavements*, International Society for Concrete Pavements, Quebec City, pp. 561-76.

Hveem, F. N. 1951, 'Slab Warping Affects Pavement Joint Performance', *Journal of the American Concrete Institute*, vol. 22, no. 10, pp. 797-808.

Hveem, F. N. & Bailey, T. 1957, 'Some Factors Influencing Shrinkage of Concrete Pavements', *Journal of the American Concrete Institute*, vol. 53, no. 2, pp. 781-9.

Ioannides, A., Karanth, R. & Sanjeevirao, K. 1998, 'Mechanistic-Empirical Approach to Assessing Relative Pavement Damage', *Transportation Research Record*, no. 1639, pp. 113-9.

Ioannides, A. M. & Khazanovich, L. 1998a, 'General Formulation for Multilayered Pavement Systems', *Journal of Transportation Engineering*, vol. 124, no. 1, pp. 82-90.

Ioannides, A. M. & Khazanovich, L. 1998b, 'Nonlinear Temperature Effects in Multi-Layered Concrete Pavements', *ASCE Journal of Transportation Engineering*, vol. 124, no. 2, pp. 128-36.

Ioannides, A. M., Khazanovich, L. & Becque, J. L. 1992, 'Structural Evaluation of Base Layers in Concrete Pavement Systems', *Transportation Research Record*, no. 1370, pp. 20-8.

Ioannides, A. M. & Salsilli-Murua, R. A. 1989, 'Temperature Curling in Rigid Pavements: An Application of Dimensional Analysis', *Transportation Research Record*, no. 1227, pp. 1-11.

Ioannides, A. M., Thompson, M. R. & Barenberg, E. J. 1985, 'Westergaard Solutions Reconsidered', *Transportation Research Record*, no. 1043, pp. 13-23.

Janda, H. F. 1935, 'Longitudinal Cracking of Concrete Pavements on State Highway 13 in Clark and Taylor Counties, Wisconsin', in *Highway Research Board*, National Research Council, Washington D.C., p. 157.

Janssen, D. J. 1987, 'Moisture in Portland Cement Concrete', *Transportation Research Record*, no. 1121, pp. 40-4.

Jiang, Y. J. & Darter, M. I. 2005, 'Structural Factors of Jointed Plain Concrete Pavements: SPS-2 - Initial Evaluation and Analysis', Federal Highway Administration, McLean, VA.

Khazanovich, L. 1994, Structural Analysis of Multi-Layered Concrete Pavement Systems, University of Illinois Urbana-Champaign.

Khazanovich, L. & Darter, M. I. 2012, 'Lessons Learned from MEPDG Development: A Confession of the JPCP MEPDG Developers', in *10th International Conference on Concrete Pavements*, International Society of Concrete Pavements, Quebec City, Quebec, Canada.

Khazanovich, L., Darter, M. I. & Yu, H. T. 2004, 'Mechanistic-Empirical Model to Predict Transverse Joint Faulting', *Transportation Research Record*, no. 1896, pp. 34-45.

Khazanovich, L. & Roesler, J. R. 1997, 'DIPLOBACK: Neural-Network Based Backcalculation Program for Composite Pavements', *Transportation Research Record*, no. 1570, pp. 143-50.

Khazanovich, L., Selezneva, O., Yu, H. T. & Darter, M. I. 2001, 'Development of Rapid Solutions for Prediction of Critical Continuously Reinforced Concrete Pavement Stresses', *Transportation Research Record*, no. 1778, pp. 64-72.

Khazanovich, L. & Yu, H. T. 1988, 'ILSL2 - A Finite Element Program for Analysis of Concrete Pavements and Overlays', in *Fifth International Conference on Bearing Capacity of Roads and Airfields*, Trondheim Norway.

Khazanovich, L., Yu, H. T., Rao, S., Galasova, K., Shats, E. & Jones, R. 2000a, 'ISLAB2000 - Finite Element Analysis Program for Rigid and Composite Pavements', ERES Consultants, Champaign, Illinois.

Khazanovich, L., Yu, H. T., Rao, S., Galasova, K., Shats, E. & Jones, R. 2000b, 'ISLAB2000 - Finite Element Analysis Program for Rigid and Composite Pavements. User's Guide', ERES Consultants, Champaign, Ill.

Khazanovich, L., Yut, I., Husein, S., Turgeon, C. & Burnham, T. 2008, 'Adaption of Mechanistic-Empirical Pavement Design Guide for Design of Minnesota Low-Volume Portland Cement Concrete Pavements', *Transportation Research Record*, no. 2087, pp. 57-67.

Korenev, B. G. & Chernigovskaya, E. I. 1962, 'Analysis of Plates on Elastic Foundation', *Gosstroiizdat*.

L'Hermite, R. 1947, 'Le Retrait des Ciments, Mortiers et Beton', in *Compte Rendu des Recherches*, Laboratoires du Batiment de des Travaux Publics, pp. 13-91.

L'Hermite, R., Chefdeville, J. & Grieu, J. J. 1949, 'Memoires sur la Mechanique-Physique du Beton: Nouvelle Contribution a L'Etude du Retrait des Ciments', *Liants Hydrauliques, Annales de L'Institut Technique du Batiment et des Travaux Publics*, vol. 106, no. 5, pp. 2-28.

Larson, G. & Dempsey, B. J. 1997, 'Enhanced Integrated Climatic Model', University of Illinois - Urbana Champaign, Urbana Illinois.

Lederle, R. E. & Hiller, J. E. 2012, 'New Warping and Differential Drying Shrinkage Models for Jointed Plain Concrete Pavements Derived with a Nonlinear Shrinkage Distribution', *Transportation Research Record*, no. 2305, pp. 3-13.

Lederle, R. E. & Hiller, J. E. 2013, 'Reversible Shrinkage of Concrete Made with RCA and Other Aggregate Types', *ACI Materials Journal*, vol. 110, no. 4.

Meier, R. W. & Rix, G. J. 1994, 'Backcalculation of Flexible Pavement Moduli Using Artificial Neural Networks', *Transportation Research Record*, no. 1448, pp. 75-82.

Miner, M. 1945, 'Cumulative Damage in Fatigue', *Transactions of the ASME*, vol. 67, pp. A159-A64.

Mohamed, A. R. & Hansen, W. 1997, 'Effect of Nonlinear Temperature Gradient on Curling Stress in Concrete Pavement', *Transportation Research Record*, no. 1568, pp. 65-71.

NCHRP 2003a, 'Guide for Mechanistic-Empirical Design for New and Rehabilitated Pavement Structures: Appendix KK - Transverse Cracking of JPCP', Transportation Research Board, Washington DC.

NCHRP 2003b, 'Guide for Mechanistic-Empirical Design for New and Rehabilitated Pavement Structures: Appendix QQ: Structural Response Models for Rigid Pavements', National Research Council, Washington D.C.

NCHRP 2004, 'Guide for Mechanistic-Empirical Design of New and Rehabilitated Pavement Structures: Part 3 Design Analysis: Chapter 4: Design of New and Reconstructed Rigid Pavements', Transportation Research Board, Washington DC.

NCHRP 2006, 'Mechanistic Empirical Pavement Design Guide', Transportation Research Board, Washington DC.

Neville, A. M. 1997, *Properties of Concrete*, 4th edn, Wiley & Sons, Inc, New York.

Owusu-Ababio, S. & Schmitt, R. 2013, 'Longitudinal Cracking in Widened Portland Cement Concrete Pavements', Wisconsin Department of Transportation, Madison WI.

Packard, R. G. & Tayabji, S. D. 1985, 'New PCA Thickness Design Procedure for Concrete Highway and Street Pavements', in *Third International Conference on Concrete Pavement Design*, Purdue University, West Lafayette, IN, pp. 225-36.

Pane, I., Hansen, W. & Mohamed, A. R. 1998, 'Three-Dimensional Finite Element Study on Effects of Nonlinear Temperature Gradients in Concrete Pavements', *Transportation Research Record*, no. 1629, pp. 58-66.

PCA, P. C. A. 1984, 'Thickness Design of Concrete Highway and Street Pavements', Skokie, IL, pp. 1-47.

Poblete, M., Ceza, P., David, J., Espinosa, R., Garcia, A. & Gonzalez, J. 1991, 'Model of Slab Cracking for Portland Cement Concrete Pavements', *Transportation Research Record*, no. 1307, pp. 154-61.

Poblete, M., Salsilli, R., Valenzuela, R., Bull, A. & Spratz, P. 1988, 'Field Evaluation of Thermal Deformations in Undoweled PCC Pavement Slabs', *Transportation Research Record*, no. 1207, pp. 217-27(+?).

Rao, C., Barenberg, E. J., Snyder, M. B. & Schmidt, S. 2001, 'Effects of Temperature and Moisture on the Response of Jointed Concrete Pavements', in *7th International Conference on Concrete Pavements*, Orlando, FL.

Rao, S. & Roesler, J. R. 2005, 'Characterizing Effective Built-In Curling from Concrete Pavement Field Measurements', *Journal of Transportation Engineering*, vol. 131, no. 4, pp. 320-7.

Reddy, A. S., Leonards, G. A. & Harr, M. E. 1963, 'Warping Stresses and Deflections in Concrete Pavements: Part III', in *Highway Research Board Proceedings*, pp. 1-24.

Richardson, J. M. & Armaghani, J. M. 1987, 'Stress Caused by Temperature Gradients in Portland Cement Concrete Pavements', *Transportation Research Record*, no. 1121, pp. 7-13.

Saxena, P. 2011, Cracking of the PCC Layer in Composite Pavements, PhD Dissertation, University of Minnesota.

Shacklock, B. W. & Keene, P. W. 1957, 'The Effect of Mix Proportions and Testing Conditions on Drying Shrinkage and Moisture Movement of Concrete', Cement and Concrete Association.

Siddique, Z., Hossain, M. & Meggers, D. 2006, 'Curling and Curling Stresses of New Concrete', in *Airfield and Highway Pavements Specialty Conference*, American Society of Civil Engineers, pp. 671-82.

Sondag, S. K. & Snyder, M. B. 2003, 'Analysis of "Built-in" Curling and Warping of PCC Pavements'.

Tabatabaie, A. M. & Barenberg, E. J. 1978, 'Finite Element Analysis of Jointed or Cracked Concrete Pavements', *Transportation Research Record*, no. 671, pp. 11-8.

Teller, L. W. & Sutherland, E. C. 1935, 'The Structural Design of Concrete Pavements: Observed Effects of Variations in Temperature and Moisture on the Size, Shape, and Stress Resistance of Concrete Pavement Slabs', *Public Roads*, vol. 16, no. 9, pp. 169-200.

Thomlinson, J. 1940, 'Temperature Variations and Consequent Stresses Produced by Daily and Seasonal Temperature Cycles in Concrete Slabs', *Concrete and Constructional Engineering*, vol. 35, no. 7, pp. 352-60.

Thompson, M. R. & Barenberg, E. J. 1992, 'Calibrated Mechanistic Structural Analysis Procedure for Pavements - Phase 2', Transportation Research Board, National Research Council, Washington DC.

Timoshenko, S. & Goodier, J. N. 1951, *Theory of Elasticity*, 2nd edn, McGraw Hill Book Company, New York.

Timoshenko, S. & Woinowsky-Krieger, S. 1959, *Theory of Plates and Shells*, 2nd edn, McGraw Hill Book Company.

Voight, G. F. 2002, 'Early Cracking in Concrete Pavements - Causes and Repairs', in *Federal Aviation Administration Airport Technology Transfer Conference*, Federal Aviation Administration.

Wells, S. A., Phillips, B. M. & Vandenbossche, J. M. 2006, 'Characterizing Strain Induced by Environmental Loads in Jointed Plain Concrete Pavements', *Transportation Research Record*, no. 1947, pp. 36-48.

Westergaard, H. M. 1926, 'Stresses in Concrete Pavements Computed by Theoretical Analysis', *Public Roads*, vol. 7, no. 2, pp. 25-35.

Westergaard, H. M. 1927, 'Theory of Concrete Pavement Design', *Proceedings of the Highway Research Board*.

Yu, H. T. & Khazanovich, L. 2001, 'Effects of Construction Curling on Concrete Pavement Behavior', in *7th International Conference on Concrete Pavements*, Orlando, FL.

Yu, H. T., Smith, K. D., Darter, M. I., Jiang, J. & Khazanovich, L. 1998, 'Performance of Concrete Pavements Volume III - Improving Concrete Pavement Performance', Federal Highway Administration, MnLean, VA.

Zollinger, D. G. & Barenberg, E. J. 1989, 'Proposed Mechanistic Based Design Procedures for Jointed Concrete Pavements', University of Illinois at Urbana-Champaign, Champaign IL.

Appendix A: Example Stress Computations

To demonstrate how the principles of similarity work, four examples are presented. The first three examples are for the unbonded case and illustrate in detail how the principles of similarity are used. The first example is for the case of traffic loads only, while the second example considers only temperature loads. The third example is for the case of combined temperature and axle loads. In each of these examples, two similar two-layer slab systems and one similar single layer slab system are presented. The two-layer original systems and the similar single layer system were analyzed using finite element analysis to determine the stresses and deflections under various load conditions. The results of the analysis of the single layer system were used to calculate the stresses and deflections in both original two-layer systems. Theses calculated results were then compared to the finite element results obtained for each original system. The fourth example repeats this process for the bonded case with both thermal and axle loads to show the differences between a bonded and an unbonded problem when compared with Example 3.

For all examples, the systems were analyzed as a system of three slabs in each direction, see Figure A1. The slab of interest was the center slab. Slab dimensions were 12 feet by 15 feet, and the load transfer efficiency was assumed to be 70% at all joints. When a load was considered, it was placed at the mid-slab edge on the slab of interest, six inches from the joint, again see Figure A1. Analysis was conducted using ISLAB2000 (Khazanovich et al. 2000b).

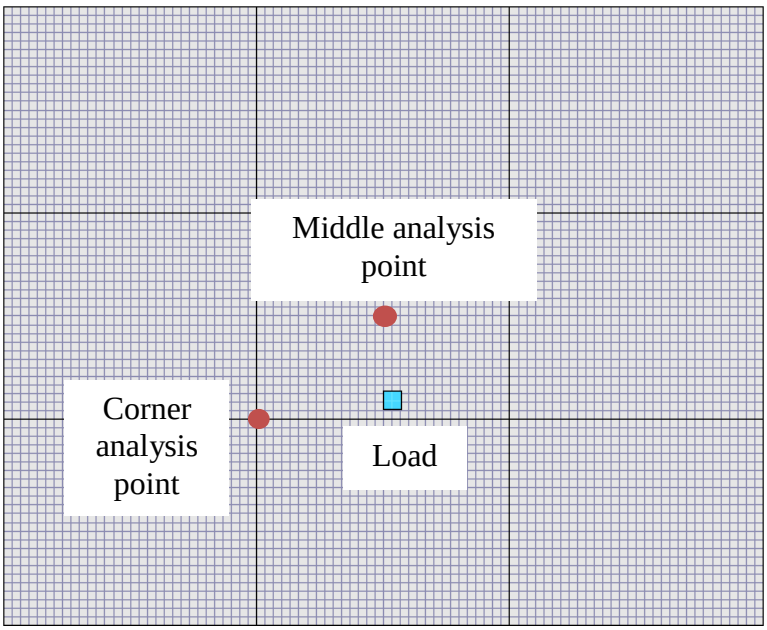

Figure A1: Finite element model used to compute actual stresses, shown with load and analysis points

A1. Example 1: Stress Computations for Similar Slabs with Axle Loads

The first three examples use the same two-layer systems and same similar single layer system. It is important note that, while the single layer system is similar to the two layered systems, it is not an equivalent single layer system. The two-layer systems were called System A and System B; the single layer system was called System C. These systems are defined in Table A1.

Table A1:Properties of Systems A, B, and C

Parameter	System A	System B	System C
Concrete Thickness h pcc (in)	12	10	13.67
Concrete Elastic Modulus E pcc (psi)	4,000,000	5,030,811	4,000,000
Concrete Poisson's Ratio μ pcc	0.15	0.15	0.15
Concrete Coefficient of Thermal Expansion αpcc (in/in/°F)	$4.40*10^{-6}$	$4.40*10^{-6}$	$4.40*10^{-6}$
Concrete Unit Weight γ pcc (lb/in^3)	0.087	0.07	0.0764
Base Thickness h base (in)	20	12	-
Base Modulus of Elasticity E base (psi)	30,000	45,000	-
Base Poisson's Ratio μ base	0.15	0.15	-
Base Coefficient of Thermal Expansion CTE base (in/in/°F)	$4.40*10^{-6}$	$4.40*10^{-6}$	-
Base Unit Weight γ base (lb/in^3)	0 (unbonded)	0 (unbonded)	-
Modulus of Subgrade Reaction k (psi/in)	350	250	500
Temperature Gradient ΔT (°F)	-25.0	-19.19	-19.26590958
Load P (lbs)	18,000	12,069	18000
Tire pressure p (psi)	100	100	67.04980843

For Systems A, B, and C to be considered similar by the equivalent system concept, the following conditions must be satisfied (Khazanovich et al. 2001; NCHRP 2003b):

1. $L_A = L_B = L_C$
2. $\ell_A = \ell_B = \ell_C$
3. $\phi_A = \phi_B = \phi_C$
4. $\frac{AGG_A}{k_A \ell_A} = \frac{AGG_B}{k_B \ell_B} = \frac{AGG_C}{k_C \ell_C}$

5. $\frac{P_A}{h_A \gamma_A} = \frac{P_B}{h_B \gamma_B} = \frac{P_C}{h_C \gamma_C}$
6. $s_A = s_B = s_C$
7. $f_A = f_B = f_C$

Where:

L = slab length

ℓ = radius of relative stiffness (Westergaard 1926)

$$\ell = \sqrt[4]{\frac{Eh^3}{12(1-\mu)k}}$$

ϕ = Korenev's non-dimensional temperature gradient (Korenev & Chernigovskaya 1962)

$$\phi = \frac{2\alpha(1+\mu)\ell^2 k}{h^2 \gamma}\Delta T$$

AGG = aggregate interlock factor determined from the load transfer efficiency (Crovetti 1994)

$$AGG = \frac{0.00546k\ell}{\left(\frac{1}{LTE} - 0.01\right)^{1.178}}$$

P = applied load

s = distance from slab edge to outer wheel edge

f = tire footprint

Conditions 1, and 6, are satisfied based on the geometry of the problem. To show that conditions 2, 3, 4, 5 and 7 are satisfied, the equivalent single layer system for Systems A and B must be defined. System C does not require an equivalent single layer system because it is already a single layer system. The equivalent thickness is given as (Ioannides et al. 1992):

$$h_{eq} = \sqrt[3]{{h_{PCC}}^3 + \frac{E_{base}}{E_{PCC}}{h_{base}}^3}$$

$$h_{A,eq} = \sqrt[3]{12^3 + \frac{30000}{4000000} 20^3} = 12.137\ in$$

$$h_{B,eq} = \sqrt[3]{10^3 + \frac{45000}{5030811} 12^3} = 10.05\ in$$

The equivalent unit weight is given as (Khazanovich 1994):

$$\gamma_{eq} = \frac{\gamma_{PCC} h_{PCC} + \gamma_{base} h_{base}}{h_{eq}}$$

$$\gamma_{A,eq} = \frac{0.087 * 12 + 0 * 20}{12.137} = 0.086\ lbs/in^3$$

$$\gamma_{B,eq} = \frac{0.07 * 10 + 0 * 12}{10.05} = 0.0696\ \ lbs/in^3$$

Check that the radii of relative stiffness are equal:

$$\ell = \sqrt[4]{\frac{Eh^3}{12(1-\mu)k}}$$

$$\ell_A = \sqrt[4]{\frac{4000000 * 12.137^3}{12(1-0.15) * 350}} = 36.330$$

$$\ell_B = \sqrt[4]{\frac{5030811 * 10.05^3}{12(1-0.15) * 250}} = 36.330$$

$$\ell_C = \sqrt[4]{\frac{4000000 * 13.67^3}{12(1-0.15) * 500}} = 36.330$$

From this, it can be seen that condition 2 is satisfied.

Because there is no temperature gradient considered in Example 1, condition 3 need not be considered (technically, all have a $\phi = 0$). This condition will be considered again in Example 2.

Check that the ratios of aggregate interlock factor to $k\ell$ are equal. First, the aggregate interlock factor must be computed:

$$AGG = \frac{0.00546k\ell}{\left(\frac{1}{LTE} - 0.01\right)^{1.178}}$$

$$AGG_A = \frac{0.00546 * 350 * 36.330}{\left(\frac{1}{70} - 0.01\right)^{1.178}} = 42758.357$$

$$AGG_B = \frac{0.00546 * 250 * 36.330}{\left(\frac{1}{70} - 0.01\right)^{1.178}} = 30541.684$$

$$AGG_C = \frac{0.00546 * 500 * 36.330}{\left(\frac{1}{70} - 0.01\right)^{1.178}} = 61083.367$$

Then the ratios of aggregate interlock factor to $k\ell$ are computed:

$$\frac{AGG_A}{k_A \ell_A} = \frac{42758.357}{350 * 36.330} = 3.3627$$

$$\frac{AGG_B}{k_B \ell_B} = \frac{30541.684}{250 * 36.330} = 3.3627$$

$$\frac{AGG_C}{k_C \ell_C} = \frac{61083.367}{500 * 36.330} = 3.3627$$

From this, it can be seen that condition 4 is satisfied.

Check that the ratios of applied load to self-weight are equal:

$$\frac{P_A}{h_{A,equiv}\gamma_{A,equiv}} = \frac{18000}{12.137 * 0.086} = 17241.379$$

$$\frac{P_B}{h_{B,equiv}\gamma_{B,equiv}} = \frac{12069}{10.05 * 0.0696} = 17241.379$$

$$\frac{P_C}{h_C \gamma_C} = \frac{18000}{13.67 * 0.0764} = 17241.379$$

From this, it can be seen that condition 5 is satisfied

Check that the tire footprints are equal. The analysis program requires the length and width of the tire footprint as inputs. Given that the tires are square,

$$f = a^2$$

Where:

a = length of the tire = width of the tire

$$a = \sqrt{\frac{P}{p}}$$

Compute *a* for each system:

$$a_A = \sqrt{\frac{18000}{100}} = 13.4164$$

$$a_B = \sqrt{\frac{12068}{67.05}} = 13.4164$$

$$a_C = \sqrt{\frac{18000}{100}} = 13.4164$$

From this, it can be seen that condition 7 is satisfied.

Given that all of the conditions required by the equivalent system concept have been satisfied, the systems can be considered to be similar. Finite element analysis was conducted on System C when the load of 18000 lbs was placed at the location shown in Figure A1. Selected results for the stresses and deflections in the middle of the slab and in the lower left corner (locations also shown in Figure A1) at the top and bottom surfaces are given in Table A2.

Table A2: Stresses and Deflections in System C Due to an Applied Load

Surface	**Location**	**Deflection δ_C (in)**	**Stress in x-direction (psi)**	**Stress in y-direction (psi)**
Bottom	Corner	-0.021429	0.8408	0.8399
Bottom	Middle	0.010256	-77.942	-66.0622
Top	Corner	-0.021429	-0.8408	-0.8399
Top	Middle	0.010256	77.942	66.0622

To compute the deflections in Systems A and B from those in System C, the deflections from System C must be scaled using scaling factors. The scaling factor λ for deflections is:

$$\lambda = \frac{k_2 h_1 \gamma_1}{k_1 h_2 \gamma_2}$$

Plugging in values from Table A1, the scaling factor to go from System C to System A is:

$$\lambda_{C-A} = \frac{k_C h_A \gamma_A}{k_A h_C \gamma_C} = \frac{500 * 12 * 0.087}{350 * 13.67 * 0.076} = 1.43$$

The scaling factor to go from System C to System B is:

$$\lambda_{C-B} = \frac{k_C h_B \gamma_B}{k_B h_C \gamma_C} = \frac{500 * 10 * 0.0696}{250 * 13.67 * 0.076} = 1.34$$

The deflections from System C, δ_C, given in Table A2 are multiplied by the appropriate scaling factor to find the deflections in Systems A and B, as shown in Table A3.

Table A3: Deflections due to an Applied Load in Systems A and B Computed from those in System C

Surface	**Location**	**δ_C (in)**	**$\delta_A = \lambda_{C\text{-}A} * \delta_C$ (in)**	**$\delta_B = \lambda_{C\text{-}B} * \delta_C$ (in)**
Bottom	Corner	-0.021429	-0.03	-0.03
Bottom	Middle	0.010256	0.01	0.013753
Top	Corner	-0.021429	-0.03	-0.02874
Top	Middle	0.010256	0.01	0.013753

The computed defections in Systems A and B are compared with those determined from the finite element analysis in Table A4. From this table, it can be seen that the computed deflections match the actual deflections almost exactly.

Table A4: Computed versus Actual Deflections due to an Applied Load in Systems A and B

System A				
Surface	**Location**	**Computed δ_A (in)**	**Actual δ_A (in)**	**Computed/Actual System A**
Bottom	Corner	-0.030613	-0.030620	1.00023
Bottom	Middle	0.014651	0.014653	1.00011
Top	Corner	-0.030613	-0.030620	1.00023
Top	Middle	0.014651	0.014653	1.00011
System B				
Surface	**Location**	**Computed δ_B (in)**	**Actual δ_B (in)**	**Computed/Actual System B**
Bottom	Corner	-0.028736	-0.028743	1.00024
Bottom	Middle	0.013753	0.013754	1.00005
Top	Corner	-0.028736	-0.028743	1.00024
Top	Middle	0.013753	0.013754	1.00005

The stresses in Systems A and B are computed from those in System C using the following equation:

$$\sigma_{1,total} = \lambda(\sigma_{2,Linear}) + \sigma_{1,nonlinear}$$

Where:

$\sigma_{2,Linear=}\sigma_{2,\,total} - \sigma_{2,nonlinear}$

$\sigma_{1,total}$ = total stress in the unsolved system, in this case System A or B

$\sigma_{2,total}$ = total stress in the solved system, in this case System C

λ = Scaling factor

$\sigma_{1,nonlinear}$ = non-linear stress in the unsolved system, in this case System A or B

$\sigma_{2,nonlinear}$ = non-linear stress in the solved system, in this case System C

$\sigma_{2,Linear}$ = linear stress in the solved system, in this case System C

The stresses in System C as computed using finite element analysis were given in Table A2. The scaling factor λ for the case of converting stresses in a single layer non-equivalent system to those in an unbonded two layer system is:

$$\lambda = -\frac{h_1^2 h_2 \gamma_1}{h_{1,eq}^3 \gamma_2}$$

Plugging in values from Table A1, the scaling factor to go from System C to System A is:

$$\lambda_{C-A} = -\frac{h_A^2 h_C \gamma_A}{h_{A,eq}^3 \gamma_C} = -\frac{12^2 * 13.67 * 0.087}{12.1374^3 * 0.0764} = 1.2541$$

The scaling factor to go from System C to System B is:

$$\lambda_{C-B} = -\frac{h_B^2 h_C \gamma_B}{h_{B,eq}^3 \gamma_C} = -\frac{10^2 * 13.67 * 0.07}{10.05^3 * 0.0764} = 1.2338$$

The non-linear component of stress needs to be computed for each system. Because there is no temperature loading in this case, that non-linear component will be zero in all cases.

Compute the linear stress component of System C. In this case, because the non-linear component of stress is zero, the linear component will be equal to the total stress in System C, as shown in Table A5.

$$\sigma_{2,Linear} = \sigma_{2,\,total} - \sigma_{2,nonlinear}$$

Table A5: Linear Component of Stress due to an Applied Load in System C

		Total Stress σ_{total}		Linear Stress σ_{Linear}	
Surface	**Location**	**Stress in x-direction (psi)**	**Stress in y-direction (psi)**	**Stress in x-direction (psi)**	**Stress in y-direction (psi)**
Bottom	Corner	0.4349	0.3743	0.4349	0.3743
Bottom	Middle	-19.1008	14.3876	-19.1008	14.3876
Top	Corner	-0.4349	-0.3743	-0.4349	-0.3743
Top	Middle	19.1008	-14.3876	19.1008	-14.3876

The linear component of stress in System C is scaled to find the linear component of stress in Systems A and B, see Table A6.

$$\sigma_{A,Linear} = \lambda_{C-A}\sigma_{C,Linear}$$

$$\sigma_{B,Linear} = \lambda_{C-B}\sigma_{C,Linear}$$

Table A6: Linear Stresses in Systems A and B due to an Applied Load as Computed from those in System C

		System A		System B	
Surface	**Location**	**Linear Stress in x-direction (psi)**	**Linear Stress in y-direction (psi)**	**Linear Stress in x-direction (psi)**	**Linear Stress in y-direction (psi)**
Bottom	Corner	0.5454012	0.4694037	0.536585	0.461816
Bottom	Middle	-23.95401	18.043263	-23.5668	17.7516
Top	Corner	-0.545401	-0.469404	-0.53658	-0.46182
Top	Middle	23.954012	-18.04326	23.5668	-17.7516

The total stress in Systems A and B can be computed by summing the linear component of stress shown in Table A6 and the nonlinear component of stress in the system. Recall that in this case, the non-linear component of stress was equal to zero for each system because no temperature gradients are present. Therefore, the total stress is equal to the

linear temperature gradient for each system. See Table A7 for the total computed stresses in Systems A and B calculated using the following equations.

$$\sigma_{A,total} = \lambda(\sigma_{C,Linear}) + \sigma_{A,nonlinear}$$

$$\sigma_{B,total} = \lambda(\sigma_{C,Linear}) + \sigma_{B,nonlinear}$$

Table A7: Total Stresses in Systems A and B due to an Applied Load, as Computed from System C

		System A		**System B**	
Surface	**Location**	**Total Stress in x-direction (psi)**	**Total Stress in y-direction (psi)**	**Total Stress in x-direction (psi)**	**Total Stress in y-direction (psi)**
Bottom	Corner	0.5454012	0.4694037	0.536585	0.461816
Bottom	Middle	-23.95401	18.043263	-23.5668	17.7516
Top	Corner	-0.545401	-0.469404	-0.53658	-0.46182
Top	Middle	23.954012	-18.04326	23.5668	-17.7516

The computed stresses in Systems A and B are compared with those determined from the finite element analysis in Table A8. From this table, it can be seen that the computed stresses match the actual stresses almost exactly.

Table A8: Computed versus Actual Stresses due to an Applied Load in Systems A and B

System A							
Surface	**Location**	**Computed σ_A (psi) x-direction**	**Actual σ_A (psi) x-direction**	**Computed/ Actual**	**Computed σ_A (psi) y-direction**	**Actual σ_A (psi) y-direction**	**Computed/ Actual**
Bottom	Corner	0.5454	0.5454	0.9999977	0.4694	0.4693	0.999779
Bottom	Middle	-23.954	-23.954	0.9999995	18.0433	18.0433	1.0000021
Top	Corner	-0.5454	-0.5454	0.9999977	-0.4694	-0.4693	0.999779
Top	Middle	23.954	23.954	0.9999995	-18.0433	-18.0433	1.0000021
System B							
Surface	**Location**	**Computed σ_A (psi) x-direction**	**Actual σ_A (psi) x-direction**	**Computed/ Actual**	**Computed σ_A (psi) y-direction**	**Actual σ_A (psi) y-direction**	**Computed/ Actual**
Bottom	Corner	0.536585	0.5366	1.000028	0.461816	0.4618	0.999965
Bottom	Middle	-23.5668	-23.5668	1.000000	17.7516	17.7516	1.000000
Top	Corner	-0.53658	-0.5366	1.000028	-0.46182	-0.4618	0.999965
Top	Middle	23.5668	23.5668	1.000000	-17.7516	-17.7516	1.000000

A2. Example 2: Stress Computations for Similar Slabs with Thermal Loads

Example 2 is a repetition of Example 1, using a thermal load instead of an axle load. The temperature gradients used in this example are given in Table A9. The remaining properties of the slabs considered are given in Table A1, though it should be noted that the load was equal to zero for all systems in this example.

Table A9: Temperature Gradients Used in Example 2

	System A	**System B**	**System C**
Temperature Gradient ΔT (°F)	-25.0	-19.19	-19.27

The similarity of Systems A, B, and C was proven in Example 1, with the exception of proving condition 3, that all of the systems had the same Korene'vs non-dimensional temperature gradient. To check that Korenev's non-dimensional temperature gradients are equal, first, the equivalent temperature gradient for Systems A and B must be computed using:

$$\Delta T_{eq} = \frac{h_{PCC}}{5h_{eq}^2}\sum_{i=1}^{10}\left(T_i * (3i-17) * \frac{h_{PCC}}{10} \quad + T_{i+1}(3i-16) * \frac{h_{PCC}}{10}\right)$$

Where:

T_i = temperature at 11 evenly spaced pointes from the top to the bottom of the slab

Using this equation and a spreadsheet program:

$\Delta T_{A,eq}$ = -24.4375

$\Delta T_{B,eq}$ = -19.1921

The equivalent temperature gradient for System C is equal to its temperature gradient. Korenev's non-dimensional temperature gradient can then be computed as:

$$\phi = \frac{2\alpha(1+\mu)\ell^2 k}{h^2\gamma}\Delta T$$

$$\phi_A = \frac{2 * 4.4 * 10^{-6}(1+0.15) * 36.330^2 * 350}{12.137^2 * 0.086} * -24.4375 = -9.016$$

$$\phi_B = \frac{2 * 4.4 * 10^{-6}(1+0.15) * 36.330^2 * 250}{10.05^2 * 0.0696} * -19.1921 = -9.016$$

$$\phi_C = \frac{2 * 4.4 * 10^{-6}(1+0.15) * 36.330^2 * 500}{13.6696^2 * 0.0764} * -19.266 = -9.016$$

From this, it can be seen that condition 3 is satisfied.

Now that the systems have been shown to be similar, the deflections and stresses in Systems A and B due to a thermal load can be calculated from those previously determined for System C. Finite element analysis was conducted on System C when the slab was exposed to a -19.27°F temperature gradient. Selected results for the stresses and deflections in the middle of the slab and in the lower left corner (locations shown in Figure A1) at the top and bottom surfaces are given in Table A10.

Table A10: Stresses and Deflections in System C due to a Temperature Gradient

Surface	**Location**	**Deflection δ_C (in)**	**Stress in x-direction (psi)**	**Stress in y-direction (psi)**
Bottom	Corner	-0.023914	0.283	0.2708
Bottom	Middle	0.008759	-52.2247	-77.4116
Top	Corner	-0.023914	-0.283	-0.2708
Top	Middle	0.008759	52.2247	77.4116

To compute the deflections in Systems A and B from those in System C, the deflections from System C must be scaled using scaling factors. The scaling factor λ for deflections is:

$$\lambda = \frac{k_2 h_1 \gamma_1}{k_1 h_2 \gamma_2}$$

Plugging in values from Table A1, the scaling factor to go from System C to System A is:

$$\lambda_{C-A} = \frac{k_C h_A \gamma_A}{k_A h_C \gamma_C} = \frac{500 * 12 * 0.087}{350 * 13.67 * 0.076} = 1.43$$

The scaling factor to go from System C to System B is:

$$\lambda_{C-B} = \frac{k_C h_B \gamma_B}{k_B h_C \gamma_C} = \frac{500 * 10 * 0.0696}{250 * 13.67 * 0.076} = 1.34$$

The deflections from System C, δ_C, given in are multiplied by the appropriate scaling factor to find the deflections in Systems A and B, as shown in Table A11.

Table A11: Deflections due to a Temperature Gradient in Systems A and B Computed from those in System C

Surface	**Location**	**δ_C (in)**	**$\delta_A = \lambda_{C-A} * \delta_C$ (in)**	**$\delta_B = \lambda_{C-B} * \delta_C$ (in)**
Bottom	Corner	-0.023914	-0.03416	-0.03207
Bottom	Middle	0.008759	0.01251	0.01175
Top	Corner	-0.023914	-0.03416	-0.03207
Top	Middle	0.008759	0.01251	0.01175

The computed defections in Systems A and B are compared with those determined from the finite element analysis in Table A12. From this table, it can be seen that the computed deflections match the actual deflections almost exactly.

Table A12: Computed versus Actual Deflections due to a Temperature Gradient in Systems A and B

System A				
Surface	**Location**	**Computed δ_A (in)**	**Actual δ_A (in)**	**Computed/Actual System A**
Bottom	Corner	-0.034162857	-0.034163	1.00000
Bottom	Middle	0.012512857	0.012513	1.00001
Top	Corner	-0.034162857	-0.034163	1.00000
Top	Middle	0.012512857	0.012513	1.00001
System B				
Surface	**Location**	**Computed δ_B (in)**	**Actual δ_B (in)**	**Computed/Actual System B**
Bottom	Corner	-0.03207	-0.03207	1.00001
Bottom	Middle	0.011746	0.011746	1.00002
Top	Corner	-0.03207	-0.03207	1.00001
Top	Middle	0.011746	0.011746	1.00002

The stresses in Systems A and B are computed from those in System C using the following equation:

$$\sigma_{1,total} = \lambda(\sigma_{2,Linear}) + \sigma_{1,nonlinear}$$

Where:

$\sigma_{2,Linear=}\sigma_{2,\,total} - \sigma_{2,nonlinear}$

$\sigma_{1,total}$ = total stress in the unsolved system, in this case System A or B

$\sigma_{2,total}$ = total stress in the solved system, in this case System C

λ = Scaling factor

$\sigma_{1,nonlinear}$ = non-linear stress in the unsolved system, in this case System A or B

$\sigma_{2,nonlinear}$ = non-linear stress in the solved system, in this case System C

$\sigma_{2,Linear}$ = linear stress in the solved system, in this case System C

The stresses in System C as computed using finite element analysis were given in Table A2. The scaling factor λ for the case of converting stresses in a single layer non-equivalent system to those in an unbonded two layer system is:

$$\lambda = -\frac{h_1^2 h_2 \gamma_1}{h_{1,eq}^3 \gamma_2}$$

Plugging in values from Table A1, the scaling factor to go from System C to System A is:

$$\lambda_{C-A} = -\frac{h_A^2 h_C \gamma_A}{h_{A,eq}^3 \gamma_C} = -\frac{12^2 * 13.67 * 0.087}{12.1374^3 * 0.0764} = 1.2541$$

The scaling factor to go from System C to System B is:

$$\lambda_{C-B} = -\frac{h_B^2 h_C \gamma_B}{h_{B,eq}^3 \gamma_C} = -\frac{10^2 * 13.67 * 0.07}{10.05^3 * 0.0764} = 1.2338$$

Compute the non-linear component of stress σ_{NL} for each case. Note that the non-linear stress in System C should be equal to zero because it is a one layer system exposed to a linear temperature gradient; thus no non-linear stresses are induced.

$$\sigma_{NL,bott} = \frac{-E_{PCC}\alpha_{PCC}}{(1-\mu_{PCC})}\left[\frac{\Delta T_{eq}}{2h_{eq}}h_{PCC} - \frac{\sum_{i=1}^{10} T_i}{10} + \frac{T_1}{20} + \frac{21T_{11}}{10}\right]$$

$$\sigma_{NL,top} = \frac{-E_{PCC}\alpha_{PCC}}{(1-\mu_{PCC})}\left[T_1 - T_{11} - \frac{\Delta T_{eq}}{2h_{eq}}h_{PCC} - \frac{\sum_{i=1}^{10} T_i}{10} + \frac{T_1}{20} + \frac{21T_{11}}{10}\right]$$

Where:

$\sigma_{NL,top}$ = nonlinear component of stress at the top of the slab

$\sigma_{NL,bott}$ = nonlinear component of stress at the bottom of the slab

T_1 = temperature at the top surface of the slab

T_{11} = temperature at the bottom surface of the slab

T_i = temperature at evenly spaced pointes from the top to the bottom of the slab

$$\sigma_{A,NL,bott} = \frac{-4000000 * 4.4 * 10^{-6}}{(1-0.15)}\left[\frac{-24.4375}{2*12.137} * 12 - \frac{1500}{10} + \frac{-25}{20} + \frac{21*0}{10}\right]$$

$$\sigma_{A,NL,bott} = -8.6854$$

$$\sigma_{A,NL,top} = \frac{-4000000 * 4.4 * 10^{-6}}{(1-0.15)} * \left[-25 - 0 - \frac{-24.4375}{2*12.137} * 12 - \frac{1500}{10} + \frac{-25}{20} + \frac{21*0}{10}\right]$$

$$\sigma_{A,NL,top} = 8.6854$$

$$\sigma_{B,NL,bott} = \frac{-5030811 * 4.4 * 10^{-6}}{(1-0.15)}\left[\frac{-18.9968}{2*10.05} * 10 - \frac{959.6}{10} + \frac{-19.192}{20} + \frac{21*0}{10}\right]$$

$$\sigma_{B,NL,bott} = -3.8038$$

$$\sigma_{B,NL,top} = \frac{-5030811 * 4.4 * 10^{-6}}{(1-0.15)} * \left[-19.192 - 0 - \frac{-18.9968}{2*10.05} * 10 - \frac{959.6}{10} + \frac{-19.192}{20} + \frac{21*0}{10}\right]$$

$$\sigma_{B,NL,top} = 3.8038$$

$$\sigma_{C,NL.bott} = \frac{-4000000 * 4.4 * 10^{-6}}{(1-0.15)}\left[\frac{-19.266}{2*13.67} * 13.37 - \frac{1316.8}{10} + \frac{-19.266}{20} + \frac{21*0}{10}\right]$$

$$\sigma_{C,NL,bott} = 0$$

$$\sigma_{C,NL.top} = \frac{-4000000 * 4.4 * 10^{-6}}{(1-0.15)} * \left[-19.266 - 0 - \frac{-19.266}{2 * 13.67} * 13.37 - \frac{1316.8}{10} + \frac{-19.266}{20} + \frac{21 * 0}{10}\right]$$

$$\sigma_{C,NL,top} = 0$$

Compute the linear stress component of System C. Because the non-linear component of stress is zero, the linear component will be equal to the total stress in System C, as shown in Table A13.

$$\sigma_{2,Linear=}\sigma_{2,\,total} - \sigma_{2,nonlinear}$$

Table A13: Linear Component of Stress due to a Temperature Gradient in System C

		Total Stress σ_{total}		**Linear Stress σ_{Linear}**	
Surface	**Location**	**Stress in x-direction (psi)**	**Stress in y-direction (psi)**	**Stress in x-direction (psi)**	**Stress in y-direction (psi)**
Bottom	Corner	0.2830	0.2708	0.2830	0.2708
Bottom	Middle	-52.2247	-77.4116	-52.2247	-77.4116
Top	Corner	-0.2830	-0.2708	-0.2830	-0.2708
Top	Middle	52.2247	77.4116	52.2247	77.4116

The linear component of stress in System C is scaled to find the linear component of stress in Systems A and B, see Table A14.

$$\sigma_{A,Linear} = \lambda_{C-A}\sigma_{C,Linear}$$

$$\sigma_{B,Linear} = \lambda_{C-B}\sigma_{C,Linear}$$

Table A14: Linear Stresses in Systems A and B due to a Temperature Gradient as Computed from those in System C

		System A		System B	
Surface	**Location**	**Linear Stress in x-direction (psi)**	**Linear Stress in y-direction (psi)**	**Linear Stress in x-direction (psi)**	**Linear Stress in y-direction (psi)**
Bottom	Corner	0.3549	0.3396	0.3492	0.3341
Bottom	Middle	-65.4942	-97.0807	-64.4355	-95.5114
Top	Corner	-0.3549	-0.3396	-0.3492	-0.3341
Top	Middle	65.4942	97.0807	64.4355	95.5114

The total stress in Systems A and B can be computed by summing the linear component of stress shown in Table A14 and the nonlinear component of stress in the system. See Table A15 for the total computed stresses in Systems A and B calculated using the following equations.

$$\sigma_{A,total} = \lambda\left(\sigma_{C,Linear}\right) + \sigma_{A,nonlinear}$$

$$\sigma_{B,total} = \lambda\left(\sigma_{C,Linear}\right) + \sigma_{B,nonlinear}$$

Table A15: Total Stresses in Systems A and B due to a Temperature Gradient, as Computed from System C

		System A		System B	
Surface	**Location**	**Total Stress in x-direction (psi)**	**Total Stress in y-direction (psi)**	**Total Stress in x-direction (psi)**	**Total Stress in y-direction (psi)**
Bottom	Corner	-8.3304	-8.3457	-3.4547	-3.4697
Bottom	Middle	-74.1795	-105.7660	-68.2393	-99.3152
Top	Corner	8.3304	8.3457	3.4547	3.4697
Top	Middle	74.1795	105.7660	68.2393	99.3152

The computed stresses in Systems A and B are compared with those determined from the finite element analysis in Table A16. From this table, it can be seen that the computed stresses match the actual stresses almost exactly.

Table A16: Computed versus Actual Stresses due to a Temperature Graident in Systems A and B

System A							
Surface	**Location**	**Computed σ_A (psi) x-direction**	**Actual σ_A (psi) x-direction**	**Computed/ Actual**	**Computed σ_A (psi) y-direction**	**Actual σ_A (psi) y-direction**	**Computed/ Actual**
Bottom	Corner	-8.3304	-8.3304	0.9999943	-8.3457	-8.3458	1.0000063
Bottom	Middle	-74.1795	-74.1795	0.9999996	-105.7660	-105.766	0.9999998
Top	Corner	8.3304	8.3304	0.9999943	8.3457	8.3458	1.0000063
Top	Middle	74.1795	74.1795	0.9999996	105.7660	105.766	0.9999998
System B							
Surface	**Location**	**Computed σ_A (psi) x-direction**	**Actual σ_A (psi) x-direction**	**Computed/ Actual**	**Computed σ_A (psi) y-direction**	**Actual σ_A (psi) y-direction**	**Computed/ Actual**
Bottom	Corner	-3.4547	-3.4546	0.999984	-3.4697	-3.4698	1.000026
Bottom	Middle	-68.2393	-68.2393	1.000000	-99.3152	-99.3152	1.000000
Top	Corner	3.4547	3.4546	0.999984	3.4697	3.4698	1.000026
Top	Middle	68.2393	68.2393	1.000000	99.3152	99.3152	1.000000

A3. Example 3: Stress Computations for Similar Slabs with Both Axle and Thermal Loads – Unbonded Case

Example 3 combines Examples 1 and 2 in that it has both temperature and traffic loading. The temperature gradients used in this example are given in Table A9. The remaining properties of the slabs considered are given in Table A1. It was previously shown in examples 1 and 2 that Systems A, B, and C satisfy all the conditions necessary to be considered as similar systems. Therefore, the deflections and stresses in Systems A and

B due to a thermal load can be calculated from those previously determined for System C. Finite element analysis was conducted on System C when the slab was exposed to a -19.27°F temperature gradient and a 18000 lb load. Selected results for the stresses and deflections in the middle of the slab and in the lower left corner (locations also shown in Figure A1) at the top and bottom surfaces are given in Table A17.

Table A17: Stresses and Deflections in System C Due to an Applied Load and a Temperature Gradient

Surface	**Location**	**Deflection δ_C (in)**	**Stress in x-direction (psi)**	**Stress in y-direction (psi)**
Bottom	Corner	-0.021429	0.8408	0.8399
Bottom	Middle	0.010256	-77.942	-66.0622
Top	Corner	-0.021429	-0.8408	-0.8399
Top	Middle	0.010256	77.942	66.0622

To compute the deflections in Systems A and B from those in System C, the deflections from System C must be scaled using scaling factors. The scaling factor λ for deflections is:

$$\lambda = \frac{k_2 h_1 \gamma_1}{k_1 h_2 \gamma_2}$$

Plugging in values from Table A1, the scaling factor to go from System C to System A is:

$$\lambda_{C-A} = \frac{k_C h_A \gamma_A}{k_A h_C \gamma_C} = \frac{500 * 12 * 0.087}{350 * 13.67 * 0.076} = 1.43$$

The scaling factor to go from System C to System B is:

$$\lambda_{C-B} = \frac{k_C h_B \gamma_B}{k_B h_C \gamma_C} = \frac{500 * 10 * 0.0696}{250 * 13.67 * 0.076} = 1.34$$

The deflections from System C, δ_C, given in are multiplied by the appropriate scaling factor to find the deflections in Systems A and B, as shown in Table A18.

Table A18: Deflections due to an Applied Load and a Temperature Gradient in Systems A and B Computed from those in System C

Surface	**Location**	**δ_C (in)**	**$\delta_A = \lambda_{C\text{-}A} * \delta_C$ (in)**	**$\delta_B = \lambda_{C\text{-}B} * \delta_C$ (in)**
Bottom	Corner	-0.021429	-0.03061	-0.02874
Bottom	Middle	0.010256	0.01465	0.01375
Top	Corner	-0.021429	-0.03061	-0.02874
Top	Middle	0.010256	0.01465	0.01375

The computed defections in Systems A and B are compared with those determined from the finite element analysis in Table A19. From this table, it can be seen that the computed deflections match the actual deflections almost exactly.

Table A19: Computed versus Actual Deflections due to an Applied Load and a Temperature Gradient in Systems A and B

System A				
Surface	**Location**	**Computed δ_A (in)**	**Actual δ_A (in)**	**Computed/Actual System A**
Bottom	Corner	-0.03061	-0.03062	1.00023
Bottom	Middle	0.01465	0.014653	1.00011
Top	Corner	-0.03061	-0.03062	1.00023
Top	Middle	0.01465	0.014653	1.00011
System B				
Surface	**Location**	**Computed δ_B (in)**	**Actual δ_B (in)**	**Computed/Actual System B**
Bottom	Corner	-0.02874	-0.02874	1.00024
Bottom	Middle	0.01375	0.013754	1.00005
Top	Corner	-0.02874	-0.02874	1.00024
Top	Middle	0.01375	0.013754	1.00005

The stresses in Systems A and B are computed from those in System C using the following equation:

$$\sigma_{1,total} = \lambda(\sigma_{2,Linear}) + \sigma_{1,nonlinear}$$

Where:

$\sigma_{2,Linear=}\sigma_{2,\,total} - \sigma_{2,nonlinear}$

$\sigma_{1,total}$ = total stress in the unsolved system, in this case System A or B

$\sigma_{2,total}$ = total stress in the solved system, in this case System C

λ = Scaling factor

$\sigma_{1,nonlinear}$ = non-linear stress in the unsolved system, in this case System A or B

$\sigma_{2,nonlinear}$ = non-linear stress in the solved system, in this case System C

$\sigma_{2,Linear}$ = linear stress in the solved system, in this case System C

The stresses in System C as computed using finite element analysis were given in Table A2. The scaling factor λ for the case of converting stresses in a single layer non-equivalent system to those in an unbonded two layer system is:

$$\lambda = -\frac{h_1^2 h_2 \gamma_1}{h_{1,eq}^3 \gamma_2}$$

Plugging in values from Table A1, the scaling factor to go from System C to System A is:

$$\lambda_{C-A} = -\frac{h_A^2 h_C \gamma_A}{h_{A,eq}^3 \gamma_C} = -\frac{12^2 * 13.67 * 0.087}{12.1374^3 * 0.0764} = 1.2541$$

The scaling factor to go from System C to System B is:

$$\lambda_{C-B} = -\frac{h_B^2 h_C \gamma_B}{h_{B,eq}^3 \gamma_C} = -\frac{10^2 * 13.67 * 0.07}{10.05^3 * 0.0764} = 1.2338$$

Compute the non-linear component of stress for each case. Note that the non-linear stress in System C should be equal to zero because it is a one layer system exposed to a linear temperature gradient; thus no non-linear stresses are induced.

$$\sigma_{NL,bott} = \frac{-E_{PCC}\alpha_{PCC}}{(1-\mu_{PCC})}\left[\frac{\Delta T_{equiv}}{2h_{equiv}}h_{PCC} - \frac{\sum_{i=1}^{10} T_i}{10} + \frac{T_1}{20} + \frac{21T_{11}}{10}\right]$$

$$\sigma_{NL,top} = \frac{-E_{PCC}\alpha_{PCC}}{(1-\mu_{PCC})}\left[T_1 - T_{11} - \frac{\Delta T_{equiv}}{2h_{equiv}}h_{PCC} - \frac{\sum_{i=1}^{10} T_i}{10} + \frac{T_1}{20} + \frac{21T_{11}}{10}\right]$$

Where:

$\sigma_{NL,top}$ = nonlinear component of stress at the top of the slab

$\sigma_{NL,bott}$ = nonlinear component of stress at the bottom of the slab

T_1 = temperature at the top surface of the slab

T_{11} = temperature at the bottom surface of the slab

T_i = temperature at evenly spaced pointes from the top to the bottom of the slab

$$\sigma_{A,NL,bott} = \frac{-4000000 * 4.4 * 10^{-6}}{(1-0.15)}\left[\frac{-24.4375}{2 * 12.137} * 12 - \frac{1500}{10} + \frac{-25}{20} + \frac{21 * 0}{10}\right]$$

$$\sigma_{A,NL,bott} = -8.6854$$

$$\sigma_{A,NL,top} = \frac{-4000000 * 4.4 * 10^{-6}}{(1-0.15)} * \left[-25 - 0 - \frac{-24.4375}{2 * 12.137} * 12 - \frac{1500}{10} + \frac{-25}{20} + \frac{21 * 0}{10}\right]$$

$$\sigma_{A,NL,top} = 8.6854$$

$$\sigma_{B,NL,bott} = \frac{-5030811 * 4.4 * 10^{-6}}{(1-0.15)}\left[\frac{-18.9968}{2 * 10.05} * 10 - \frac{959.6}{10} + \frac{-19.192}{20} + \frac{21 * 0}{10}\right]$$

$$\sigma_{B,NL,bott} = -3.8038$$

$$\sigma_{B,NL,top} = \frac{-5030811 * 4.4 * 10^{-6}}{(1-0.15)} * \left[-19.192 - 0 - \frac{-18.9968}{2 * 10.05} * 10 - \frac{959.6}{10} + \frac{-19.192}{20} + \frac{21 * 0}{10}\right]$$

$$\sigma_{B,NL,top} = 3.8038$$

$$\sigma_{C,Nl,bott} = \frac{-4000000 * 4.4 * 10^{-6}}{(1-0.15)}\left[\frac{-19.266}{2 * 13.67} * 13.37 - \frac{1316.8}{10} + \frac{-19.266}{20} + \frac{21 * 0}{10}\right]$$

$$\sigma_{C,NL,bott} = 0$$

$$\sigma_{C,Nl,bott} = \frac{-4000000 * 4.4 * 10^{-6}}{(1-0.15)} * \left[-19.266 - 0 - \frac{-19.266}{2 * 13.67} * 13.37 - \frac{1316.8}{10} + \frac{-19.266}{20} + \frac{21 * 0}{10}\right]$$

$$\sigma_{C,NL,top} = 0$$

Compute the linear stress component of System C. Because the non-linear component of stress is zero, the linear component will be equal to the total stress in System C, as shown in Table A20.

$$\sigma_{2,Linear=}\sigma_{2,\,total} - \sigma_{2,nonlinear}$$

Table A20: Linear Component of Stress due to an Applied Load and a Temperature Gradient in System C

		Total Stress σ_{total}		**Linear Stress σ_{Linear}**	
Surface	**Location**	**Stress in x-direction (psi)**	**Stress in y-direction (psi)**	**Stress in x-direction (psi)**	**Stress in y-direction (psi)**
Bottom	Corner	0.8408	0.8399	0.8408	0.8399
Bottom	Middle	-77.942	-66.0622	-77.942	-66.0622
Top	Corner	-0.8408	-0.8399	-0.8408	-0.8399
Top	Middle	77.942	66.0622	77.942	66.0622

The linear component of stress in System C is scaled to find the linear component of stress in Systems A and B, see Table A21.

$$\sigma_{A,Linear} = \lambda_{C-A}\sigma_{C,Linear}$$

$$\sigma_{B,Linear} = \lambda_{C-B}\sigma_{C,Linear}$$

Table A21: Linear Stresses in Systems A and B due to an Applied Load and a Temperature Gradient as Computed from those in System C

		System A		**System B**	
Surface	**Location**	**Linear Stress in x-direction (psi)**	**Linear Stress in y-direction (psi)**	**Linear Stress in x-direction (psi)**	**Linear Stress in y-direction (psi)**
Bottom	Corner	1.0544	1.0533	1.0374	1.0363
Bottom	Middle	-97.7458	-82.8476	-96.1658	-81.5084
Top	Corner	-1.0544	-1.0533	-1.0374	-1.0363
Top	Middle	97.7458	82.8476	96.1658	81.5084

The total stress in Systems A and B can be computed by summing the linear component of stress shown in Table A21 and the nonlinear component of stress in the system. See Table A22 for the total computed stresses in Systems A and B calculated using the following equations.

$$\sigma_{A,total} = \lambda\left(\sigma_{C,Linear}\right) + \sigma_{A,nonlinear}$$

$$\sigma_{B,total} = \lambda\left(\sigma_{C,Linear}\right) + \sigma_{B,nonlinear}$$

Table A22: Total Stresses in Systems A and B due to an Applied Load and a Temperature Gradient, as Computed from System C

		System A		**System B**	
Surface	**Location**	**Total Stress in x-direction (psi)**	**Total Stress in y-direction (psi)**	**Total Stress in x-direction (psi)**	**Total Stress in y-direction (psi)**
Bottom	Corner	-7.6309	-7.6320	-2.7664	-2.7675
Bottom	Middle	-106.4312	-91.5329	-99.9696	-85.3122
Top	Corner	7.6309	7.6320	2.7664	2.7675
Top	Middle	106.4312	91.5329	99.9696	85.3122

The computed stresses in Systems A and B are compared with those determined from the finite element analysis in Table A23. From this table, it can be seen that the computed stresses match the actual stresses almost exactly.

Table A23: Computed versus Actual Stresses due to an Applied Load and a Temperature Gradient in Systems A and B

System A							
Surface	**Location**	**Computed σ_A (psi) x-direction**	**Actual σ_A (psi) x-direction**	**Computed/ Actual**	**Computed σ_A (psi) y-direction**	**Actual σ_A (psi) y-direction**	**Computed/ Actual**
Bottom	Corner	-7.6309	-7.6308	0.9999844	-7.6320	-7.632	0.9999937
Bottom	Middle	-106.4312	-106.4382	1.0000659	-91.5329	-91.5401	1.0000785
Top	Corner	7.6309	7.6308	0.9999844	7.6320	7.632	0.9999937
Top	Middle	106.4312	106.4382	1.0000659	91.5329	91.5401	1.0000785
System B							
Surface	**Location**	**Computed σ_B (psi) x-direction**	**Actual σ_B (psi) x-direction**	**Computed/ Actual**	**Computed σ_B (psi) y-direction**	**Actual σ_B (psi) y-direction**	**Computed/ Actual**
Bottom	Corner	-2.7664	-2.7663	0.999951	-2.7675	-2.7675	0.999983
Bottom	Middle	-99.9696	-99.9765	1.000069	-85.3122	-85.3193	1.000083
Top	Corner	2.7664	2.7663	0.999951	2.7675	2.7675	0.999983
Top	Middle	99.9696	99.9765	1.000069	85.3122	85.3193	1.000083

A4. Example 4: Stress Computations for Similar Slabs with Both Axle and Thermal Loads – Bonded Case

Example 4 serves to show the process of solving one system using the results of another and the principles of similarity when the two layered system is bonded. This procedure can be compared with that of Example 3, which was for the unbonded case. It should be noted that the properties of the slab systems used in Example 4 differ from those used in the first three examples because those examples were all for unbonded systems. Therefore, the results of Example 4 cannot be compared with the results of the previous three examples, but the differences in procedure for bonded and unbonded cases can be examined by comparing Examples 3 and 4.

Example 4 has one two-layer systems and one similar single layer system. It is important note that, while the single layer system is similar to the two layered systems, it is not an equivalent single layer system. The two-layer system was called System D; the single layer system was called System E. Properties for the two systems are given in Table A24. A second two-layer system was not considered in this example for brevity and because the fact that one single layer system can be used to compute stresses in different two-layer systems was already illustrated in the first three examples.

Table A24: Properties of Systems D and E

Parameter	**System D**	**System E**
Concrete Thickness h pcc (in)	8	17.68
Concrete Elastic Modulus E pcc (psi)	4,000,000	4,000,000
Concrete Poisson's Ratio μ pcc	0.15	0.15
Concrete Coefficient of Thermal Expansion αpcc (in/in/°F)	4.40E-06	4.40E-06
Concrete Unit Weight γ pcc (lb/in^3)	0.087	0.187
Base Thickness h base (in)	30	-
Base Modulus of Elasticity E base (psi)	60000	-
Base Poisson's Ratio μ base	0.15	-
Base Coefficient of Thermal Expansion CTE base (in/in/°F)	4.40E-06	-
Base Unit Weight γ base (lb/in^3)	0.087	-
Modulus of Subgrade Reaction k (psi/in)	250	500
Temperature Gradient ΔT (°F)	-50	-18.009
Load P (lbs)	18000	18000
Tire pressure p (psi)	100	100

For Systems D, and E, to be considered similar by the equivalent system concept (Khazanovich et al. 2001; NCHRP 2003b), the following conditions must be satisfied:

1. $L_D = L_E$
2. $\ell_D = \ell_E$
3. $\phi_D = \phi_E$
4. $\frac{AGG_D}{k_D \ell_D} = \frac{AGG_E}{k_E \ell_E}$
5. $\frac{P_D}{h_D \gamma_D} = \frac{P_E}{h_E \gamma_E}$
6. $s_D = s_E$
7. $f_D = f_E$

Where:

L = slab length

ℓ = radius of relative stiffness (Westergaard 1926)

$$\ell = \sqrt[4]{\frac{Eh^3}{12(1-\mu)k}}$$

ϕ = Korenev's non-dimensional temperature gradient (Korenev & Chernigovskaya 1962)

$$\phi = \frac{2\alpha(1+\mu)\ell^2 k}{h^2 \gamma}\Delta T$$

AGG = aggregate interlock factor determined from the load transfer efficiency (Crovetti 1994)

$$AGG = \frac{0.00546k\ell}{\left(\frac{1}{LTE} - 0.01\right)^{1.178}}$$

P = applied load

s = distance from slab edge to outer wheel edge

f = tire footprint

Conditions 1, and 6, are satisfied based on the geometry of the problem. To show that conditions 2, 3, 4, 5 and 7 are satisfied, the equivalent single layer system for System D

must be defined. System E does not require an equivalent single layer system because it is already a single layer system. The equivalent thickness is given as (Ioannides et al. 1992):

$$h_{eq} = \sqrt[3]{\begin{matrix} {h_{PCC}}^3 + \frac{E_{base}}{E_{PCC}} {h_{base}}^3 + \\ 12\left[\left(x - \frac{h_{PCC}}{2}\right)^2 h_{PCC} + \frac{E_{base}}{E_{PCC}}\left(h_{PCC} - x + \frac{h_{base}}{2}\right)^2\right] \end{matrix}}$$

$$x = \frac{E_{PCC}h_{PCC}\frac{h_{PCC}}{2} + E_{base}h_{base}\left(h_{PCC} + \frac{h_{base}}{2}\right)}{E_{PCC}h_{PCC} + E_{base}h_{base}}$$

$$h_{D,eq} = \sqrt[3]{\begin{matrix} 8^3 + \frac{60000}{4000000} 30^3 + \\ 12\left[\left(5.01 - \frac{8}{2}\right)^2 * 8 + \frac{60000}{4000000}\left(8 - 5.01 + \frac{30}{2}\right)^2\right] \end{matrix}} = 14.032$$

$$x_D = \frac{4000000 * 8 * \frac{8}{2} + 60000 * 30 * \left(8 + \frac{30}{2}\right)}{4000000 * 8 + 60000 * 30} = 5.01$$

The equivalent unit weight is given as (Khazanovich 1994):

$$\gamma_{eq} = \frac{\gamma_{PCC}h_{PCC} + \gamma_{base}h_{base}}{h_{eq}}$$

$$\gamma_{D,eq} = \frac{0.087 * 8 + 0.087 * 30}{14.032} = 0.236\, lbs/in^3$$

Check that the radii of relative stiffness are equal:

$$\ell = \sqrt[4]{\frac{Eh^3}{12(1-\mu)k}}$$

$$\ell_D = \sqrt[4]{\frac{4000000 * 14.032^3}{12(1-0.15) * 250}} = 44.059$$

$$\ell_E = \sqrt[4]{\frac{4000000 * 17.68^3}{12(1-0.15) * 500}} = 44.059$$

From this, it can be seen that condition 2 is satisfied.

To check that Korenev's non-dimensional temperature gradients are equal, first, the equivalent temperature gradient for Systems D must be computed using:

$$\Delta T_{eq} = \frac{h_{PCC}}{5h_{eq}^2}\sum_{i=1}^{10}\left(T_i\left((3i-2)\frac{h_{PCC}}{10} - 3x\right) + T_{i+1}\left((3i-1)\frac{h_{PCC}}{10} - 3x\right)\right) - \frac{T_{11}}{2}h_{PCC}(h_{PCC} - 2x)$$

Where:

T_i = temperature at 11 evenly spaced pointes from the top to the bottom of the slab

Using this equation and a spreadsheet program:

$\Delta T_{A,eq}$ = -28.587

The equivalent temperature gradient for System F is equal to its temperature gradient.

Korenev's non-dimensional temperature gradient can then be computed as:

$$\phi = \frac{2\alpha(1+\mu)\ell^2 k}{h^2\gamma}\Delta T$$

$$\phi_D = \frac{2 * 4.4 * 10^{-6}(1 + 0.15) * 44.059^2 * 250}{14.032^2 * 0.236} * -28.587 = -3.0266$$

$$\phi_E = \frac{2 * 4.4 * 10^{-6}(1 + 0.15) * 36.330^2 * 500}{17.678^2 * 0.187} * -18.009 = -3.0266$$

From this, it can be seen that condition 3 is satisfied.

Check that the ratios of aggregate interlock factor to kℓ are equal. First, the aggregate interlock factor must be computed:

$$AGG = \frac{0.00546k\ell}{\left(\frac{1}{LTE} - 0.01\right)^{1.178}}$$

$$AGG_D = \frac{0.00546 * 250 * 44.059}{\left(\frac{1}{70} - 0.01\right)^{1.178}} = 37039.2$$

$$AGG_E = \frac{0.00546 * 500 * 44.0590}{\left(\frac{1}{70} - 0.01\right)^{1.178}} = 74078.5$$

Then the ratios of aggregate interlock factor to kℓ are computed:

$$\frac{AGG_A}{k_A\ell_A} = \frac{37039.2}{250 * 44.059} = 3.3627$$

$$\frac{AGG_C}{k_C\ell_C} = \frac{74078.5}{500 * 44.059} = 3.3627$$

From this, it can be seen that condition 4 is satisfied.

Check that the ratios of applied load to self-weight are equal:

$$\frac{P_D}{h_{D,eq}\gamma_{D,eq}} = \frac{18000}{14.032 * 0.236} = 5444.65$$

$$\frac{P_E}{h_E\gamma_E} = \frac{18000}{17.68 * .187} = 5444.65$$

From this, it can be seen that condition 5 is satisfied

Check that the tire footprints are equal. The analysis program requires the length and width of the tire footprint as inputs. Given that the tires are square,

$$f = a^2$$

Where:

a = length of the tire = width of the tire

$$a = \sqrt{\frac{P}{p}}$$

Compute a for each system:

$$a_D = \sqrt{\frac{18000}{100}} = 13.4164$$

$$a_E = \sqrt{\frac{18000}{100}} = 13.4164$$

From this, it can be seen that condition 7 is satisfied.

Given that all of the conditions required by the equivalent system concept have been satisfied, the systems can be considered to be similar. Finite element analysis was conducted on System F when the slab was exposed to a -18.009°F temperature gradient and a 18000 lb load, as shown in Figure A1. Selected results for the stresses and deflections in the middle of the slab and in the lower left corner (locations also shown in Figure A1) at the top and bottom surfaces are given in Table A25.

Table A25: Stresses and Deflections in System F Due to an Applied Load and a Temperature Gradient

Surface	**Location**	**Deflection δ_C (in)**	**Stress in x-direction (psi)**	**Stress in y-direction (psi)**
Bottom	Corner	-0.008818	0.2036	0.1441
Bottom	Middle	0.015236	-42.4834	-48.5598
Top	Corner	-0.008818	-0.2036	-0.1441
Top	Middle	0.015236	42.4834	48.5598

To compute the deflections in Systems D from those in System E, the deflections from System E must be scaled scaling factors. The scaling factor λ for deflections is:

$$\lambda = \frac{k_2 h_1 \gamma_1}{k_1 h_2 \gamma_2}$$

Plugging in values from Table A1, the scaling factor to go from System E to System D is:

$$\lambda = \frac{500 * 8 * 0.87}{250 * 17.68 * 0.187} = 2.0$$

The deflections from System E, δ_C, given in are multiplied by the appropriate scaling factor to find the deflections in System D, as shown in Table A26.

Table A26: Deflections due to an Applied Load and a Temperature Gradient in System D Computed from those in System E

Surface	Location	δ_E (in)	$\delta_D = \lambda * \delta_E$ (in)
Bottom	Corner	-0.008818	-0.017636
Bottom	Middle	0.015236	0.030472
Top	Corner	-0.008818	-0.017636
Top	Middle	0.015236	0.030472

The computed defections in System D are compared with those determined from the finite element analysis in Table A27. From this table, it can be seen that the computed deflections match the actual deflections almost exactly.

Table A27: Computed versus Actual Deflections due to an Applied Load and a Temperature Gradient in System D

Surface	Location	Computed δ_D (in)	Actual δ_D (in)	Computed/Actual System D
Bottom	Corner	-0.017636	-0.017636	1.00000
Bottom	Middle	0.030472	0.030473	1.00003
Top	Corner	-0.017636	-0.017636	1.00000
Top	Middle	0.030472	0.030473	1.00003

The stresses in System D are computed from those in System E using the following equation:

$$\sigma_{1,total} = \lambda(\sigma_{2,Linear}) + \sigma_{1,nonlinear}$$

Where:

$\sigma_{2,Linear=}\sigma_{2,\,total} - \sigma_{2,nonlinear}$

$\sigma_{1,total}$ = total stress in the unsolved system, in this case System D or B

$\sigma_{2,total}$ = total stress in the solved system, in this case System E

λ = Scaling factor

$\sigma_{1,nonlinear}$ = non-linear stress in the unsolved system, in this case System D or B

$\sigma_{2,nonlinear}$ = non-linear stress in the solved system, in this case System E

$\sigma_{2,Linear}$ = linear stress in the solved system, in this case System E

The stresses in System E as computed using finite element analysis were given in Table A2. The scaling factor λ for the case of converting stresses in a single layer non-equivalent system to those in an unbonded two layer system is:

$$\lambda_{bottom} = \frac{2(h_1 - x)\gamma_{1,eq} h_2}{h_{1,eq}^2 \gamma_2}$$

$$\lambda_{top} = \frac{2x\gamma_{1,eq} h_2}{h_{1,eq}^2 \gamma_2}$$

Plugging in values from Table A1, the scaling factors to go from System E to System D are, for the bottom and top surfaces, respectively:

$$\lambda_{bott} = \frac{2 * (8 - 5.01) * 0.236 * 17.68}{14.032^2 * 0.187} = 0.6761$$

$$\lambda_{top} = \frac{2 * 5.01 * 0.236 * 17.68}{14.032^2 * 0.187} = 1.134$$

Compute the non-linear component of stress for each case $\sigma_{NL.}$ The non-linear stresses for System D are computed using equations for the bonded case. Note that the non-linear stress in System E should be equal to zero because it is a one layer system exposed to a linear temperature gradient; thus no non-linear stresses are induced.

$$\sigma_{D,NL,bott} = \frac{-E_{PCC}\alpha_{PCC}}{(1-\mu_{PCC})}\left[\frac{\Delta T_{eq}}{h_{eq}}(h_{PCC}-x) - \frac{h_{PCC}}{h_{PCC}+\frac{E_{base}}{E_{PCC}}h_{base}}\left(\frac{\sum_{i=1}^{10}T_i}{10}-\frac{T_1}{20}-\frac{21T_{11}}{10}\right)\right]$$

$$\sigma_{D,NL,bott} = \frac{-4000000 * 4.4 * 10^{-6}}{(1-0.15)}\left[\frac{-28.587}{14.032}(8-5.01) - \frac{8}{8+\frac{60000}{4000000}*30}\left(\frac{3517.75}{10}-\frac{-50}{20}-\frac{21*0}{10}\right)\right]$$

$$\sigma_{D,NL,bott} = -364.02$$

$$\sigma_{D,NL,top} = \frac{-E_{PCC}\alpha_{PCC}}{(1-\mu_{PCC})}\left[T_1 - T_{11} - \frac{\Delta T_{eq}}{h_{eq}}x - \frac{h_{PCC}}{h_{PCC}+\frac{E_{base}}{E_{PCC}}h_{base}}\left(\frac{\sum_{i=1}^{10}T_i}{10}-\frac{T_1}{20}-\frac{21T_{11}}{10}\right)\right]$$

$$\sigma_{D,NL,top} = \frac{-4000000 * 4.4 * 10^{-6}}{(1-0.15)}\left[-50-0-\frac{28.587}{14.032}*5.01 - \frac{8}{8+\frac{60000}{4000000}*30}\left(\frac{3517.75}{10}-\frac{-50}{20}-\frac{21*0}{10}\right)\right]$$

$$\sigma_{D,NL,top} = 333.79$$

$$\sigma_{E,NL,bott} = \frac{-E_{PCC}\alpha_{PCC}}{(1-\mu_{PCC})}\left[\frac{\Delta T_{eq}}{2h_{eq}}h_{PCC} - \frac{\sum_{i=1}^{10} T_i}{10} + \frac{T_1}{20} + \frac{21T_{11}}{10}\right]$$

$$\sigma_{E,NL,bott} = \frac{-4000000 * 4.4 * 10^{-6}}{(1-0.15)} * \left[\frac{-19.266}{2 * 13.67} * 13.37 - \frac{1316.8}{10} + \frac{-19.266}{20} + \frac{21 * 0}{10}\right]$$

$$\sigma_{E,NL,bott} = 0$$

$$\sigma_{E,NL,top} = \frac{-E_{PCC}\alpha_{PCC}}{(1-\mu_{PCC})}\left[T_1 - T_{11} - \frac{\Delta T_{eq}}{2h_{eq}}h_{PCC} - \frac{\sum_{i=1}^{10} T_i}{10} + \frac{T_1}{20} + \frac{21T_{11}}{10}\right]$$

$$\sigma_{E,NL,bott} = \frac{-4000000 * 4.4 * 10^{-6}}{(1-0.15)} * \left[19.226 - 0 - \frac{-19.266}{2 * 13.67} * 13.37 - \frac{1316.8}{10} + \frac{-19.266}{20} + \frac{21 * 0}{10}\right]$$

$$\sigma_{E,NL,top} = 0$$

Compute the linear stress component of System E. Because the non-linear component of stress is zero, the linear component will be equal to the total stress in System E, as shown in Table A28.

$$\sigma_{2,Linear=}\sigma_{2,\,total} - \sigma_{2,nonlinear}$$

Table A28: Linear Component of Stress due to an Applied Load and a Temperature Gradient in System E

		Total Stress σ_{total}		**Linear Stress σ_{Linear}**	
Surface	**Location**	**Stress in x-direction (psi)**	**Stress in y-direction (psi)**	**Stress in x-direction (psi)**	**Stress in y-direction (psi)**
Bottom	Corner	0.2036	0.1441	0.2036	0.1441
Bottom	Middle	-42.4834	-48.5598	-42.4834	-48.5598
Top	Corner	-0.2036	-0.1441	-0.2036	-0.1441
Top	Middle	42.4834	48.5598	42.4834	48.5598

The linear component of stress in System E is scaled to find the linear component of stress in System D, see Table A29.

$$\sigma_{D,Linear,bott} = \lambda_{bott}\sigma_{E,Linear,bott}$$

$$\sigma_{D,Linear,top} = \lambda_{top}\sigma_{E,Linear,top}$$

Table A29: Linear Stresses in System D due to an Applied Load and a Temperature Gradient as Computed from those in System E

		System D	
Surface	**Location**	**Linear Stress in x-direction (psi)**	**Linear Stress in y-direction (psi)**
Bottom	Corner	0.1377	0.0974
Bottom	Middle	-28.7234	-32.8317
Top	Corner	-0.2309	-0.1634
Top	Middle	48.1756	55.0662

The total stress in System D can be computed by summing the linear component of stress shown in Table A29 and the nonlinear component of stress in the system. See Table A30 for the total computed stresses in System D calculated using the following equations.

$$\sigma_{D,total,bott} = \lambda_{bott}\left(\sigma_{D,Linear}\right) + \sigma_{D,NL,bott}$$

$$\sigma_{D,total,top} = \lambda_{top}\left(\sigma_{D,Linear}\right) + \sigma_{D,NL,top}$$

Table A30: Total Stresses in System D due to an Applied Load and a Temperature Gradient, as Computed from System E

		System D	
Surface	**Location**	**Total Stress in x-direction (psi)**	**Total Stress in y-direction (psi)**
Bottom	Corner	-363.8852	-363.9254
Bottom	Middle	-392.7462	-396.8545
Top	Corner	333.55649	333.62396
Top	Middle	381.963	388.85356

The computed stresses in System D are compared with those determined from the finite element analysis in Table A31. From this table, it can be seen that the computed stresses match the actual stresses almost exactly.

Table A31: Computed versus Actual Stresses due to an Applied Load and a Temperature Gradient in System D

Surface	**Location**	**Computed σ_A (psi) x-direction**	**Actual σ_A (psi) x-direction**	**Computed/ Actual**	**Computed σ_A (psi) y-direction**	**Actual σ_A (psi) y-direction**	**Computed/ Actual**
Bottom	Corner	-363.8852	-363.8851	0.9999998	-363.9254	-363.9254	1.0000000
Bottom	Middle	-392.7462	-392.7462	1.0000000	-396.8545	-396.8545	1.0000000
Top	Corner	333.55649	333.5564	0.9999997	333.62396	333.6239	0.9999998
Top	Middle	381.963	381.963	1.0000000	388.85356	388.8536	1.0000001

Appendix B: Example of Damage Computations

The program created in this research computes bottom-up damage for each combination pavement age, month, load level, axle type, temperature gradient, and vehicle wander that the pavement is predicted to see. For brevity, this example will only consider one load level and axle type, one vehicle wander, one temperature distribution, and one hour of the day. To illustrate how damage is computed, this example will show sample calculations.

The properties of the pavement in this example are given in Table B1 for the pavement at age 1 month, in the month of October. As the pavement ages, properties like the modulus of elasticity and modulus of rupture will change as the concrete gains strength. Other properties, like the modulus of subgrade reaction will change seasonally. Still other properties will change with time and vary seasonally, such as load transfer efficiency. This pavement was purposely under-designed in the MEPDG to ensure that it would accumulate sufficient damage to be calculable.

The load considered was a 22,000 lb single axle load occurring at a wander of 6 inches. The equivalent linear temperature gradient considered was 8°F, and nonlinear temperature gradients were considered from 0-24°F. The month was selected as October, and the hour as noon. There are two parts to damage computation: the number of allowable loads and the number of applied loads. These will each be considered separately.

Table B1: Pavement Properties at Pavement Age 1 Month

Property	Value
Concrete Thickness	8 in
Concrete Modulus of Elasticity	4946180 psi
Concrete Unit Weight	0.087 lb/in^3
Concrete Coefficient of Thermal Expansion	5.5E-06 in/in/°F
Concrete Poisson's Ratio	0.2
Concrete Modulus of Rupture	775 psi
Base Material	A-1-a
Base Thickness	12 in
Base Modulus of Elasticity	52710 psi
Base Unit Weight	0.074 lb/in^3
Base Coefficient of Thermal Expansion	5.5E-06 in/in/°F
Subgrade Material A-7-6	
Modulus of Subgrade Reaction	180.1 psi/in
Bond Condition	unbonded
Load Transfer Efficiency	92%

B1. Number of Allowable Loads

The number of allowable loads is computed based on the magnitude of the stress induced by each specific load combination. Stresses were computed as the sum of the linear and nonlinear components of stress. The linear stresses were computed using the neural networks, while the nonlinear stresses were computed directly from the original system inputs. To make these computations, the equivalent system was defined.

The equivalent thickness h_{eq} and equivalent unit weight γ_{eq} are defined as:

$$h_{eq} = \sqrt[3]{{h_{PCC}}^3 + \frac{E_{base}}{E_{PCC}} {h_{base}}^3}$$

$$\gamma_{eq} = \frac{\gamma_{PCC} h_{PCC}}{h_{eq}}$$

Where:

h_{PCC} = concrete thickness in the original system

E_{base} = base modulus of elasticity in the original system

E_{PCC} = concrete modulus of elasticity in the original system

h_{base} = base thickness in the original system

γ_{PCC} = concrete unit weight in the original system

The concrete in the equivalent system will have the same elastic modulus, Poisson's ratio, and coefficient of thermal expansion as the concrete in the original system. Both systems will also have the same modulus of subgrade reaction, and wheel load magnitude. From these equations, it can be seen that the equivalent thickness and equivalent unit weight will change as the moduli of elasticity of the concrete and the base change. Results of these calculations for the first four months of pavement age are given in Table B2. For the remainder of the sample calculations, the equivalent system for a pavement age of 1 month will be used.

Table B2: Equivalent System for First Four Months of Pavement Life

Age (months)	**h_{PCC} (in)**	**h_{base} (in)**	**E_{PCC} (psi)**	**E_{base} (psi)**	**γ_{PCC} (lb/in^3)**	**h_{eq} (in)**	**γ_{eq} (lb/in^3)**
1	8	12	4946180	52710	0.087	8.0948	0.08598
2	8	12	4958085	53930	0.087	8.0967	0.08596
3	8	12	4969075	53660	0.087	8.0960	0.08597
4	8	12	4979270	53760	0.087	8.0960	0.08597

B1.1 Computing Nonlinear Component of Stress

The nonlinear component of stress on the bottom surface was computed directly from the original system:

$$\sigma_{NL} = \frac{-E_{PCC}\alpha_{PCC}}{1-\mu_{PCC}} T_{NL}$$

Where:

σ_{NL} = nonlinear component of stress

α_{PCC} = coefficient of thermal expansion in the original system

μ_{PCC} = Poisson's ratio in the original system

T_{NL} = nonlinear component of temperature gradient

In order to compute the probability of a given combination of linear and nonlinear temperature gradient as discussed in Section___, nonlinear temperature gradients between -24 and 24°F were considered in 1 degree increments. The stress associated with select nonlinear temperature gradients for age 1 month are given in Table B3.

Table B3: Select Nonlinear Stress Associated with Nonlinear Temperature Gradients

Nonlinear Temperature Gradient (°F)	**Nonlinear Stress (psi)**
-5	-170.0
-4	-136.0
-3	-102.0
-2	-68.0
-1	-34.0
0	0.0
1	34.0
2	68.0
3	102.0
4	136.0
5	170.0

B1.2 Computing Linear Component of Stress

The linear component of stress was computed using a neural network. First, the equivalent system must be transformed into a neural network system, which requires computing the modulus of elasticity E_{NN}, the temperature gradient T_{NN}, the aggregate interlock factor AGG_{NN}, and the tire pressure p_{NN} specific to the neural network. This is accomplished as follows:

$$E_{NN} = \frac{h_{eq}^3 E_{eq}(1-\mu_{NN}^2)k_{NN}}{(1-\mu_{eq}^2)k_{eq}}$$

$$\Delta T_{NN} = \frac{h_{NN}^2 \gamma_{NN}\alpha_{eq}(1+\mu_{eq})\ell_{eq}^2 k_{eq}}{h_{eq}^2 \gamma_{eq}\alpha_{NN}(1+\mu_{NN})k_{NN}\ell_{NN}^2}\Delta T_{eq}$$

$$\rho_{NN} = \frac{P_{NN}}{a_{stnd}}$$

$$P_{NN} = \frac{P_{eq}h_{NN}\gamma_{NN}}{h_{eq}\gamma_{eq}}$$

$$AGG_{NN} = \frac{AGG_{eq}k_{NN}\ell_{NN}}{k_{eq}\ell_{eq}}$$

Where:

E_{eq} = elastic modulus of the equivalent system

h_{NN} = pavement thickness of the neural network system, 10 in

γ_{NN} = concrete unit weight in the neural network system, 0.087 lb/in^3

μ_{NN} = Poisson's ratio of the neural network system

μ_{eq} = Poisson's ratio of the equivalent system

k_{eq} = modulus of subgrade reaction of the equivalent system

k_{NN} = modulus of subgrade reaction of the neural network system, 250 psi/in

α_{eq} = coefficient of thermal expansion of the equivalent system

ℓ_{eq} = radius of relative stiffness of the equivalent system

ℓ_{NN} = radius of relative stiffness of the neural network system

P_{eq} = wheel load in the equivalent system

P_{NN} = wheel load in the neural network system

a_{stnd} = standard tire footprint in the neural network system, 45.5625 in^2

AGG_{eq} = aggregate interlock factor in the equivalent system

The final variable required by the neural network is the vehicle wander x_{NN}, which is equal to the vehicle wander in the original system. The inputs required to compute similar space stresses using the neural network for each combination of wheel load and temperature gradient can then be computed. Note that the neural network takes an input of $Log(E_{NN})$ instead of E_{NN}. The required inputs for the neural network for pavement age 1 month are given in Table B4.

Table B4: Neural Network Inputs for Pavement Age 1 Month

$Log(E_{NN})$	**AGG_{NN}**	**p_{NN}**	**T_{NN}**	**x_{NN}**
6.569157	184515.7	151.22	11.63353	6

The stress output by the neural network for the inputs specified in Table B4 is 99.66 psi. This stress is in similar space; to convert this stress into real space, it must be multiplied by the scaling factor λ, given as:

$$\lambda = \frac{h_{PCC}^2 h_{NN} \gamma_{PCC}}{h_{eq}^3 \gamma_{NN}}$$

For the pavement age of 1 month, λ is equal to 1.204, resulting in a linear component of stress in real space of 119.9896.

The linear component of stress in real space is then added to the nonlinear component of stress calculated previously to find the total stress in real space of the system. The results of these computations for the select nonlinear temperature gradients shown in Table B3 are given in Table B5.

Table B5: Select Total Stress Associated with Nonlinear Temperature Gradients

Nonlinear Temperature Gradient (°F)	**Nonlinear Stress (psi)**	**Total Stress (psi)**
-5	-170.0	-50.0104
-4	-136.0	-16.0104
-3	-102.0	17.9896
-2	-68.0	51.9896
-1	-34.0	85.9896
0	0.0	119.9896
1	34.0	153.9896
2	68.0	187.9896
3	102.0	221.9896
4	136.0	255.9896
5	170.0	289.9896

Once total stress is known, the number of allowable loads can be computed using the transfer function from the MEPDG:

$$Log(N) = 2\left(\frac{MOR}{\sigma_{total}}\right)^{1.22}$$

Where:

MOR = modulus of rupture of the concrete

The modulus of rupture of the concrete changes as the concrete gains strength; at a pavement age of 1 month, the modulus of rupture was 775.0735 psi. Only tensile stresses

can cause cracks, therefore the number of allowable loads producing compression is essentially infinite. For practical purposes, N was capped at a very large value of 10^{15} to avoid complications associated with including infinity as a value in a program. The number of allowable loads N was computed for the select nonlinear temperature gradients shown in Table B5; results are shown in Table B6.

Table B6: Select Number of Allowable Loads

Nonlinear Temperature Gradient (°F)	Total Stress (psi)	Log (N)	N
-5	-50.0104	-	1.00E+15
-4	-16.0104	-	1.00E+15
-3	17.97462	29.24389	1.75E+29
-2	51.9796	54.0396	1.10E+54
-1	85.98459	197.3984	1.00E+15
0	119.9896	19.47481	2.98E+19
1	153.9946	14.36388	2.31E+14
2	187.9996	11.26048	1.82E+11
3	222.0045	9.193203	1.56E+09
4	256.0095	7.72602	5.32E+07
5	290.0145	6.63554	4.32E+06

B2. Number of Applied Loads

The number of applied loads is computed for each loading condition, i.e. for each combination of axle type, load magnitude, vehicle wander, and combination of linear and nonlinear temperature gradient, in a given month, hour, and year.

To begin, the number of 22,000 lb single axle loads in year 1 of pavement life was determined from the MEPDG SingleAxleOutput.txt file as 11.5/day. This number was multiplied by 30 days in a standard month to determine the number of 22,000 lb single

axle loads in a standard month in the first year of pavement life n_{ijkl} = 345 vehicles/month.

The number of given axle loads in a standard month of the given year of pavement life was then multiplied by the probability of a given traffic wander occurring. The probability of the traffic wander P_n of a vehicle being 6 inches from the pavement edge was 0.135. This means that 46.575 22,000 lb single axle loads will travel across the pavement with a wander of 6 inches in a standard month in the first year of pavement life. This quantity is denoted as n_{ijkln}.

Next, the hourly traffic distribution is taken into account by multiplying n_{ijkln} by the hourly traffic distribution P_o. From the MEPDG _HourlyTrafficPerc.txt file, the percentage of daily traffic occurring in hour 12 was .059. Thus n_{ijklno} = 2.748.

The final step is account for the probability of a given linear and nonlinear temperature gradient combination occurring in the same hour, month, and year, P_m. This probability was computed for all of the nonlinear temperature gradients considered, from -24 to 24°F. P_m and the associated final number for applied loads $n_{ijklmno}$ for select nonlinear temperature gradients are shown in Table B7.

Table B7: Select values of P_m and $n_{ijklmno}$

Nonlinear Temperature Gradient (°F)	P_m	$n_{ijklmno}$
-5	0	0
-4	0	0
-3	0	0
-2	0	0
-1	0	0
0	0.0068	0.018703
1	0.0303	0.083339
2	0.0744	0.204634
3	0	0
4	0	0
5	0	0

B3. Damage Computation

The total damage in the pavement is computed as

$$Fatigue\ Damage = \sum \frac{n_{ijklmno}}{N_{ijklmno}}$$

For the select nonlinear temperature gradients used throughout this example, the resulting fatigue damage is given in Table B8.

Table B8: Select Values of Fatigue Damage

Nonlinear Temperature Gradient (°F)	$n_{ijklmno}$	$N_{ijklmno}$	Fatigue Damage
-5	0	1.00E+15	0
-4	0	1.00E+15	0
-3	0	1.75E+29	0
-2	0	1.10E+54	0
-1	0	1.00E+15	0
0	0.018703	2.98E+19	6.28E-22
1	0.083339	2.31E+14	3.61E-16
2	0.204634	1.82E+11	1.12E-12
3	0	1.56E+09	0
4	0	5.32E+07	0
5	0	4.32E+06	0

The total fatigue damage accumulated was for 22000 lb single axle loads traveling at a wander of 6 inches in the twelfth hour of the day when at 8°F linear temperature gradient was present for the entire 240 months of pavement life was $4.94*10^{-10}$. Similar calculations were made for every value of load magnitude, every axle type, all vehicle wanders, and all hours to the day to find the total damage seen by the pavement equal to .068 at the location considered.

Other locations have different values of damage. For example, a location 12 inches closer to the middle of the transverse joint of the pavement was .373. When designing a pavement, the highest level of damage seen along the transverse joint should be taken as the value of damage associated with longitudinal cracking in that pavement.